

AD-A188 895

REMOVING RESONANT OSCILLATION SIGNALS FROM SHALLOW
FLOAT DATA(U) SCRIPPS INSTITUTION OF OCEANOGRAPHY LA
JOLLA CA MARINE PHYSIC. R L CULVER ET AL. MAY 87

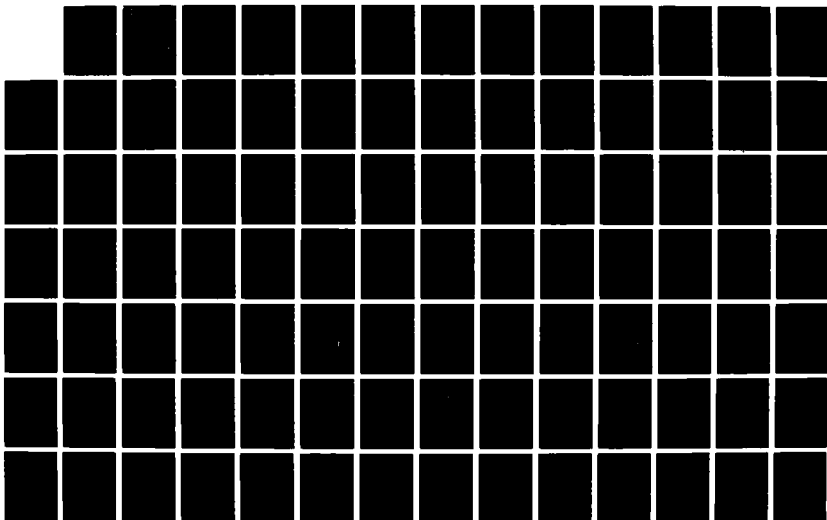
1/2

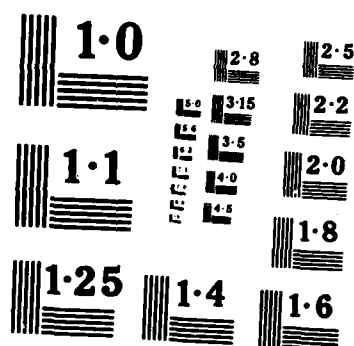
UNCLASSIFIED

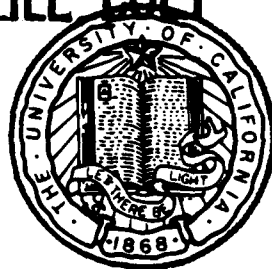
MPL-TN-395 N00014-87-K-0010

F/G 28/1

NL







MARINE PHYSICAL LABORATORY

SCRIPPS INSTITUTION OF OCEANOGRAPHY

San Diego, California 92152

AD-A188 895

REMOVING RESONANT OSCILLATION SIGNALS FROM SWALLOW FLOAT DATA

R.L. Culver, W.S. Hodgkiss, G.L. Edmonds, and V.C. Anderson

Sponsored by the
Office of Naval Research
Contract N00014-87-K-0010

DTIC
ELECTE
DEC 28 1987
S H D

MPL TECHNICAL MEMORANDUM 395

MPL-U-21/87
May 1987

Approved for public release; distribution unlimited.

87 12 16 002

REPORT DOCUMENTATION PAGE

1a. REPORT SECURITY CLASSIFICATION UNCLASSIFIED			1b. RESTRICTIVE MARKINGS UNCLASSIFIED		
2a. SECURITY CLASSIFICATION AUTHORITY			3. DISTRIBUTION/AVAILABILITY OF REPORT Approved for public release; distribution unlimited.		
2b. DECLASSIFICATION/DOWNGRADING SCHEDULE					
4. PERFORMING ORGANIZATION REPORT NUMBER(S) MPL TM-395 [MPL-U-21/87]			5. MONITORING ORGANIZATION REPORT NUMBER(S)		
6a. NAME OF PERFORMING ORGANIZATION Marine Physical Laboratory		6b. OFFICE SYMBOL (If applicable) MPL	7a. NAME OF MONITORING ORGANIZATION Office of Naval Research		
6c. ADDRESS (City, State, and ZIP Code) University of California, San Diego Scripps Institution of Oceanography San Diego, California 92152			7b. ADDRESS (City, State, and ZIP Code) Department of the Navy 800 North Quincy Street Arlington, VA 22217-5000		
8a. NAME OF FUNDING / SPONSORING ORGANIZATION Office of Naval Research		8b. OFFICE SYMBOL (If applicable)	9. PROCUREMENT INSTRUMENT IDENTIFICATION NUMBER N00014-87-K-0010		
8c. ADDRESS (City, State, and ZIP Code) Department of the Navy 800 North Quincy Street Arlington, VA 22217-5000			10. SOURCE OF FUNDING NUMBERS		
			PROGRAM ELEMENT NO.	PROJECT NO.	TASK NO.
					WORK UNIT ACCESSION NO.
11. TITLE (Include Security Classification) REMOVING RESONANT OSCILLATION SIGNALS FROM SWALLOW FLOAT DATA					
12. PERSONAL AUTHOR(S) R.L. Culver, W.S. Hodgkiss, G.L. Edmonds, and V. C. Anderson					
13a. TYPE OF REPORT Technical Memorandum		13b. TIME COVERED FROM _____ TO _____		14. DATE OF REPORT (Year, Month, Day) May 1987	
15. PAGE COUNT 80					
16. SUPPLEMENTARY NOTATION					
17. COSATI CODES			18. SUBJECT TERMS (Continue on reverse if necessary and identify by block number)		
FIELD	GROUP	SUB-GROUP	Swallow floats; ambient ocean noise; resonant oscillation		
19. ABSTRACT (Continue on reverse if necessary and identify by block number)					
<p>Self-contained, freely-drifting Swallow floats capable of recording very low frequency (VLF) ambient ocean noise are under development at the Marine Physical Laboratory, Scripps Institution of Oceanography, San Diego, California. The floats are ballasted to neutral buoyancy at a desired depth, whereupon they record the components of particle velocity, from which sound pressure levels may be derived. A high frequency acoustic mutual interrogation system is incorporated to provide relative float positions, permitting the combination of data from an array of floats.</p> <p>During an experiment conducted between 16 and 18 September 1986 approximately 50 miles west of San Diego, twelve Swallow float buoys were deployed to depths of 1000 to 2000 meters for a 24 hour period. Data from four of the floats were found to contain strong signals due to resonant float oscillation excited by their internal tape recorder. This paper develops and applies a method of processing data to attenuate the resonant oscillation signals. The method can be applied when the mean square resonant oscillation signal is large relative to the background noise power.</p> <p>Consecutive records are averaged together to produce an estimate of the float's resonant oscillation signal. The resonant oscillation signal estimate is then correlated with each record to yield a weighting coefficient, and the weighted signal subtracted from that record. The method was applied to three of the four 1986 deployment floats, and it significantly attenuated resonant oscillation signals between 0.36 Hz and 6.1 Hz.</p>					
20. DISTRIBUTION / AVAILABILITY OF ABSTRACT <input type="checkbox"/> UNCLASSIFIED/UNLIMITED <input checked="" type="checkbox"/> SAME AS RPT <input type="checkbox"/> DTIC USERS			21. ABSTRACT SECURITY CLASSIFICATION UNCLASSIFIED		
22a. NAME OF RESPONSIBLE INDIVIDUAL W. S. Hodgkiss			22b. TELEPHONE (Include Area Code) (619) 534-1798		22c. OFFICE SYMBOL MPL

Table of Contents

Section	Page
Abstract	iii
Introduction	1
1. Swallow Float System Description	2
2. The Resonant Oscillation Problem	3
3. Theoretical Solution	5
4. Application	12
References	22



Accession For	
NTIS GFA&I	<input checked="" type="checkbox"/>
ERIC TDS	<input type="checkbox"/>
Unpublished	<input type="checkbox"/>
Justification	
By	
Distribution/	
Availability	
Available and/or	
Dist. Special	
A-1	

Removing Resonant Oscillation Signals from Swallow Float Data

R.L. Culver, W.S. Hodgkiss, G.L. Edmonds, and V.C. Anderson

Marine Physical Laboratory
Scripps Institution of Oceanography
University of California, San Diego
San Diego, CA. 92152

ABSTRACT

Self-contained, freely-drifting Swallow floats capable of recording very low frequency (VLF) ambient ocean noise are under development at the Marine Physical Laboratory, Scripps Institution of Oceanography, San Diego, California. The floats are ballasted to neutral buoyancy at a desired depth, whereupon they record the components of particle velocity, from which sound pressure levels may be derived. A high frequency acoustic mutual interrogation system is incorporated to provide relative float positions, permitting the combination of data from an array of floats.

During an experiment conducted between 16 and 18 September 1986 approximately 50 miles west of San Diego, twelve Swallow float buoys were deployed to depths of 1000 to 2000 meters for a 24 hour period. Data from four of the floats were found to contain strong signals due to resonant float oscillation excited by their internal tape recorder. This paper develops and applies a method of processing data to attenuate the resonant oscillation signals. The method can be applied when the mean square resonant oscillation signal is large relative to the background noise power.

Consecutive records are averaged together to produce an estimate of the float's resonant oscillation signal. The resonant oscillation signal estimate is then correlated with each record to yield a weighting coefficient, and the weighted signal subtracted from that record. The method was applied to three of the four 1986 deployment floats, in which it significantly attenuated resonant oscillation signals between 0.36 Hz and 6.1 Hz.

Introduction

Under Office of Naval Research sponsorship, the Marine Physical Laboratory has designed, fabricated and deployed self-contained Swallow floats which record very low frequency (VLF) ambient ocean noise over extended periods of time. In operation, the floats are ballasted to neutral buoyancy at a desired depth or deployed to the ocean bottom. They operate autonomously to measure and record the components of particle velocity in the 1 - 20 Hz band, from which sound pressure levels may be determined. The floats periodically generate and receive 8 kHz acoustic pulses which are used to determine their relative positions. The deployment of several floats thus forms a freely drifting array of sensors.

The Swallow float design minimizes self-noise which can limit accurate ambient ocean noise measurements. Floating freely, they are not subject to flow noise or tether strumming. They measure velocity and are thus insensitive to variations in local pressure. Ambient ocean noise levels derived from single float measurements have been shown to agree closely with omni-directional hydrophone measurements made under similar conditions.¹ Operation of the floats has been described in earlier reports.^{1,2,3} Starting with the 1986 deployment data, the velocity signal sampling rate was been increased to 50 Hz and the anti-aliasing filter cutoff-frequency increased to about 21 Hz. Record duration was decreased from 90 to 45 seconds.

MPL has deployed Swallow floats annually since 1982. Between 16 and 19 September 1986, 12 floats were deployed approximately 50 miles west of San Diego, California at 32°35' N, 118°10' W. Three floats were located on the ocean bottom to serve as references for the acoustic positioning system. Five floats developed problems and yielded little data. The remaining 4 deployed to about 1000 meters depth where they acquired approximately 15 hours of acoustic data. MPL Technical Memorandum 391 contains a preliminary analysis of data from this deployment.

Velocity data from the floats deployed to 1000 meters depth in 1986 have been found to contain strong sinusoidal signals which are excited at the start of each record and decay exponentially. These signals are attributed to resonant float oscillation apparently excited by the internal tape recorder when it operates between records. In some records, the resonant oscillation causes velocity data to be clipped for up to 8 seconds at the beginning, obscuring the ambient ocean noise signal and reducing the dynamic range with which the ambient ocean noise signal is measured during the remainder of the record.

Effort is currently underway at MPL to modify the Swallow float hardware to eliminate resonant oscillation in future deployments. It is also desirable to remove these signals from the 1986 data set to permit its further use. This report derives a method of removing or significantly reducing resonant oscillation, which may be applied if certain conditions are met. The method is shown to be effective on the 1986 deployment data set.

A separate investigation focusing on occurrences of resonant oscillation at frequencies below 0.6 Hz is ongoing. Resonant oscillation at these frequencies appears to consist of an irregular rocking or wobble which is strongly excited as the floats descend, weakly but consistently excited by the tape recorder at the start of each record, and occasionally excited by strong acoustic pulses which it receives. MPL Technical Memorandum 394, *Low Frequency Oscillations in 1986 Swallow Float Data*, will probably be issued in June of this year.

1. Swallow Float System Description

The Swallow float is a 17 inch diameter glass sphere containing three geophones as directional velocity transducers, a compass for detecting float heading, an acoustic transponder for positioning, a solid state memory data buffer, a digital cartridge tape recorder, and an acoustically actuated ballast release. Signal conditioning is depicted in Figure 1.1 and hardware configuration is shown in Figure 1.2.

The three orthogonally-oriented geophones are rigidly mounted to the inside top of the glass sphere. Each transducer generates a signal proportional to the component of the float's velocity which is along the transducer's axis.

The geophone signal undergoes 95 dB of amplification before entering an automatic gain control (AGC) circuit which provides up to 26 dB of gain to make full use of the dynamic range of the analog-to-digital converter (ADC). AGC level is controlled by the float's microprocessor depending upon how much clipping occurs at the ADC.

Before sampling at 50 Hz, the signal is low-pass filtered to prevent aliasing. The filter has a 21 Hz corner frequency and is down 20 dB at 25 Hz. The ADC is an 8-bit device yielding 48 dB of dynamic range. Clipping occurs when the input rises above + 2.5 or below - 2.5 volts.

The digitized output is buffered for 44 seconds before being stored on tape because the tape drive requires approximately 75 watts of power and cannot be powered on continuously. During a one second interval, the tape drive is powered up, the buffer contents are written to tape, and the tape drive is powered down. Tape recorder capacity is limited to about 2000 45-second records, so that submergence time is limited to about 25 hours.

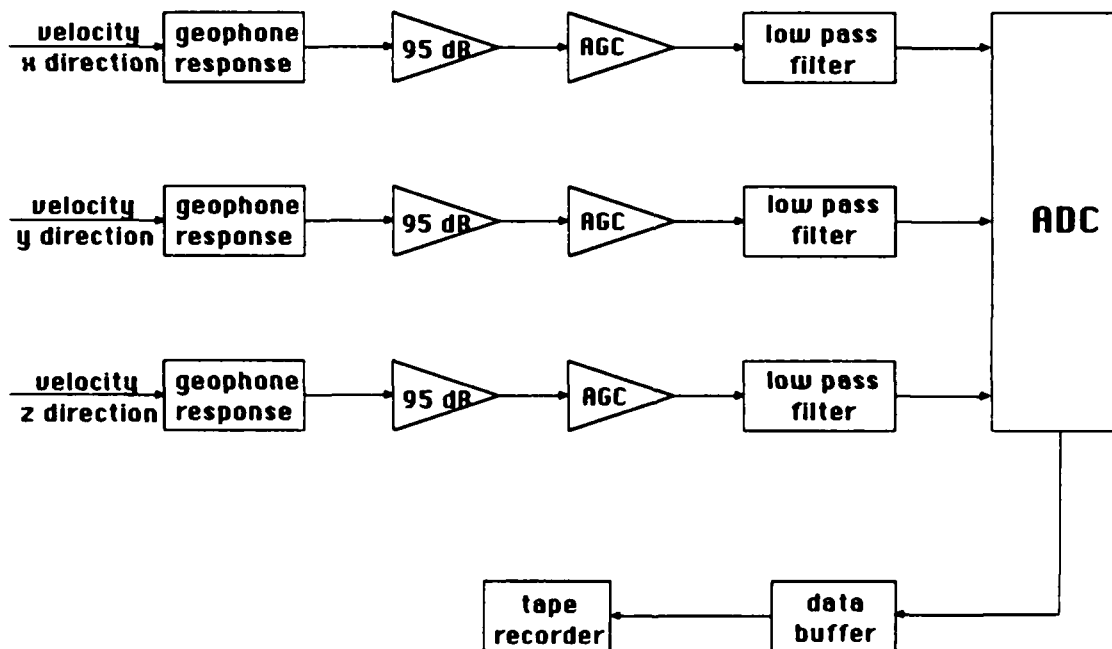


Figure 1.1: Geophone Signal Conditioning

2. The Resonant Oscillation Problem

Twelve Swallow floats were deployed during September 1986 about 50 miles west of San Diego, Ca. in approximately 2000 meters of water. Three were located on the ocean bottom to serve as references for the acoustic positioning system and the remaining nine were deployed to about 1000 meters depth to collect velocity data. Four of the nine surfaced prematurely and collected little data. A fifth float developed a ground in one geophone channel. The four remaining floats deployed successfully to approximately 1000 meters and collected about 15 hours of useful velocity data. A preliminary analysis of these data is contained in MPL Technical Memorandum 391, *September 1986 Trip Report*.⁴

The 1986 deployment velocity data were found to contain sinusoidal signals which are strong at the start of each record and decay exponentially thereafter. Some examples of geophone output with 95 dB gain are shown in Figures 2.1 through 2.8. Each Figure contains one axis of data from twelve 45-second records. Acoustic positioning pulses may be seen 10 seconds into records 1203, 1611, 1205, 1613, 1209, 1605, 1210, and 1606 in Figures 2.1 through 2.8, respectively.

Table 2.1: Key to Figures 2.1 through 2.8		
Figure	Float	Records
2.1	3	1200-1211
2.2	3	1600-1611
2.3	5	1200-1211
2.4	5	1600-1611
2.5	9	1200-1211
2.6	9	1600-1611
2.7	10	1200-1211
2.8	10	1600-1611

Floats 3, 9, and 10 contain a ≈ 4 Hz signal which is clipped for 3 to 8 seconds at the start of each record and decays away after that. Another lower amplitude sinusoid with a period of about 2.6 seconds is visible in many records in all 4 floats. The decaying sinusoids appear quite similar from record to record. Their initial phase does not change and their amplitude changes very little. For these reasons, they are thought to represent float resonances excited by one or more impulses which are nearly identical from record to record. The impulses are thought to be mechanical rather than acoustic. This is because the floats do not generate acoustic energy near the start of each record, and because mechanical impulses are quite possibly generated by the float's internal tape recorder when it is powered up and down at the end of each record.

Another indication that the tape recorder is responsible for the oscillations is that the initial amplitude and phase of the oscillation depends on the direction in which the tape recorder is writing. The tape recorder writes in a serpentine manner, i.e. it traverses the entire tape in one direction writing the first track, reverses direction and writes the second track, again reverses direction and writes the third track, and so on. Each track is about 500 records long, with direction reversals occurring near records 500, 1000 and 1500. An example of the effect which tape recorder direction has on the resonant oscillation can be seen in data from float 3. X-axis clipping near record 1200 (track 3) in Figure 2.1 has an initial phase which is about π radians different from that near record 1600 (track 4) in Figure 2.2. Similar indications can be found in the other floats.

The resonant float oscillation causes at least two problems. First, it can obscure the ambient noise signal. Certainly the ambient noise signal is obscured at the start of the record in floats 3, 9, and 10. How much of the record is affected by the oscillations it is not readily evident. The 0.4 Hz oscillation appears to extend to the end of some records.

Second, resonant oscillation can dominate the AGC level and reduce the dynamic response applied to the ambient noise signal. To understand why this can occur requires some understanding of how the AGC level is set. The AGC level is controlled by a microprocessor which keeps track of the number of clipped samples during each record. The AGC is stepped down between records when there is too much clipping and is stepped up when there is too little. The resonant oscillation can raise the AGC level by causing clipping. When the AGC level is set too high, too few bits are available to quantize the ambient ocean noise signal. This reduces the dynamic range with which the noise is measured. The microprocessor can be programmed to wait after the start of a record before looking for clipped samples. This works well enough but requires knowing how long the oscillation-induced clipping will last.

Fundamentally there are two ways of modifying the Swallow float design to eliminate resonant oscillation in the velocity data: remove the excitation or change the float's response to the excitation. Eliminating the excitation is impractical because it would be expensive to redesign the tape recorder or would require long, very soft "springs" to decouple it from the rest of the float down to 1 Hz. Changing the response is easier done and effort is ongoing at MPL to dampen the resonant response, move it out of band, or both. One design was tested during a February 1987 sea trip but proved unsatisfactory. Several other designs will be tested during an April 1987 sea trip.

There is also sufficient value in the September 1986 data set to warrant exploring a means of processing that data to remove the resonant oscillation. The intent with the 1986 data is to use the acoustic positioning system pulses to determine the floats positions while they were deployed and beamform using data from the four floats deployed to 1000 meters. The remainder of this report deals with removing the resonant oscillation from the 1986 data.

3. Theoretical Solution

The j^{th} Swallow float data record $x_j(n)$ is composed of an ambient noise signal $s_j(n)$ and a resonant oscillation signal $r_j(n)$. The resonant oscillation $r_j(n)$ consists of a fixed but unknown sequence $r(n)$, multiplied by a gain factor a_j which may vary from record to record. See Figure 3.1. The j^{th} data record is therefore

$$x_j(n) = a_j \cdot r(n) + s_j(n). \quad (3.1)$$

We define $r(n)$ such that the average value of a_j is 1. It can be seen from Figures 2.1 through 2.8 that the value of a_j changes little from record to record. Therefore we assume that for M greater than 10,

$$\bar{a} = \frac{1}{M} \sum_{j=1}^M a_j \approx 1 \quad (M > 10) \quad (3.2)$$

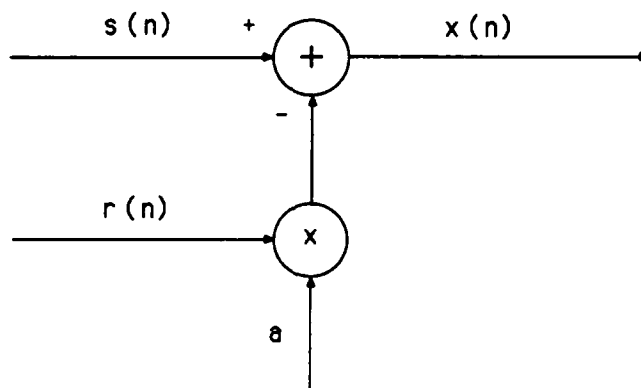


Figure 3.1: The geophone signal $x(n)$ is composed of an ambient noise signal $s(n)$ and a resonant oscillation signal $r(n)$.

A method is sought by which the resonant oscillation $a_j \cdot r(n)$ may be removed from each record $x_j(n)$ leaving behind the noise, $s_j(n)$, which is the desired signal. The approach is to estimate $r(n)$ and a_j and substitute them into a rearranged equation (3.1):

$$\hat{s}_j(n) = x_j(n) - \hat{a}_j \cdot \hat{r}(n) \quad (3.3)$$

Estimating $r(n)$

Under certain conditions, a good estimate of $r(n)$ may be obtained by coherently averaging data from a large number of records. The M record average of $x_j(n)$ is

$$\begin{aligned}\bar{x}(n) &= \frac{1}{M} \sum_{j=1}^M x_j(n) = \frac{1}{M} \sum_{j=1}^M [a_j \cdot r(n) + s_j(n)] \\ &= r(n) \frac{1}{M} \sum_{j=1}^M a_j + \frac{1}{M} \sum_{j=1}^M s_j(n) = \bar{a} \cdot r(n) + \bar{s}(n)\end{aligned}\quad (3.4)$$

Equation (3.4) tells us that if M is large enough for \bar{a} to be approximately equal to 1, and if $|r(n)|$ is much larger than $|\bar{s}(n)|$, then $r(n)$ will be approximately equal to $\bar{x}(n)$.

$$\text{If } |r(n)| \gg |\bar{s}(n)|, \quad (3.5)$$

$$\text{then } \bar{r}(n) = \frac{1}{M} \sum_{j=1}^M x_j(n) \approx r(n) \quad (M > 10) \quad (3.6)$$

We can ensure that equation (3.5) is satisfied in the mean square sense. Squaring both sides and averaging over all values of n yields

$$\frac{1}{L} \sum_{n=1}^L r^2(n) \gg \frac{1}{L} \sum_{n=1}^L \bar{s}^2(n) \quad (3.5a)$$

Using equations (3.5a) and (3.6), we can say that if the mean square value of $r(n)$ is much greater than the mean square value of $\bar{s}(n)$, then the M record average provides a good estimate of $r(n)$. We need to know the mean square values of $r(n)$ and $\bar{s}(n)$.

The sequence $r(n)$ consists of fixed but unknown values which may be positive, negative or zero. No assumption is made about its mean value

$$\mu_r = \lim_{L \rightarrow \infty} \frac{1}{L} \sum_{n=1}^L r(n) \quad (3.7a)$$

except that it is well approximated by the estimate $\hat{\mu}_r$

$$\hat{\mu}_r = \frac{1}{L} \sum_{n=1}^L r(n) \approx \mu_r \quad (L = 2250) \quad (3.7b)$$

when $L = 2250$, the number of points in a record. There is no a priori assumption about the mean square value of $r(n)$,

$$\gamma_r^2 = \lim_{L \rightarrow \infty} \frac{1}{L} \sum_{n=1}^L r^2(n) \quad (3.8a)$$

except that it is well approximated by the estimate

$$\hat{\gamma}_r^2 = \frac{1}{L} \sum_{n=1}^L r^2(n) \approx \gamma_r^2 \quad (L = 2250) \quad (3.8b)$$

The sequence $s_j(n)$ is one realization of a random process which we assume to be stationary over M record intervals. We assume that $s_j(n)$ is mean zero

$$\mu_s = \lim_{M \rightarrow \infty} \frac{1}{M} \sum_{j=1}^M s_j(n) = 0 \quad (3.9a)$$

and has mean square value

$$\gamma_s^2 = \lim_{M \rightarrow \infty} \frac{1}{M} \sum_{j=1}^M s_j^2(n) \quad (3.9b)$$

The stationarity assumption also allows us to equate the time and ensemble averages of $s_j(n)$, and we assume that they are well approximated by the $L = 2250$ estimate,

$$\hat{\mu}_s = \frac{1}{L} \sum_{n=1}^L s_j(n) \approx 0 \quad (L = 2250) \quad (3.10a)$$

$$\hat{\gamma}_s^2 = \frac{1}{L} \sum_{n=1}^L s_j^2(n) \approx \gamma_s^2 \quad (L = 2250) \quad (3.10b)$$

We also assume that the noise is uncorrelated from record to record

$$R_{s,s_k}(0) = \lim_{L \rightarrow \infty} \frac{1}{L} \sum_{n=1}^L s_j(n) s_k(n) = \begin{cases} 0, & j \neq k \\ \gamma_s^2, & j = k \end{cases} \quad (3.11a)$$

and that the estimate of the cross correlation (with $L = 2250$) is

$$\hat{R}_{s,s_k}(0) = \frac{1}{L} \sum_{n=1}^L s_j(n) s_k(n) = \begin{cases} 0 & j \neq k \\ \hat{\gamma}_s^2 & j = k \end{cases} \quad (L = 2250) \quad (3.11b)$$

Lastly, we assume that $r(n)$ and $s_j(n)$ are uncorrelated for all j

$$R_{rs_k}(0) = \lim_{L \rightarrow \infty} \frac{1}{L} \sum_{n=1}^L r(n) s_k(n) = 0 \quad (\text{for all } j) \quad (3.12a)$$

and

$$\hat{R}_{rs}(0) = \frac{1}{L} \sum_{n=1}^L r(n) s_k(n) \approx 0 \quad (L = 2250; \text{ for all } j) \quad (3.12b)$$

Now, the estimate of the mean square value of $\bar{s}(n)$ is

$$\begin{aligned} \hat{\gamma}_{\bar{s}}^2 &= \frac{1}{L} \sum_{n=1}^L \bar{s}^2(n) \\ &= \frac{1}{L} \sum_{n=1}^L \left[\frac{1}{M} \sum_{j=1}^M s_j(n) \right]^2 = \frac{1}{L} \sum_{n=1}^L \frac{1}{M^2} \sum_{j=1}^M \sum_{k=1}^M s_j(n) s_k(n) \\ &= \frac{1}{M^2} \sum_{j=1}^M \sum_{k=1}^M \frac{1}{L} \sum_{n=1}^L s_j(n) s_k(n) \\ &= \frac{1}{M^2} \sum_{j=1}^M \hat{\gamma}_s^2 = \frac{\hat{\gamma}_s^2}{M} \end{aligned} \quad (3.13)$$

where equation (3.11b) has been used. Equation (3.13) says that the mean square value of $\bar{s}(n)$ is $1/M$ times the mean square value of $s(n)$. An estimate for the mean square value of $s(n)$, γ_s^2 , may be obtained from the mean and mean square values of $x_j(n)$ as follows. The mean value of the j^{th} data record is

$$\hat{\mu}_{x_j} = \frac{1}{L} \sum_{n=1}^L x_j(n) = a_j \frac{1}{L} \sum_{n=1}^L r(n) + \frac{1}{L} \sum_{n=1}^L s_j(n) = a_j \hat{\mu}_r \quad (3.14)$$

where equations (3.7b) and (3.10a) have been used. The mean square value of $x_j(n)$ is

$$\begin{aligned} \hat{\gamma}_{x_j}^2 &= \frac{1}{L} \sum_{n=1}^L x_j^2(n) \\ &= \frac{1}{L} \sum_{n=1}^L \left[a_j r(n) + s_j(n) \right]^2 \\ &= a_j^2 \frac{1}{L} \sum_{n=1}^L r^2(n) + \frac{1}{L} \sum_{n=1}^L s_j^2(n) \\ &= a_j^2 \hat{\gamma}_r^2 + \hat{\gamma}_s^2 \end{aligned} \quad (3.15)$$

using equation (3.12b). Now solve equation (3.14) for a_j , square the result and substitute it into equation (3.15) to get

$$\hat{\gamma}_{x_j}^2 = \hat{\mu}_{x_j}^2 \frac{\hat{\gamma}_r^2}{\hat{\mu}_r^2} + \hat{\gamma}_s^2 \quad (3.16)$$

There are M such equations and they can be written in matrix form as follows

$$\begin{bmatrix} \hat{\gamma}_{x_1}^2 \\ \hat{\gamma}_{x_2}^2 \\ \vdots \\ \hat{\gamma}_{x_M}^2 \end{bmatrix} = \begin{bmatrix} \hat{\mu}_{x_1}^2 & 1 \\ \hat{\mu}_{x_2}^2 & 1 \\ \vdots & \vdots \\ \hat{\mu}_{x_M}^2 & 1 \end{bmatrix} \begin{bmatrix} \frac{\hat{\gamma}_r^2}{\hat{\mu}_r^2} \\ \hat{\gamma}_s^2 \end{bmatrix} \quad (3.17)$$

If we identify

$$Z = \begin{bmatrix} \hat{\gamma}_{x_1}^2 \\ \hat{\gamma}_{x_2}^2 \\ \vdots \\ \hat{\gamma}_{x_M}^2 \end{bmatrix}, \quad H = \begin{bmatrix} \hat{\mu}_{x_1}^2 & 1 \\ \hat{\mu}_{x_2}^2 & 1 \\ \vdots & \vdots \\ \hat{\mu}_{x_M}^2 & 1 \end{bmatrix}, \quad \text{and} \quad X = \begin{bmatrix} \frac{\hat{\gamma}_r^2}{\hat{\mu}_r^2} \\ \hat{\gamma}_s^2 \end{bmatrix},$$

so that equation (3.17) may be written as $Z = HX$, then the least squares solution for X is

$$X_{ls} = \left[H^T H \right]^{-1} H^T Z$$

$$\begin{bmatrix} \frac{\hat{\gamma}_r^2}{\hat{\mu}_r^2} \\ \hat{\gamma}_s^2 \end{bmatrix}_{\text{least square}} = \begin{bmatrix} \sum_{j=1}^M \hat{\mu}_{x_j}^4 & \sum_{j=1}^M \hat{\mu}_{x_j}^2 \\ \sum_{j=1}^M \hat{\mu}_{x_j}^2 & M \end{bmatrix}^{-1} \begin{bmatrix} \sum_{j=1}^M \hat{\mu}_{x_j}^2 \hat{\gamma}_{x_j}^2 \\ \sum_{j=1}^M \hat{\gamma}_{x_j}^2 \end{bmatrix}$$

$$= \frac{1}{M \sum_{j=1}^M \hat{\mu}_{x_j}^4 - \left[\sum_{j=1}^M \hat{\mu}_{x_j}^2 \right]^2} \begin{bmatrix} M & - \sum_{j=1}^M \hat{\mu}_{x_j}^2 \\ - \sum_{j=1}^M \hat{\mu}_{x_j}^2 & \sum_{j=1}^M \hat{\mu}_{x_j}^4 \end{bmatrix} \begin{bmatrix} \sum_{j=1}^M \hat{\mu}_{x_j}^2 \hat{\gamma}_{x_j}^2 \\ \sum_{j=1}^M \hat{\gamma}_{x_j}^2 \end{bmatrix} \quad (3.18)$$

The least squares estimate for the mean square value of the noise is

$$\hat{\gamma}_s^2 = \frac{\sum_{j=1}^M \hat{\mu}_{x_j}^4 \sum_{j=1}^M \hat{\gamma}_{x_j}^2 - \sum_{j=1}^M \hat{\mu}_{x_j}^2 \sum_{j=1}^M \hat{\mu}_{x_j}^2 \hat{\gamma}_{x_j}^2}{M \sum_{j=1}^M \hat{\mu}_{x_j}^4 - \left[\sum_{j=1}^M \hat{\mu}_{x_j}^2 \right]^2} \quad (3.19)$$

Substituting (3.19) into (3.13) provides the estimate for the mean square value of the $\bar{s}(n)$. An estimate for γ_r^2 may be obtained from the mean square value of the M record average, $\bar{x}(n)$. Using (3.4) and (3.12b), we have

$$\begin{aligned} \hat{\gamma}_{\bar{x}}^2 &= \frac{1}{L} \sum_{n=1}^L \left[\bar{x}(n) \right]^2 \\ &= \frac{1}{L} \sum_{n=1}^L \left[\bar{a} \cdot r(n) + \bar{s}(n) \right]^2 \\ &= \bar{a}^2 \frac{1}{L} \sum_{n=1}^L r^2(n) + \frac{1}{L} \sum_{n=1}^L \bar{s}^2(n) \\ &= \bar{a}^2 \hat{\gamma}_r^2 + \hat{\gamma}_s^2 \end{aligned} \quad (3.20)$$

If M is larger than 10, we can set $\bar{a} = 1$ in equation (3.20). Solving (3.20) for $\hat{\gamma}_r^2$ yields

$$\hat{\gamma}_r^2 = \hat{\gamma}_{\bar{x}}^2 - \hat{\gamma}_s^2 \quad M > 10 \quad (3.21)$$

Recognizing that the condition (3.5a) is

$$\hat{\gamma}_r^2 \gg \hat{\gamma}_s^2, \quad (3.5b)$$

we can use equations (3.13), (3.19) and (3.21) to determine if (3.5b) is satisfied for a particular value of M. If (3.5b) is satisfied, then we are justified in using that value of M in equation (3.6) to obtain $\hat{r}(n)$.

Estimating a

An estimate for the value of a in the j th record may be obtained by correlating $x_j(n)$ with $\hat{r}(n)$:

$$\begin{aligned}
 \hat{R}_{x,r}(0) &= \frac{1}{L} \sum_{n=1}^L x_j(n) \hat{r}(n) \\
 &= \frac{1}{L} \sum_{n=1}^L \left[a_j \cdot r(n) + s_j(n) \right] \hat{r}(n) \\
 &= a_j \frac{1}{L} \sum_{n=1}^L r(n) \hat{r}(n) + \frac{1}{L} \sum_{n=1}^L r(n) s_j(n) \\
 &= a_j \hat{\gamma}_r^2
 \end{aligned} \tag{3.22}$$

where the assumption (3.12) that $r(n)$ and $s_j(n)$ are uncorrelated has been used. Equation (3.22) is valid if $\hat{r}(n)$ is a good estimate of $r(n)$, which is to say that the condition (3.5b) is satisfied. Solving (3.22) for a_j yields

$$\hat{a}_j = \frac{\hat{R}_{x,r}(0)}{\hat{\gamma}_r^2} \tag{3.23}$$

Equation (3.23) is evaluated by calculating $\hat{\gamma}_r^2$ using (3.21) and $\hat{R}_{x,r}(0)$ using (3.22). Substituting equations (3.6) and (3.23) into (3.3) yields the estimate of the ambient ocean noise in the j th record

$$\hat{s}(n) = x_j(n) - \hat{a}_j \cdot \hat{r}(n) = x_j(n) - \frac{\hat{R}_{x,r}(0)}{\hat{\gamma}_r^2} \bar{x}(n) \tag{3.24}$$

4. Application

In the previous Section, a method has been developed for removing resonant oscillation signal from Swallow float data records. In this Section, the method is applied to September 1986 deployment data.

Estimating $r(n)$

A necessary first step is to clarify the definition of $r(n)$. In Section 3 it was postulated that the resonant oscillation $r(n)$ be a fixed but unknown sequence which is different for each float. In Section 2, however, it was pointed out that the initial phase of the resonant oscillation depends upon the direction in which the tape recorder is writing. In fact, $r(n)$ is thought to change, but change very little over reasonably long intervals which do not include changes in tape recorder direction. $r(n)$ is characterized as follows:

- the resonant oscillation $r(n)$ results from impulses generated by the tape recorder when it starts and stops between records;
- the magnitude and direction of the impulses generated by the tape recorder depends upon the direction in which the tape recorder is writing, and also depends upon the relative amount of tape which is on each reel of the recorder;
- the magnitude and initial phase of the resonant oscillation depend upon tape travel direction and may vary during the interval between tape recorder direction changes.

Thus $r(n)$ is expected to change considerably when the tape recorder changes direction, and to change slowly as the tape moves from one reel to the other. The implication of this redefinition is that M record averages which are meant to approximate $r(n)$ cannot span tape recorder direction changes or be so long that $r(n)$ changes appreciably over the average.

Tape recorder direction changes have been shown to occur at records 968 and 1456 in float 9 and at records 977 and 1467 in float 10.⁵ We can assume that tape recorder direction changes occur in floats 3 and 5 at roughly the same points and avoid averaging over those records. Once we have determined the value of M which satisfies equation (3.5b) for each float, we can ensure that $r(n)$ does not change appreciably over the M record average by comparing adjacent M record averages.

We now proceed to process 1986 deployment data from floats 3, 5, 9, and 10 and start by finding the values of M which result in the mean square value of the M record averages being much greater than $1/M$ times the mean square values of the noise. This is the condition expressed in equation (3.5b).

One must establish how large the left hand side of (3.5b) is to be in order that the condition be deemed satisfied. We started with the condition (3.5) which required only that $|r(n)|$ be much larger than $|\bar{s}(n)|$. It is now stipulated that $|r(n)|$ must be at least a factor of 5 larger than $|\bar{s}(n)|$.

$$\frac{|r(n)|}{|\bar{s}(n)|} \geq 5 \quad (4.1)$$

Since equation (3.5b) is the mean square of (3.5), equation (4.1) requires that $\hat{\gamma}_r^2$ be at least a factor of 25 larger than $\hat{\gamma}_s^2$.

$$\frac{\hat{\gamma}_r^2}{\hat{\gamma}_f^2} \geq 25 \quad (4.2)$$

The problem is now to find the value of M for each float which satisfies equation (4.2). Tables 4.1 through 4.4 contain the results of evaluating equation (4.2) for various values of M for floats 3, 5, 9, and 10. The right-most column in each Table is the value of the left hand side of equation (4.2).

According to Table 4.1, setting M equal to 60 satisfies (4.2) for all three axes of float 3. Table 4.2 shows that using $M = 400$ satisfies (4.2) in the x direction only for records 1001-1400 of float 5. We cannot use a larger value of M without running the risk of including records which contain tape recorder direction changes. Thus we cannot average enough float 5 records to satisfy equation (4.2). Tables 4.3 and 4.4 show that a value of $M = 40$ satisfies (4.2) for all axes from floats 9 and 10.

From Tables 4.1, 4.3 and 4.4 we know how many records must be averaged together to get a good estimate of $r(n)$ for floats 3, 9, and 10. However, before going on to process float 3, 9, and 10 data, we must also ensure that $r(n)$ does not change significantly over the 40 or 60 record intervals which do not include tape recorder direction changes. To do this we determine the similarity of consecutive M record averages as indicated by their covariance. The covariance of the two sequences normalized by the product of their variances produces their correlation coefficient ρ .⁶ The correlation coefficient of two M record averages, $\hat{r}_j(n)$ and $\hat{r}_k(n)$, is

$$\rho_{jk} = \frac{C_{\hat{r}_j \hat{r}_k}(0)}{\sqrt{C_{\hat{r}_j \hat{r}_j}(0) \cdot C_{\hat{r}_k \hat{r}_k}(0)}} \quad (4.3)$$

where:

$$C_{\hat{r}_j \hat{r}_k}(0) = \lim_{L \rightarrow \infty} \frac{1}{L} \sum_{n=1}^L \left[\hat{r}_j(n) - \mu_{r_j} \right] \left[\hat{r}_k(n) - \mu_{r_k} \right] \quad (4.4)$$

$$C_{\hat{r}_j \hat{r}_j}(0) = \lim_{L \rightarrow \infty} \frac{1}{L} \sum_{n=1}^L \left[\hat{r}_j(n) - \mu_{r_j} \right] \left[\hat{r}_j(n) - \mu_{r_j} \right], \quad (4.5)$$

$$C_{\hat{r}_k \hat{r}_k}(0) = \lim_{L \rightarrow \infty} \frac{1}{L} \sum_{n=1}^L \left[\hat{r}_k(n) - \mu_{r_k} \right] \left[\hat{r}_k(n) - \mu_{r_k} \right], \quad (4.6)$$

$$\mu_{r_j} = \lim_{L \rightarrow \infty} \frac{1}{L} \sum_{n=1}^L \hat{r}_j(n) \quad \text{and} \quad (4.7)$$

$$\mu_{r_k} = \lim_{L \rightarrow \infty} \frac{1}{L} \sum_{n=1}^L \hat{r}_k(n). \quad (4.8)$$

When $L = 2250$ is used in equations (4.1) through (4.6), the estimates $\hat{\rho}_{jk}$, $\hat{C}_{\hat{r}_j \hat{r}_k}(0)$, $\hat{C}_{\hat{r}_j \hat{r}_j}(0)$, $\hat{C}_{\hat{r}_k \hat{r}_k}(0)$, $\hat{\mu}_{r_j}$, and $\hat{\mu}_{r_k}$ are obtained.

The correlation coefficient $\hat{\rho}_{jk}$ is normalized to take on values between -1.0 and 1.0. A value of $\hat{\rho}_{jk}$ close to 1.0 indicates that the two sequences are very similar. A value close to 0 indicates that they are unrelated, and a value close to -1.0 indicates that they are inversely related.

Figure 4.1 shows the correlation coefficients for a series of adjacent 60 record averages from float 3. The correlation coefficients are very close to 1 everywhere except in the vicinity of the tape recorder direction change, which apparently occurs somewhere between record 1360 and 1420. Figure 4.1 indicates that $r(n)$ changes little over 60 record intervals which do not include a change in tape recorder direction.

Figures 4.2 and 4.3 show the correlation coefficients for series of adjacent 40 record averages from floats 9 and 10, respectively. Again the correlation coefficients remain very close to 1 everywhere except in the vicinity of the tape recorder changes which apparently occur between records 1400 and 1440 in float 9 and records 1440 and 1480 in float 10. Figures 4.2 and 4.3 indicate that $r(n)$ in floats 9 and 10 changes little over 40 record intervals which do not include a change in tape recorder direction.

We now have full confidence in using a 60 record average as the estimate of $r(n)$ in float 3 and 40 record averages as estimates of $r(n)$ in floats 9 and 10. Before moving on to estimating a_j and processing the data, it is interesting to compare estimates of the mean square noise, or noise power, from the four floats during the same intervals, summarized in Table 4.5.

There is general agreement among measurements made by the floats, although there are some differences. The floats were separated by 1900 to 3000 meters during the two intervals and their local sound fields may not be the same. Also, there is probably variation among the sensor frequency responses. X and y direction power estimates should generally agree, as they do in floats 3, 5, and 9 during records 1201-1240 and float 5 during records 1601-1640, since all four floats were not oriented in the same direction when these measurements were made. When they do not agree, as in float 10 during records 1201-1240 and floats 3, 9, and 10 during record 1601-1640, the y direction levels are higher, perhaps due to the influence of the resonant oscillation signal.

Table 4.5 - Noise Power Estimates

Float	Axis		
	x	y	z
<u>records 1201-1240</u>			
float 3	0.040	0.058	0.0053
float 5	0.026	0.023	0.0052
float 9	0.033	0.031	0.0083
float 10	0.052	0.182	0.0009
<u>records 1601-1640</u>			
float 3	0.043	0.085	0.0072
float 5	0.041	0.034	0.0069
float 9	0.038	0.115	0.0139
float 10	0.061	0.232	0.0373

It is also interesting to compare estimates of the resonant oscillation power from the four floats, which are given in Table 4.6. Resonant oscillation is stronger in the y direction than in the x direction in floats 3, 9 and 10. Float 10's resonant oscillation is stronger than that of the other floats, and floats 3 and 9

have comparable power in their resonant oscillation.

Table 4.6 - Resonant Oscillation Power Estimates

Float	Axis		
	x	y	z
<u>records 1201-1240</u>			
float 3	0.0223	0.0606	0.0044
float 5	0.0036	0.0022	0.0004
float 9	0.0255	0.0444	0.0084
float 10	0.0567	0.1775	0.0251
<u>records 1601-1640</u>			
float 3	0.0260	0.0622	0.0033
float 5	0.0036	0.0027	0.0004
float 9	0.0273	0.0948	0.0100
float 10	0.0563	0.1985	0.0291

Estimating a

Now we can calculate values for \hat{a} , using equation (3.23). Values of a , for records 1201-1240 and 1601-1640 from floats 3, 9, and 10 are plotted in Figures 4.4 through 4.6. The mean and standard deviation of the a , values are given in Table 4.7. The mean value of a , is very close to 1.0 for all three floats and the standard deviation never exceeds 0.1. Thus it appears we are justified in our assumption (3.2).

Table 4.7 - Statistics of the scaler multiplier a

		records 1201-1240		records 1601-1640	
float	axis	$\hat{\mu}_a$	$\hat{\sigma}_a$	$\hat{\mu}_a$	$\hat{\sigma}_a$
3	x	0.9974	0.050	0.9880	0.090
	y	0.9978	0.036	0.9930	0.062
	z	0.9994	0.099	0.9970	0.050
9	x	1.0000	0.037	1.0000	0.029
	y	1.0000	0.047	1.0000	0.028
	z	1.0000	0.063	1.0000	0.034
10	x	1.0000	0.066	1.0000	0.057
	y	1.0000	0.025	1.0000	0.023
	z	1.0000	0.051	1.0000	0.020

Processing Results

Data from floats 3, 9, and 10 have been processed using $M=40$ or 60 and equation (3.24). Results are contained in Figures 4.7 through 4.12.

Figures 4.7a through 4.7h pertain to float 3. Figure 4.7a shows the x, y, and z axis geophone time series from record 1207 before any processing. These same time series were shown as the 8th traces from the top in Figures 2.1a, 2.1b, and 2.1c. The time series consist of signal due to resonant float oscillation, which is clearly visible in the first 3 to 10 seconds of the record, and signal due to ambient ocean noise.

Figure 4.7b contains the power spectrum of the time series shown in Figure 4.7a. The first 5 seconds of the record were not used in the spectral estimate because data are clipped. A 512 point (20.48 second) Fourier transform was used, and consecutive segments which were 50% overlapped. Segments were windowed using a Kaiser-Bessel window with $\alpha = 2.5$. The seven spectral estimates thus obtained from each axis of the record were incoherently averaged to produce one spectrum per axis. The acoustic pressure spectral estimate shown in the top panel was obtained by power summing spectra from each axis. It has been shown previously that acoustic pressure spectra may be derived from the power sum of directional velocity spectra.¹ Peaks in the geophone and acoustic pressure power spectra may correspond to signals present in either the resonant oscillation or the ambient ocean noise.

Figure 4.7c shows the time series from a 60 record average beginning with record 1201. This is our estimate of the resonant oscillation, $\bar{r}(n)$. The first 3 to 10 seconds of $\bar{r}(n)$ closely resemble record 1207, indicating that the first part of record 1207 is strongly affected by the resonant oscillation. Figure 4.7c shows that the resonant oscillation signal continues to be present throughout the record, although its level is low in the latter part.

Figure 4.7d shows the power spectra of the time series shown in Figure 4.7c. The levels of spectral peaks are summarized in Table 4.8. Only the peaks at 2 Hz and multiples of 2 Hz appear harmonically related. The 8 Hz peaks in the x and y direction are 2 Hz harmonics but they are dominated by another signal, as evidenced by their higher levels.

Figure 4.7e compares the power spectra of record 1207 with that of $\bar{r}(n)$. The background level of $\bar{r}(n)$'s spectra is about 18 dB below that of record 1207. This difference makes sense in light of equation (3.13), which says that the power in $\bar{s}(n)$ is $1/M$ times that in $s(n)$, and

$$10 \log \frac{1}{60} = -18\text{dB} \quad (4.9)$$

Peaks at 2.3 Hz in the x direction, 1.67 Hz, 2.3 Hz, 4 Hz, 4.5 Hz, and 6 Hz in the y direction, and 4 Hz, 4.5 Hz, and 6 Hz in the z direction have the same spectral level in $\bar{r}(n)$ and record 1207. Spectral levels below 0.5 Hz in the y and z directions are also the same in $\bar{r}(n)$ and record 1207. Signals at these frequencies were not attenuated by the averaging, are therefore coherent from record to record, and are likewise attributed to the float's resonant oscillation.

Also in Figure 4.7e, 8 Hz peaks in the x and y directions are about 18 dB lower in $\bar{r}(n)$ than in record 1207. The 18 dB attenuation indicates that the 8 Hz signals, like the background noise, are incoherent from record to record. This further indicates that the 8 Hz peaks are primarily due to ambient ocean noise, at least in the x and y directions. Peaks at about 9 Hz are also attenuated by about 20 dB in the x and y directions and 12 dB in the z direction, indicating that they too originate in the ambient ocean noise field.

Table 4.8 - Spectral Levels, Float 3, Average of Records 1201-1260

Frequency	Axis		
	x	y	z
0.97	-	93	96
1.5	92	-	-
1.67	94	104	85
2.0	91	84	88
2.3	100	96	86
4	79	72	76
4.5	64	99	81
6	73	68	68
8	75	76	66
10	66	60	65
12	66	62	64
14	66	61	63
16	64	61	61
18	64	61	58
20	63	60	62
22	61	63	58
24	61	62	58

Of further note in Figure 4.7e is that many of the 2 Hz harmonics peaks are between 4 and 10 dB lower in $\hat{r}(n)$ than in record 1207. This indicates that their frequency or initial phase varies a small amount from record to record. One plausible explanation would be that the 2 Hz fundamental frequency changes very slightly from record to record. This frequency jitter could cause the 2 Hz signal to remain essentially coherent, but the harmonics might change frequency over a larger range proportional to the ratio of their frequency to that of the fundamental. A 0.01 Hz change in the 2 Hz signal, for example, would result in a 0.1 Hz change in the 20 Hz signal. Note that in Figure 4.7e the 2 Hz signal is largely coherent from record to record, the 12 Hz is less so (attenuated about 6 dB in the x and y axes, no attenuation in the z axis), and the 20 Hz signal is largely incoherent from record to record (attenuated about 9 dB in the x axis, 18 dB in the y axis, and 8 dB in the z axis).

Figures 4.7f and 4.7g show record 1207 after processing using equation (3.24), and Figure 4.7h compares the spectra of record 1207 before and after processing. Processing reduces or removes spectral peaks attributed to resonant oscillation at 2.3 Hz, 4 Hz, and 6 Hz in the x direction, 1.67 Hz, 2.3 Hz, 4 Hz, 4.5 Hz, and 6 Hz in the y direction, and 4 Hz, 4.5 Hz, and 6 Hz in the z direction. Processing also lowers spectral levels below 1 Hz in the x and y directions.

Processing does not affect the level of spectral peaks which are attributed to the ambient noise field, such as those at 8 and 9 Hz. However, several peaks at harmonics of 2 Hz, which are attributed to the resonant oscillation, are also unaffected by processing, possibly because of the aforementioned fundamental frequency jitter.

Figures 4.8a through 4.8h contain similar results for record 1607 from float 3. The spectral comparison plots, 4.8e and 4.8h, show that processing reduces the level of spectral peaks attributed to resonant oscillation at 2.3 Hz, 4 Hz, 6 Hz, 8 Hz, 10 Hz, 12 Hz, 14 Hz, 16 Hz, and 22 Hz in the x direction; 1.67 Hz,

2.3 Hz, 4 Hz, and 4.5 Hz in the y direction; and 2.3 Hz, 4 Hz, 4.5 Hz, 6 Hz, 10 Hz, 12 Hz, 16 Hz, 18, 20 Hz, and 22 Hz in the z direction. Processing also reduces spectral levels below 1 Hz in the x and y directions. Not all of the 2 Hz harmonics attributed to resonant oscillation are reduced, as in record 1207. Signals present in the ambient noise field are not affected by the processing.

Figures 4.9 and 4.10 contain similar plots for records 1207 and 1607 from float 9, and Figures 4.11 and 4.12 contain results of processing the same records in float 10. In all cases, processing individual records using a 40 record average and an estimate for a_j removes or substantially reduces the major spectral lines attributed to resonant oscillation.

In records 1207 and 1607 of float 10, processing attenuates resonant oscillation signals at 1.5 Hz in the y axis and 4.1 Hz in all three axes by about 16 dB. However, the signals have more than 20 dB signal to noise ratio (SNR) before processing and are still visible in the processed records.

Acknowledgements

This work was supported by the Office of Naval Research, Code 112, under contract N00014-87-K-0225. Fabrication of the floats was carried out by M. Darling. Other contributors to this project include F. N. Spiess and J. C. Nickles.

Table 4.1 - Float 3, 1986 deployment

M	records	axis	$\hat{\gamma}_s^2$	$\frac{\hat{\gamma}_s^2}{M}$	$\hat{\gamma}_x^2$	$\hat{\gamma}_y^2$	$\frac{\hat{\gamma}_r^2}{\frac{\hat{\gamma}_s^2}{M}}$
20	1201-1220	x	.0427	.002135	.0239	.021765	10.19
		y	.0613	.003065	.0611	.058035	18.93
		z	.00796	.000398	.00453	.004132	10.38
20	1221-1240	x	.0382	.001910	.0237	.021790	11.40
		y	.0583	.002915	.0599	.056985	19.54
		z	.00588	.000294	.00475	.004456	15.15
20	1601-1620	x	.0451	.002255	.0281	.025845	11.46
		y	.0863	.004315	.0651	.060785	14.08
		z	.00731	.000365	.00336	.002995	8.20
20	1621-1640	x	.0407	.002035	.0250	.022965	11.28
		y	.0835	.004175	.0605	.056325	13.49
		z	.00703	.000351	.00335	.002999	8.54
40	1201-1240	x	.0402	.001005	.0233	.022295	22.18
		y	.0580	.001450	.0602	.058750	40.51
		z	.00528	.000132	.00445	.004318	32.71
40	1601-1640	x	.0429	.001072	.0260	.024928	23.25
		y	.0847	.002117	.0622	.060083	28.38
		z	.00715	.000178	.00327	.003092	17.37
60	1201-1260	x	.0409	.000681	.0234	.022719	33.36
		y	.0580	.000966	.0604	.059434	61.52
		z	.00516	.000086	.00444	.004354	50.62
60	1601-1660	x	.0437	.000728	.0266	.025872	35.53
		y	.0852	.001420	.0631	.061680	43.43
		z	.00720	.000120	.00328	.003160	26.33

Table 4.2 - Float 5, 1986 deployment

M	records	axis	$\hat{\gamma}_s^2$	$\frac{\hat{\gamma}_s^2}{M}$	$\hat{\gamma}_x^2$	$\hat{\gamma}_y^2$	$\frac{\hat{\gamma}_r^2}{\frac{\hat{\gamma}_s^2}{M}}$
40	1001-1040	x	.024137	.000603	.005064	.004461	7.39
		y	.026275	.000656	.0037718	.0031158	4.74
		z	.0040842	.000102	.00035344	.00025144	2.46
40	1201-1240	x	.026102	.000652	.0036248	.0029728	4.55
		y	.023268	.000581	.0022631	.0016821	2.89
		z	.0051705	.000129	.0003433	.0002143	1.66
40	1501-1540	x	.194700	.004867	.010289	.005422	1.11
		y	.072920	.001823	.0048317	.0030087	1.65
		z	.059752	.001493	.0017479	.0002549	.17
40	1701-1740	x	.036070	.000901	.0031857	.0022847	2.53
		y	.028199	.000704	.0022439	.0015399	2.18
		z	.0065993	.000164	.00033059	.00016659	1.01
80	1001-1080	x	.025068	.000313	.0044149	.0041019	13.10
		y	.028085	.000351	.0032843	.0029333	8.35
		z	.0042591	.000053	.00030403	.00025103	4.73
80	1201-1280	x	.035478	.000443	.0036023	.0031593	7.13
		y	.030123	.000376	.0020839	.0017079	4.54
		z	.010001	.000125	.00032428	.00019928	1.59
80	1501-1580	x	.181310	.002266	.0062007	.0039347	1.73
		y	.085152	.001064	.0040127	.0029487	2.77
		z	.052335	.000654	.03044	.029786	45.54
80	1701-1780	x	.036614	.000457	.0027925	.0023355	5.11
		y	.026466	.000330	.0019895	.0016595	5.02
		z	.0060379	.000075	.00026261	.00018761	2.50
200	1001-1200	x	.030885	.000154	.0040074	.0038534	25.02
		y	.032732	.000163	.0026009	.0024379	14.95
		z	.001521	.000007	.00028529	.00027829	39.75
200	1201-1400	x	.043546	.000217	.0039816	.0037646	17.34
		y	.086227	.000431	.0022422	.0018112	4.20
		z	.021514	.000107	.00035352	.00024652	2.30
200	1501-1700	x	.089202	.000446	.003495	.003049	6.83
		y	.087931	.000439	.0025187	.0020797	4.73
		z	.016671	.000083	.00039813	.00031513	3.79

Table 4.2 - Float 5, 1986 deployment

M	records	axis	$\hat{\gamma}_s^2$	$\frac{\hat{\gamma}_s^2}{M}$	$\hat{\gamma}_x^2$	$\hat{\gamma}_r^2$	$\frac{\hat{\gamma}_r^2}{\frac{\hat{\gamma}_s^2}{M}}$
200	1701-1900	x	.052966	.000264	.0028392	.0025752	9.75
		y	.072233	.000361	.0020118	.0016508	4.57
		z	.021281	.000106	.00026349	.00015749	1.48
400	1001-1400	x	.037920	.000094	.005064	.004970	52.87
		y	.063715	.000159	.0037718	.0036128	22.72
		z	.012528	.000031	.00035344	.00032244	10.40
400	1501-1900	x	.067506	.000168	.0029586	.0027906	16.61
		y	.083492	.000208	.0020024	.0017944	8.62
		z	.015138	.000037	.00027517	.00023817	6.43

Table 4.3 - Float 9, 1986 deployment

M	records	axis	$\hat{\gamma}_s^2$	$\frac{\hat{\gamma}_s^2}{M}$	$\hat{\gamma}_x^2$	$\hat{\gamma}_r^2$	$\frac{\hat{\gamma}_r^2}{\frac{\hat{\gamma}_s^2}{M}}$
20	1201-1220	x	.0361	.001805	.0259	.024095	13.34
		y	.0515	.002575	.0439	.041325	16.04
		z	.0107	.000535	.00847	.007935	14.83
20	1221-1240	x	.0311	.001555	.0260	.024445	15.72
		y	.0313	.001565	.0466	.045035	28.77
		z	.00751	.000375	.00864	.008265	22.04
20	1601-1620	x	.0325	.001625	.0276	.025975	15.98
		y	.1033	.005165	.0966	.091435	17.70
		z	.0147	.000735	.0102	.009465	12.87
20	1621-1640	x	.0407	.002035	.0279	.025865	12.71
		y	.120	.006000	.0951	.089100	14.85
		z	.0128	.000640	.0100	.009360	14.62
40	1201-1240	x	.0333	.000832	.0255	.024668	29.64
		y	.0311	.000777	.0444	.043623	56.14
		z	.00825	.000206	.00836	.008154	39.58
40	1601-1640	x	.0376	.000940	.0273	.026360	28.04
		y	.1151	.002877	.0948	.091923	31.95
		z	.0139	.000347	.0100	.009653	27.81

Table 4.4 - Float 10, 1986 deployment

M	records	axis	$\hat{\gamma}_s^2$	$\frac{\hat{\gamma}_s^2}{M}$	$\hat{\gamma}_x^2$	$\hat{\gamma}_r^2$	$\frac{\hat{\gamma}_r^2}{\frac{\hat{\gamma}_s^2}{M}}$
20	1201-1220	x	.0624	.003120	.0562	.053080	17.01
		y	.190	.009500	.177	.167500	17.63
		z	.0279	.001395	.0250	.023605	16.92
20	1221-1240	x	.0479	.002395	.0584	.056005	23.38
		y	.1773	.008865	.1801	.171235	19.31
		z	-.0421	-.002105	.0262	.028305	-13.44
20	1601-1620	x	.056	.002800	.0565	.053700	19.17
		y	.2375	.011875	.2000	.188125	15.84
		z	.04089	.002044	.02924	.027196	13.30
20	1621-1640	x	.0675	.003375	.0572	.053825	15.94
		y	.2296	.011480	.1981	.186620	16.25
		z	.03597	.001798	.02937	.027572	15.33
40	1201-1240	x	.05186	.001296	.0568	.055504	42.82
		y	.1823	.004557	.1775	.172943	37.95
		z	.00093	.000023	.0251	.025077	1090.30
40	1601-1640	x	.0611	.001527	.0564	.054873	35.93
		y	.2322	.005805	.1985	.192695	33.19
		z	.03734	.000933	.02917	.028237	30.26

References

1. Culver, Richard L., "Infrasonic ambient ocean noise spectra from freely drifting sensors," SIO Reference 85-22, Marine Physical Laboratory, Scripps Institution of Oceanography, San Diego, CA, 1985.
2. Culver, R. L., W. S. Hodgkiss, V. C. Anderson, J. C. Nickles, and G. L. Edmonds, "Freely drifting Swallow float array: Initial estimates of interelement range," MPL TM-380, Marine Physical Laboratory, Scripps Institution of Oceanography, San Diego, CA, 1985.
3. Hodgkiss, W. S., V. C. Anderson, G. Edmonds, J. C. Nickles, and R. L. Culver, "A freely drifting infrasonic sensor system," *Fourth Working Symposium on Oceanographic Data Systems*, February 4-6, 1986.
4. Culver, R. L., W. S. Hodgkiss, G. L. Edmonds, and V. C. Anderson, "Freely Drifting Swallow Float Array: September 1986 Trip Report," MPL TM-391, Marine Physical Laboratory, Scripps Institution of Oceanography, San Diego, CA, 1987.
5. Culver, R. L., W. S. Hodgkiss, V. C. Anderson, and G. L. Edmonds, "Low Frequency Oscillations in 1986 Swallow Float Data," MPL TM-394, Marine Physical Laboratory, Scripps Institution of Oceanography, San Diego, CA, 1987.
6. Bendat, Julius S. and Allan G. Piersol, *Engineering Applications of Correlation and Spectral Analysis*, p. 45, John Wiley and Sons, New York, 1980.

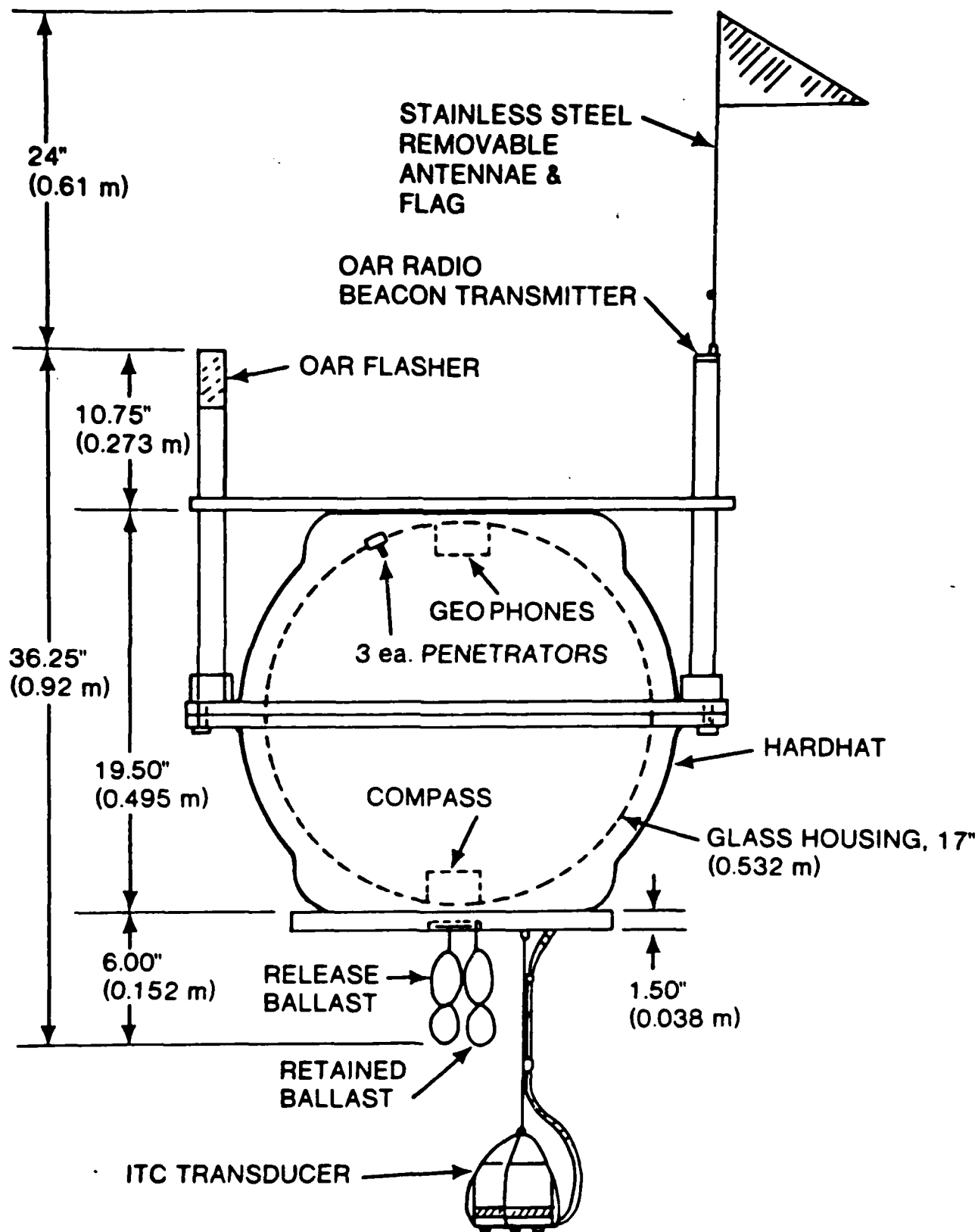
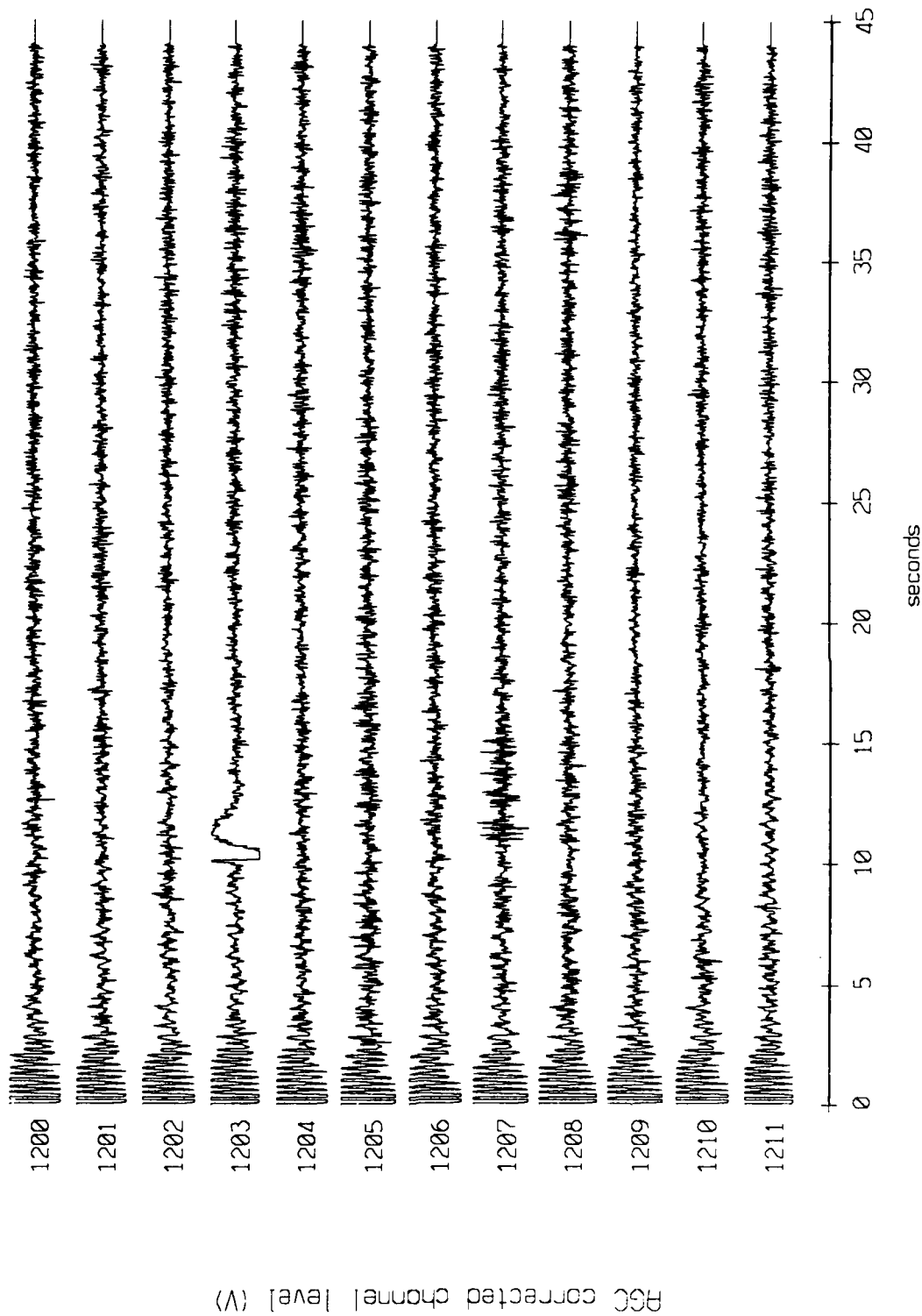


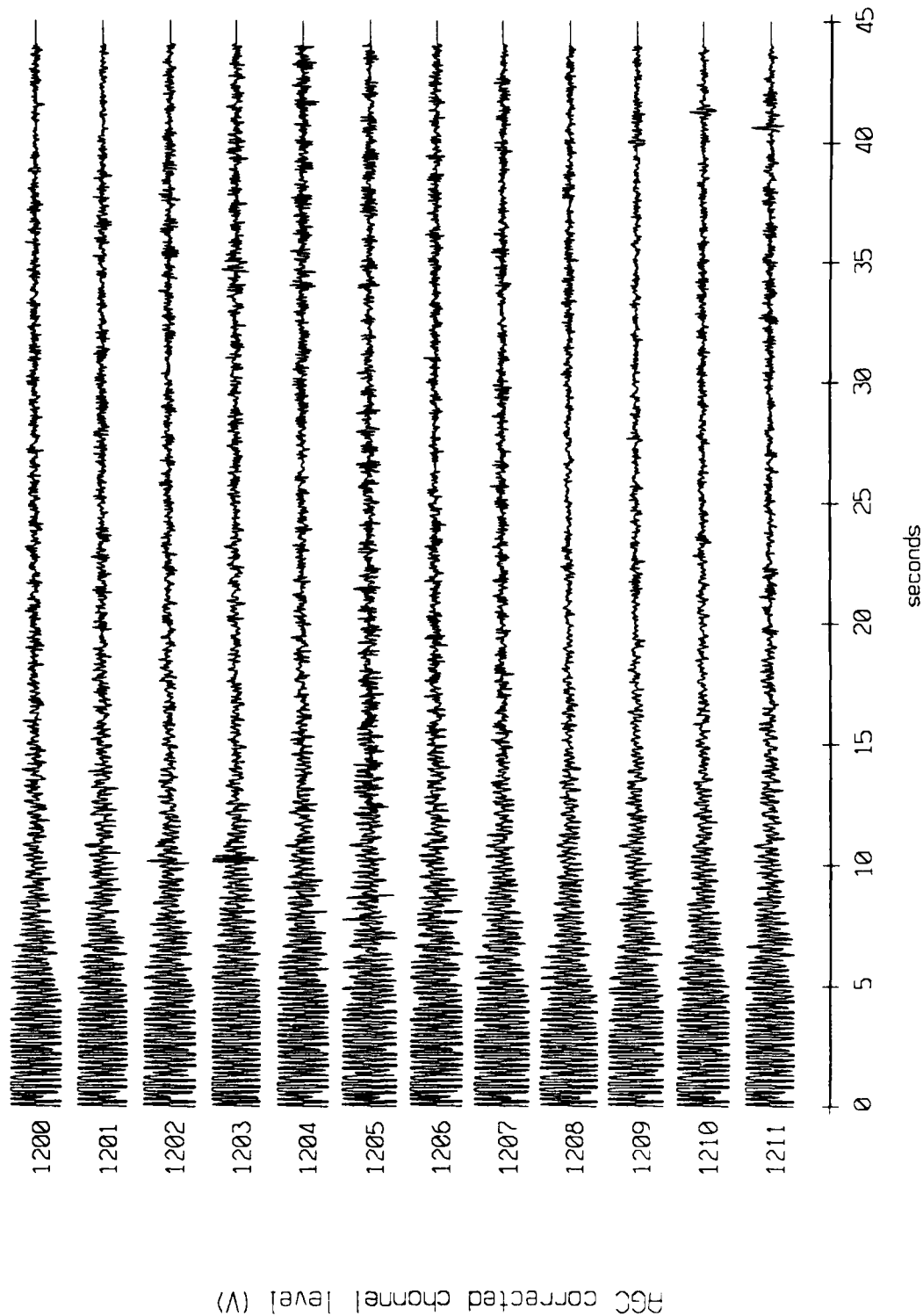
Figure 1.2

Figure 2.1a

Floot 3, 1986 Deployment - records 1200 - 1211, (x-axis)
vertical axis scale is approx. -1.0 to 1.0 volts



Floot 3, 1986 Deployment - records 1200 - 1211, (y-axis)
vertical axis scale is approx. -1.0 to 1.0 volts



AGC corrected channel level (V)

Figure 2.1b

Float 3, 1986 Deployment - records 1200 - 1211, (z-axis)
vertical axis scale is approx. -1.0 to 1.0 volts

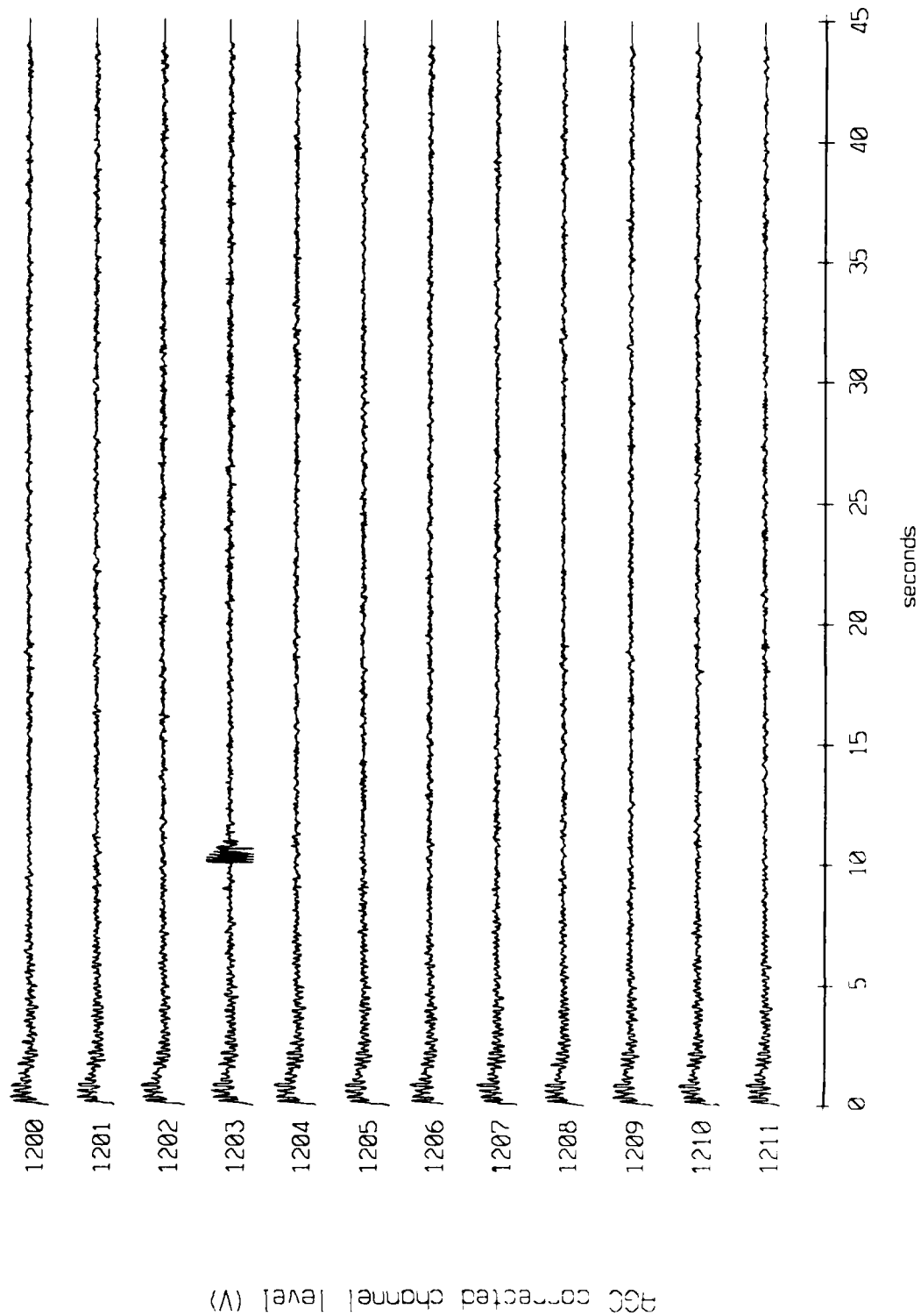


Figure 2.1c

Float 3, 1986 Deployment - records 1600 - 1611, (x-axis)
vertical axis scale is approx. -1.0 to 1.0 volts

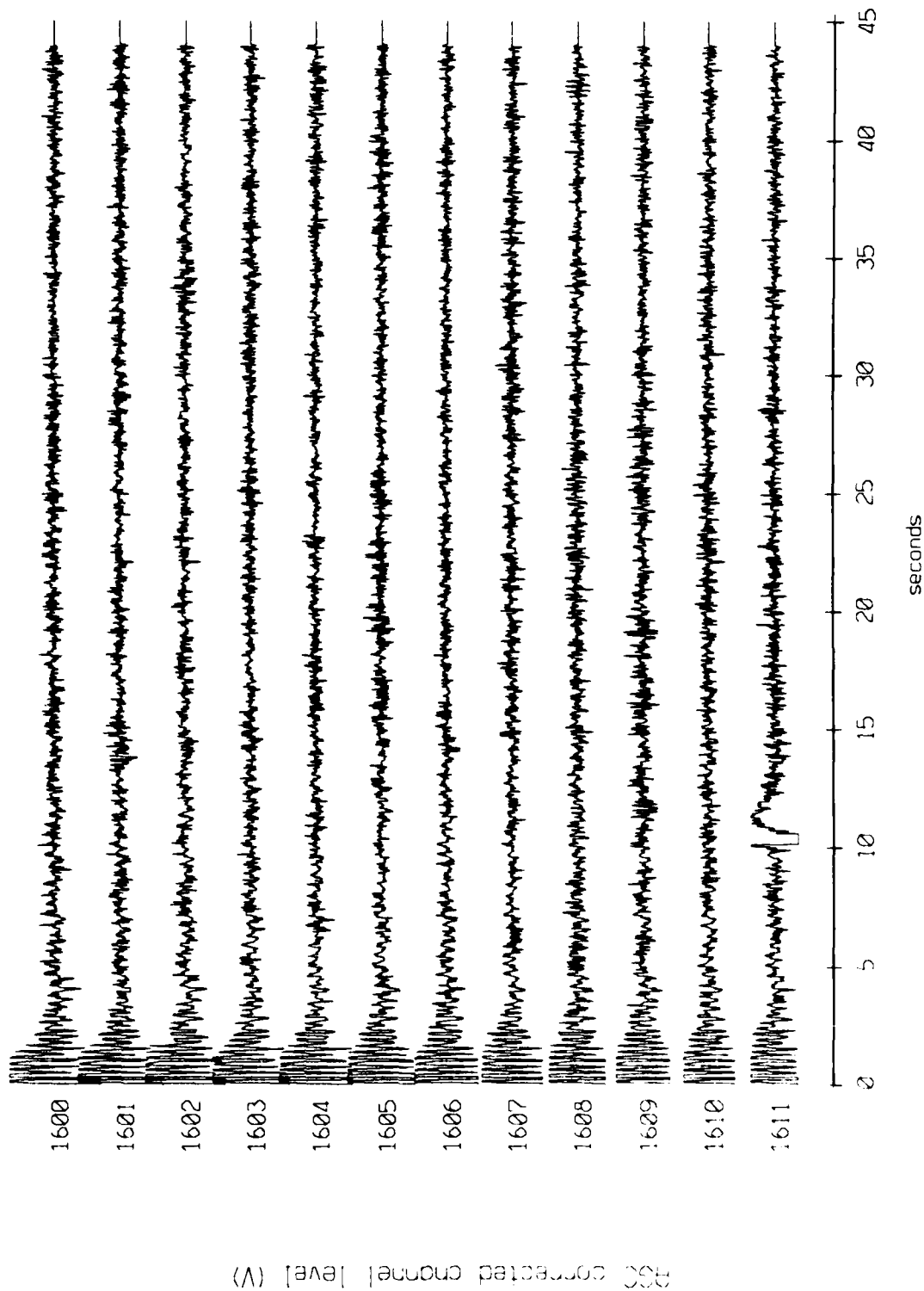
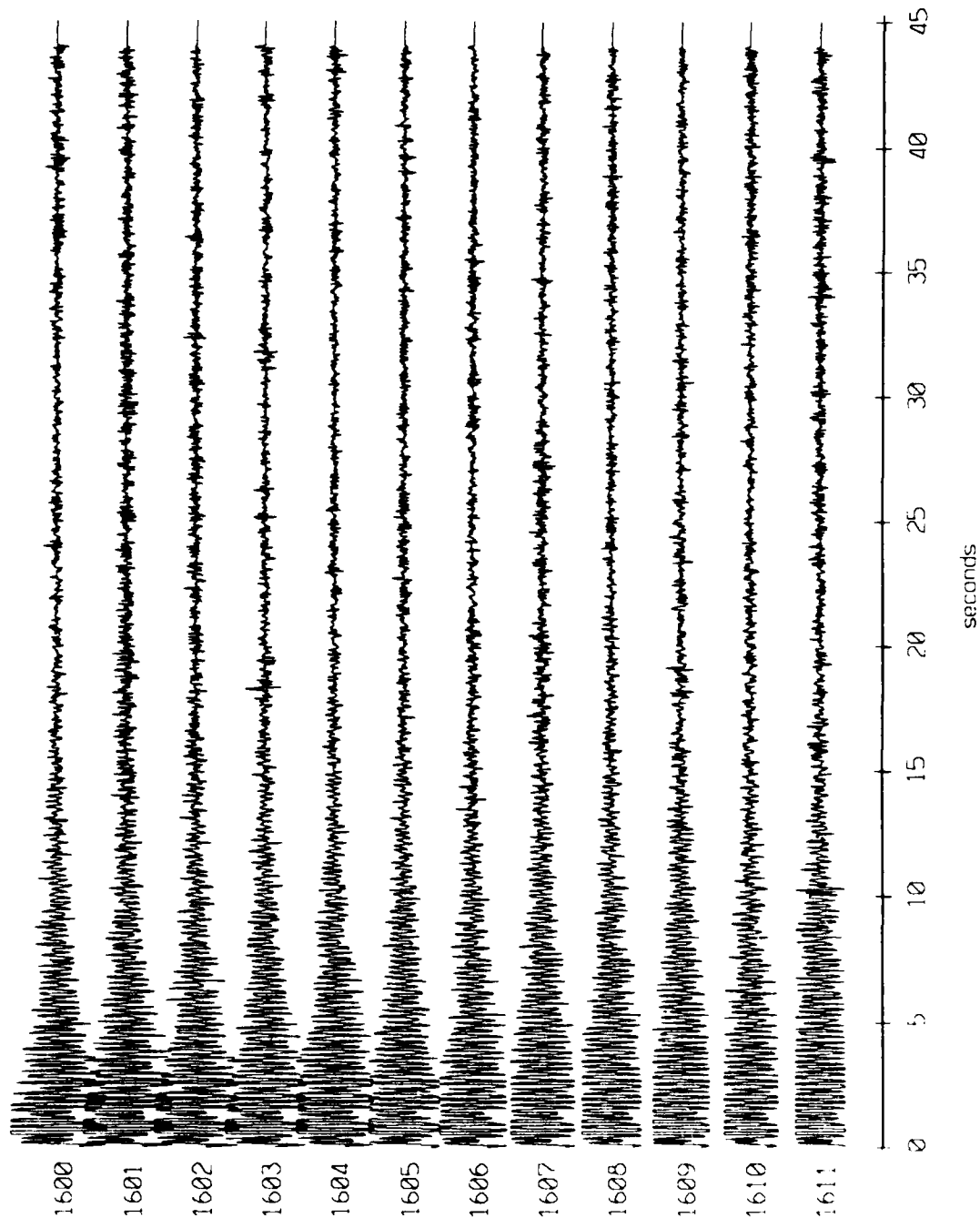


Figure 2.2a

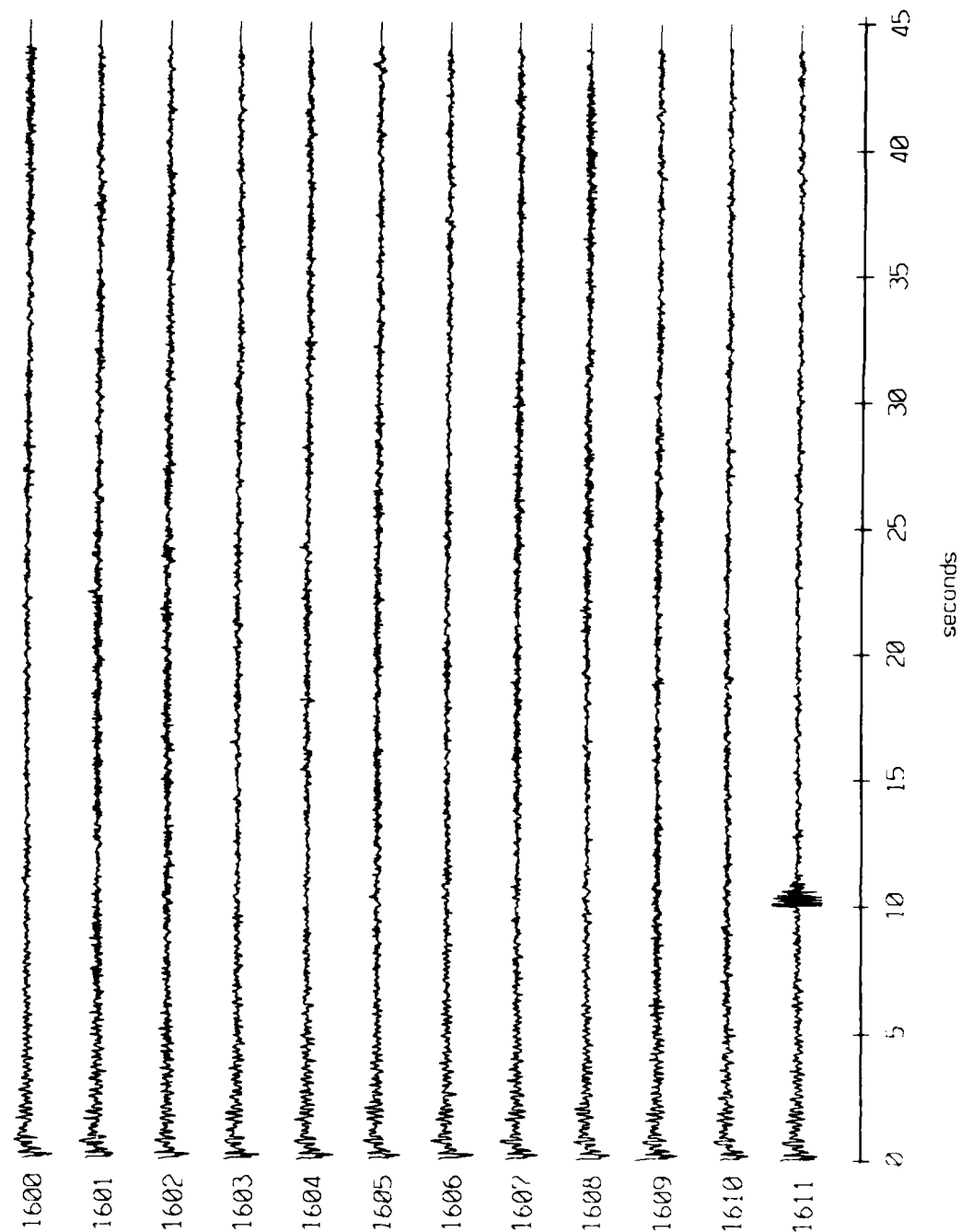
Floot 3, 1986 Deployment - records 1600 - 1611, (y-axis)
vertical axis scale is approx. -1.0 to 1.0 volts



1600 corrected channel level (V)

Figure 2.2b

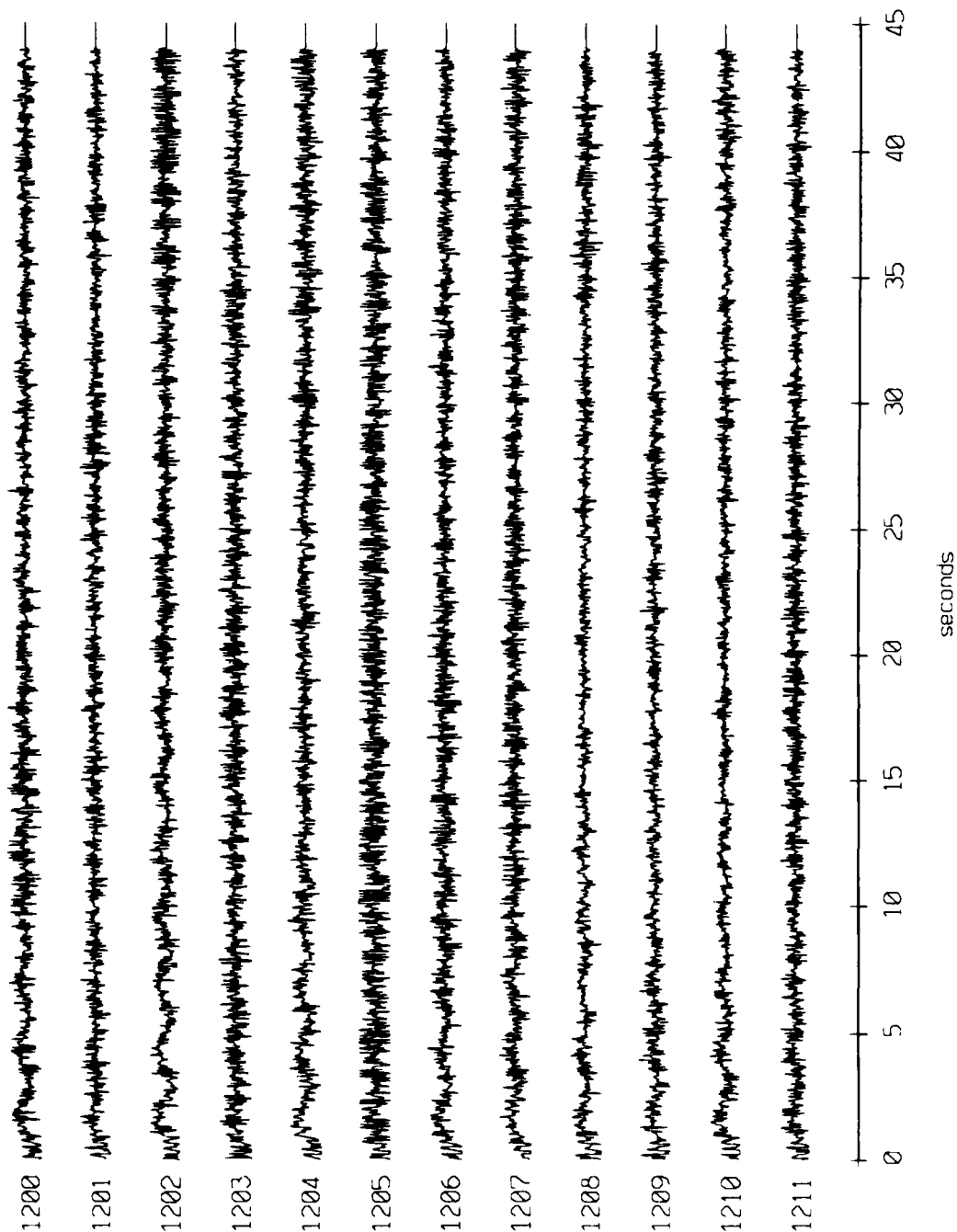
Float 3, 1986 Deployment - records 1600 - 1611, (z-axis)
vertical axis scale is approx. -1.0 to 1.0 volts



900 corrected channel level (V)

Figure 2.2c

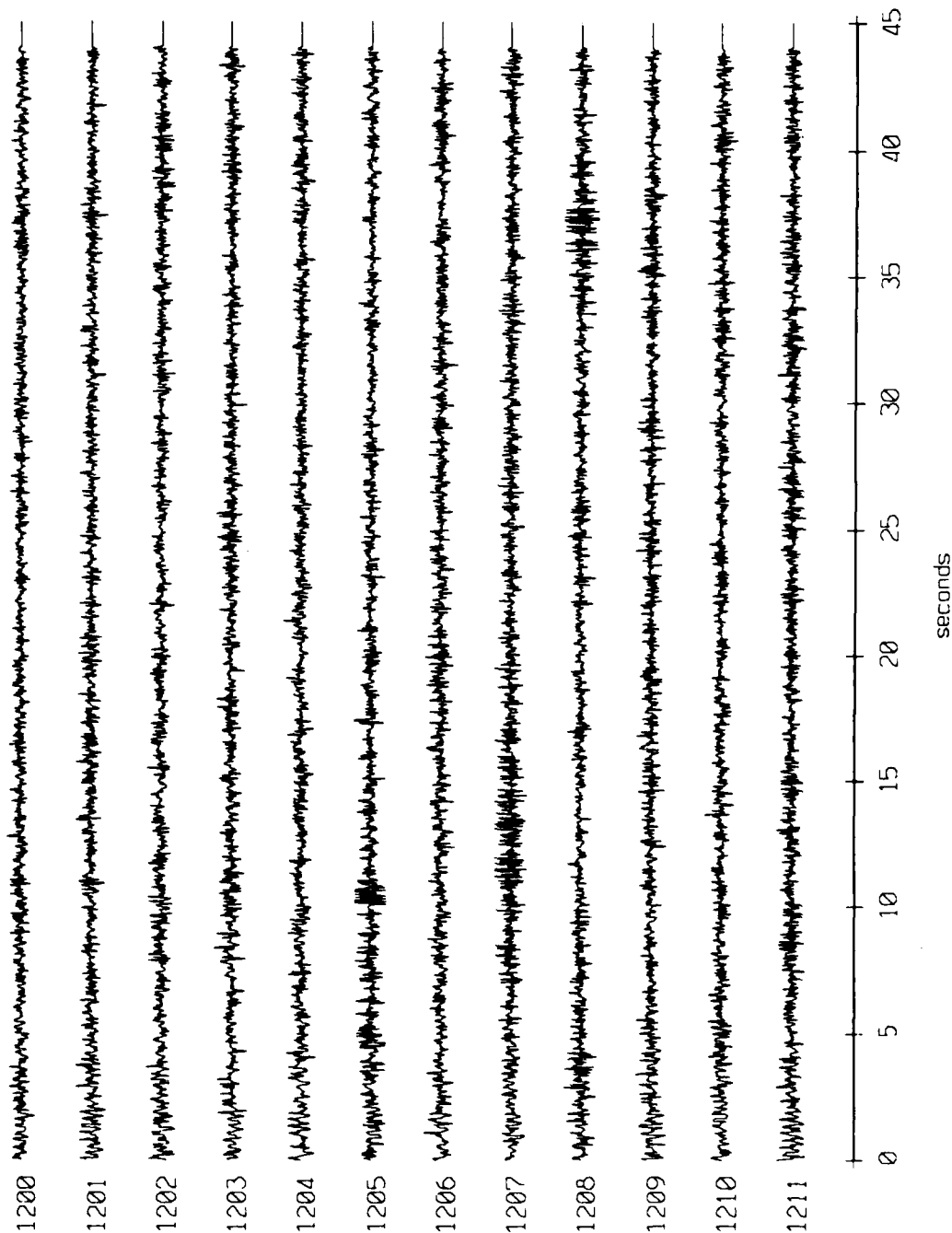
Floot 5, 1986 Deployment - records 1200 - 1211, (x-axis)
vertical axis scale is approx. -1.0 to 1.0 volts



HGC corrected channel level (V)

Figure 2.3a

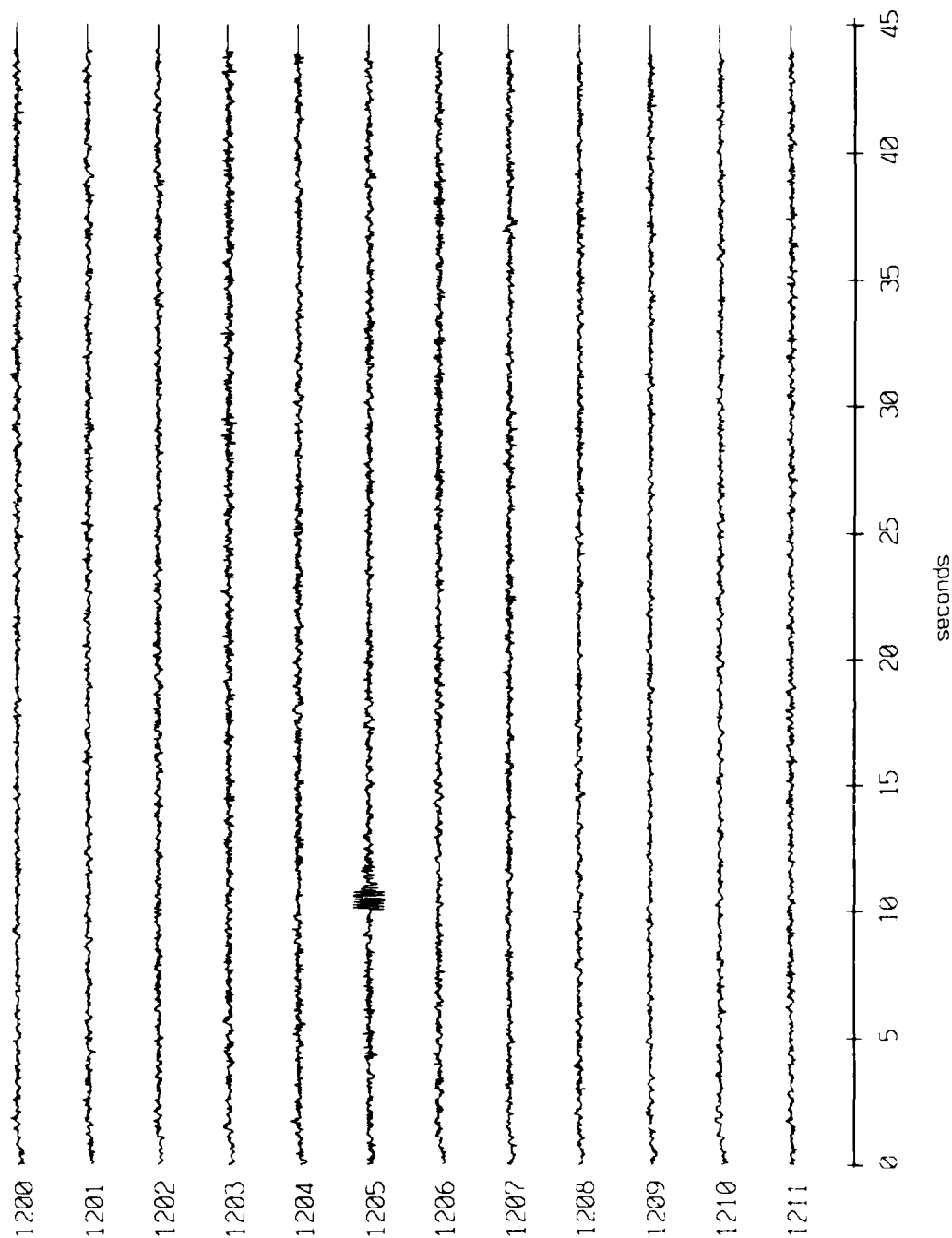
Floot 5, 1986 Deployment - records 1200 - 1211, (y-axis)
vertical axis scale is approx. -1.0 to 1.0 volts



AGC corrected channel level (V)

Figure 2.3b

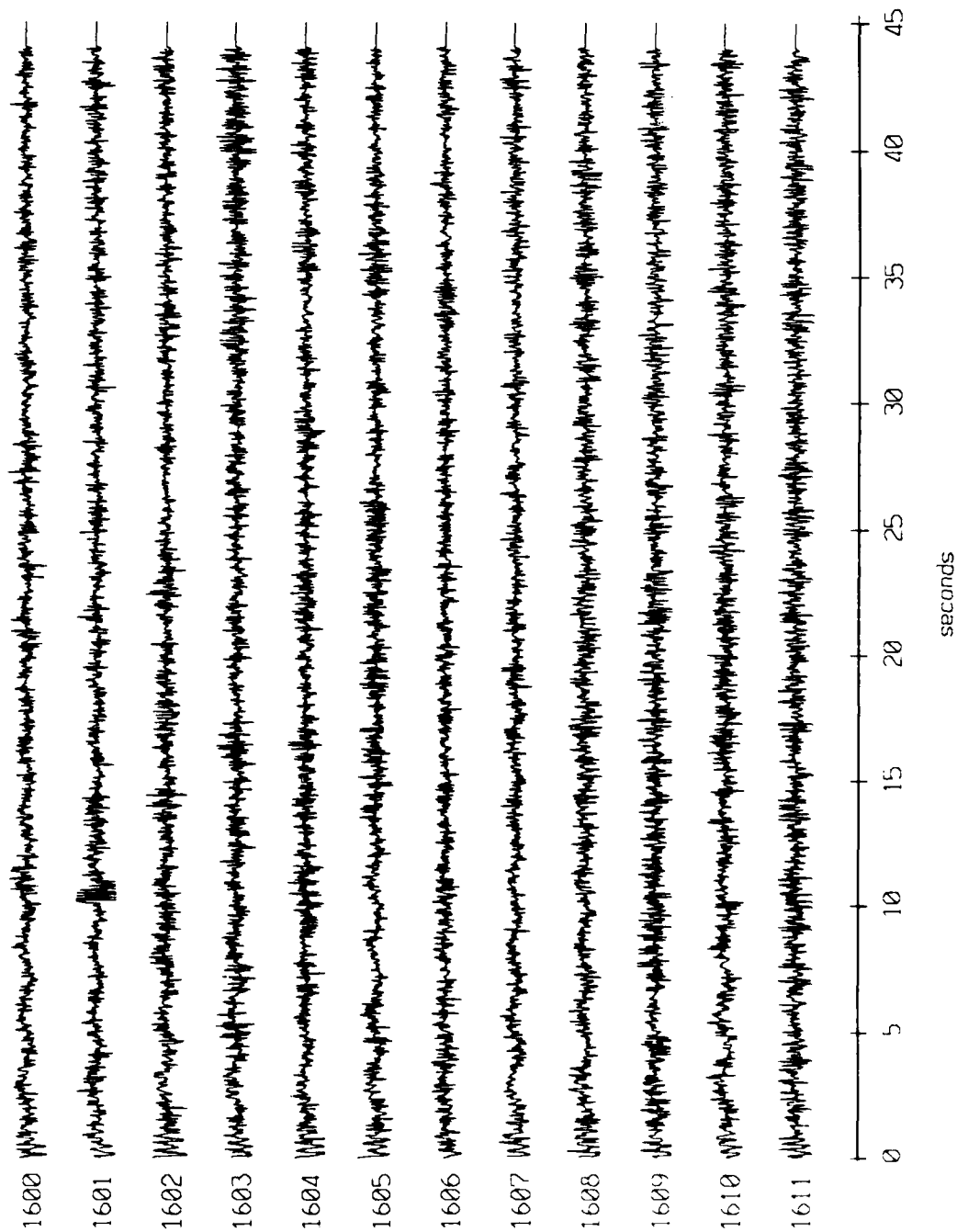
Float 5, 1986 Deployment - records 1200 - 1211, (z-axis)
vertical axis scale is approx. -1.0 to 1.0 volts



AGC corrected channel level (V)

Figure 2.3c

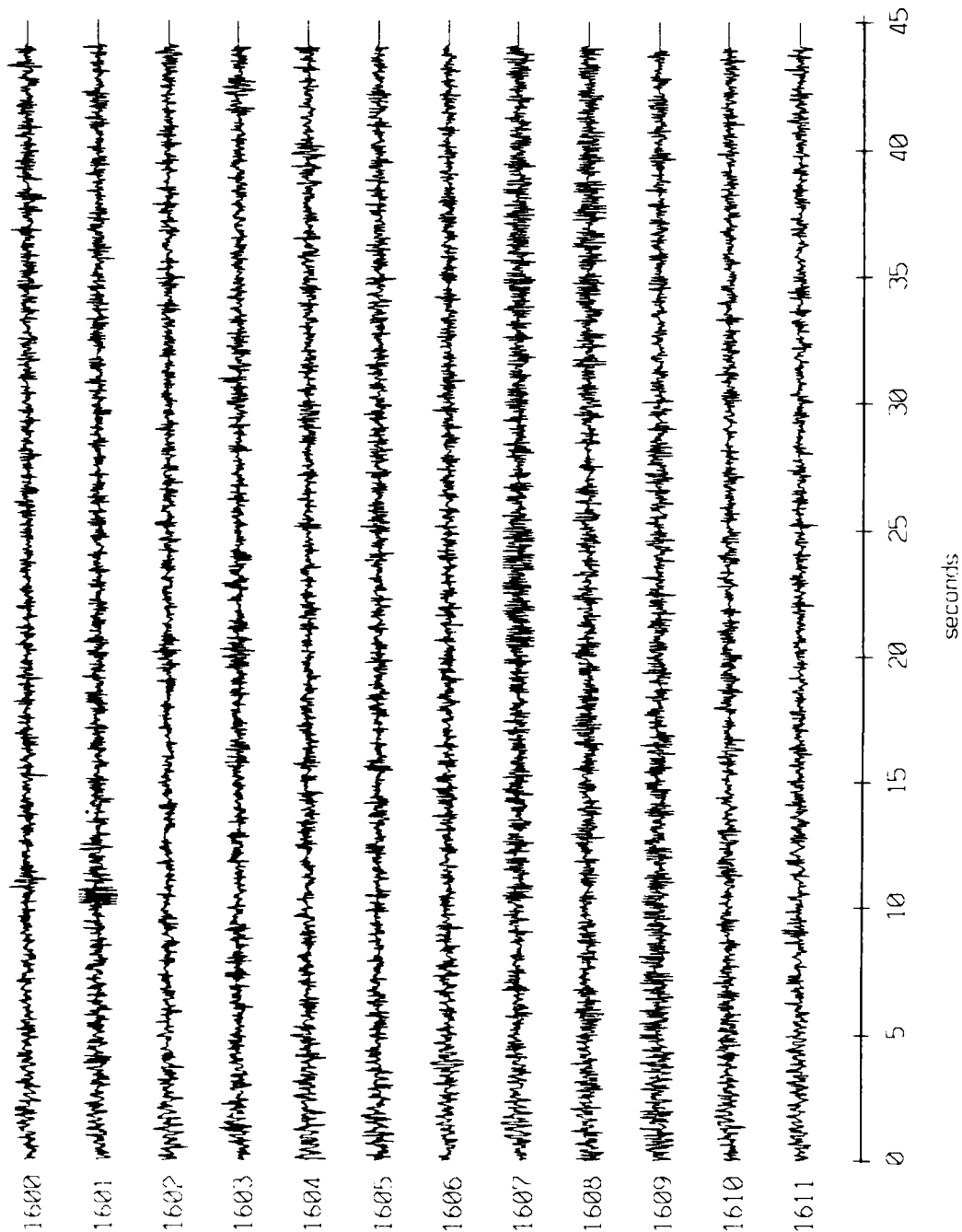
float 5, 1986 Deployment - records 1600 - 1611, (x-axis)
vertical axis scale is approx. -1.0 to 1.0 volts



300 corrected channel (v)

Figure 2.4a

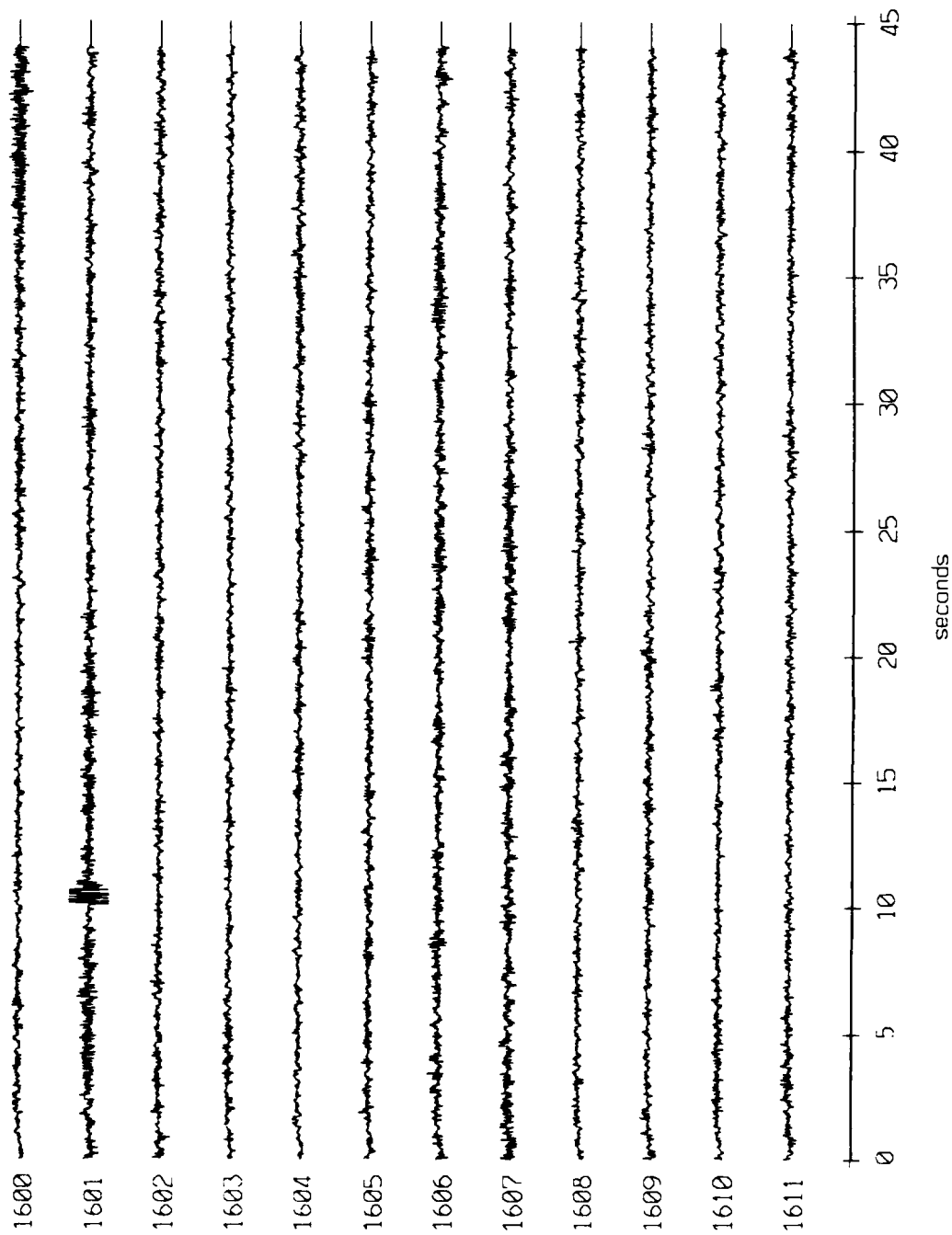
Floot 5, 1986 Deployment - records 1600 - 1611, (y-axis)
vertical axis scale is approx. -1.0 to 1.0 volts



(V) level (corrected level) (V)

Figure 2.4b

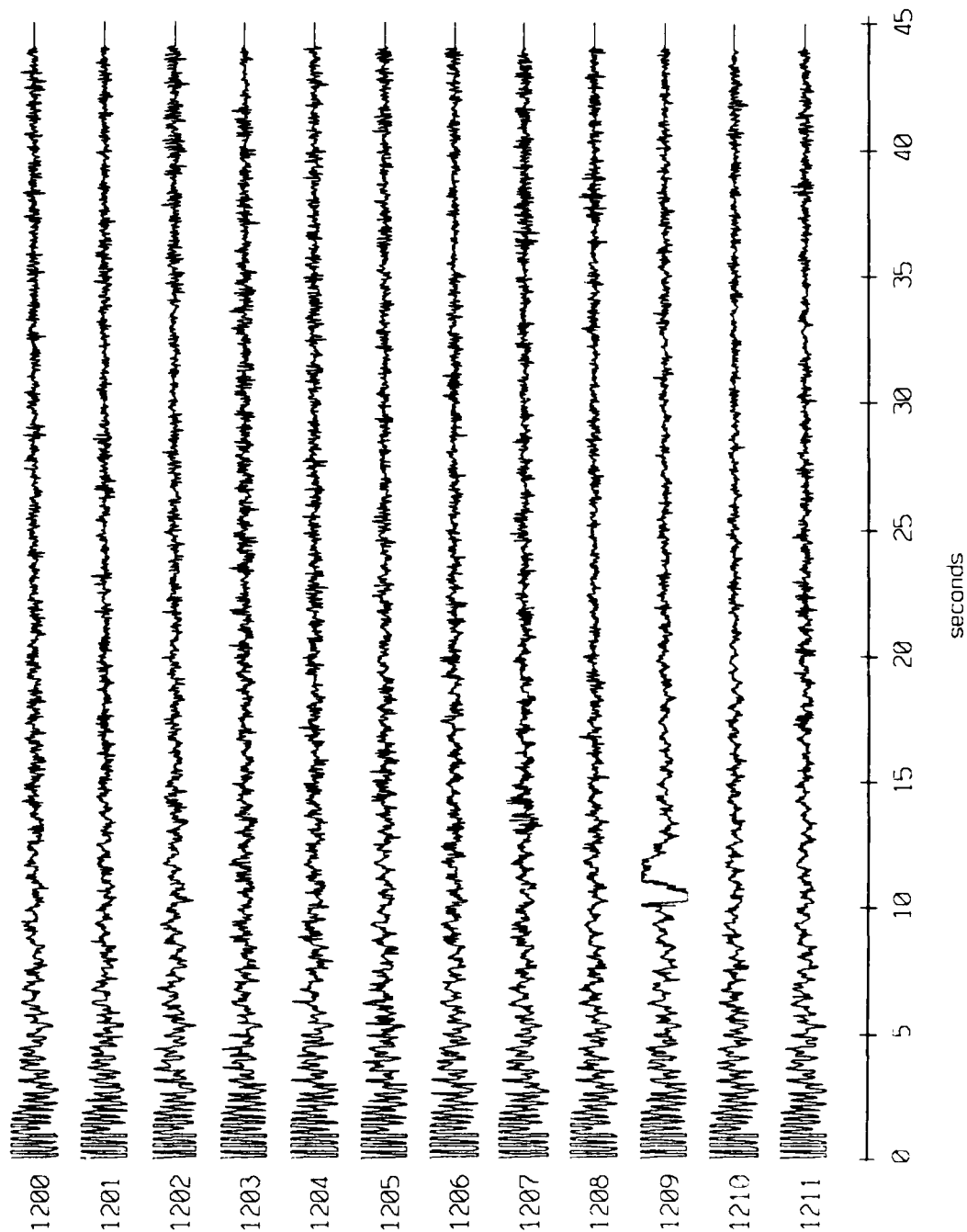
Float 5, 1986 Deployment - records 1600 - 1611, (z-axis)
vertical axis scale is approx. -1.0 to 1.0 volts



AGC corrected channel level (V)

Figure 2.4c

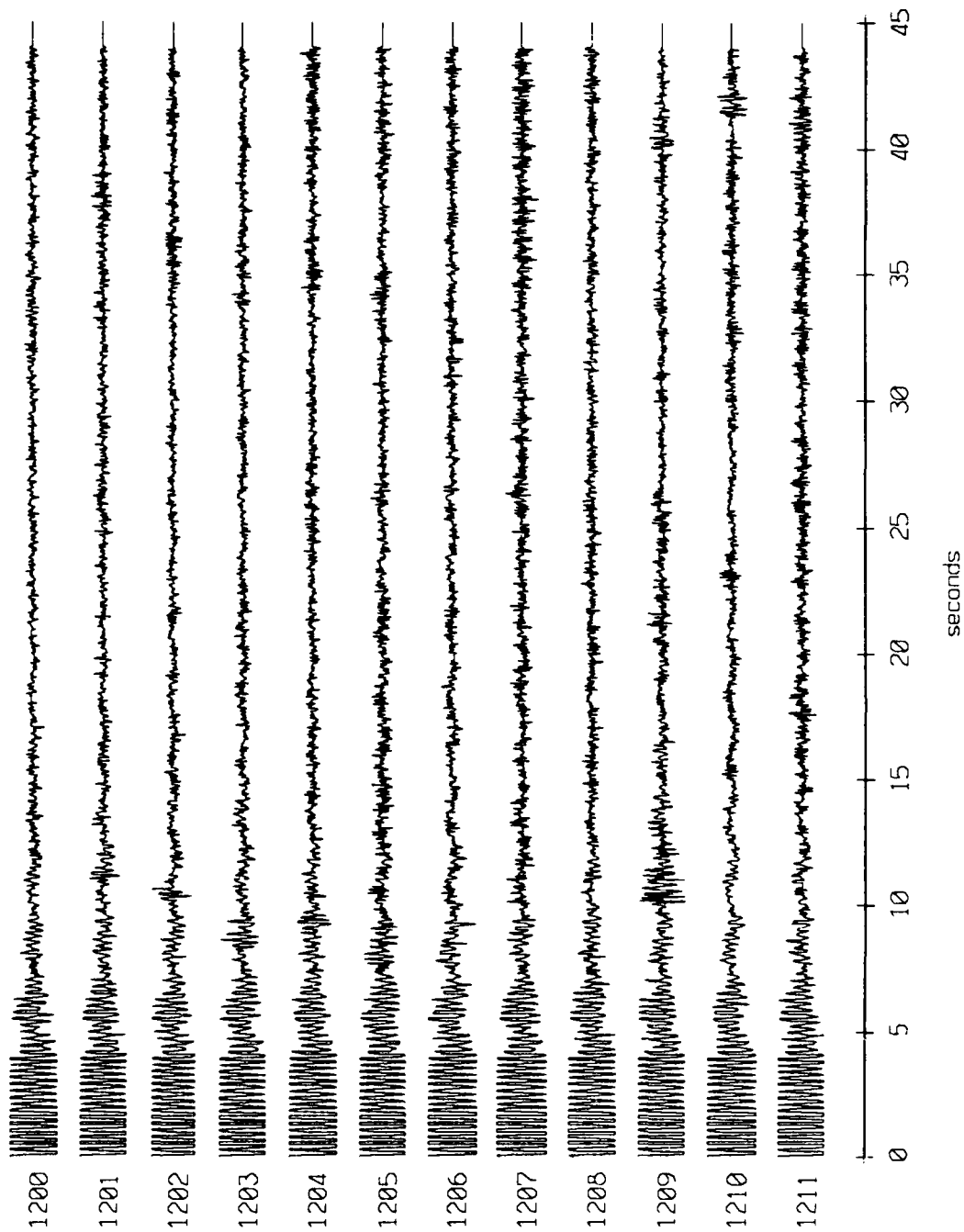
Floot 9, 1986 Deployment - records 1200 - 1211, (x-axis)
vertical axis scale is approx. -1.0 to 1.0 volts



AGC corrected channel level (V)

Figure 2.5a

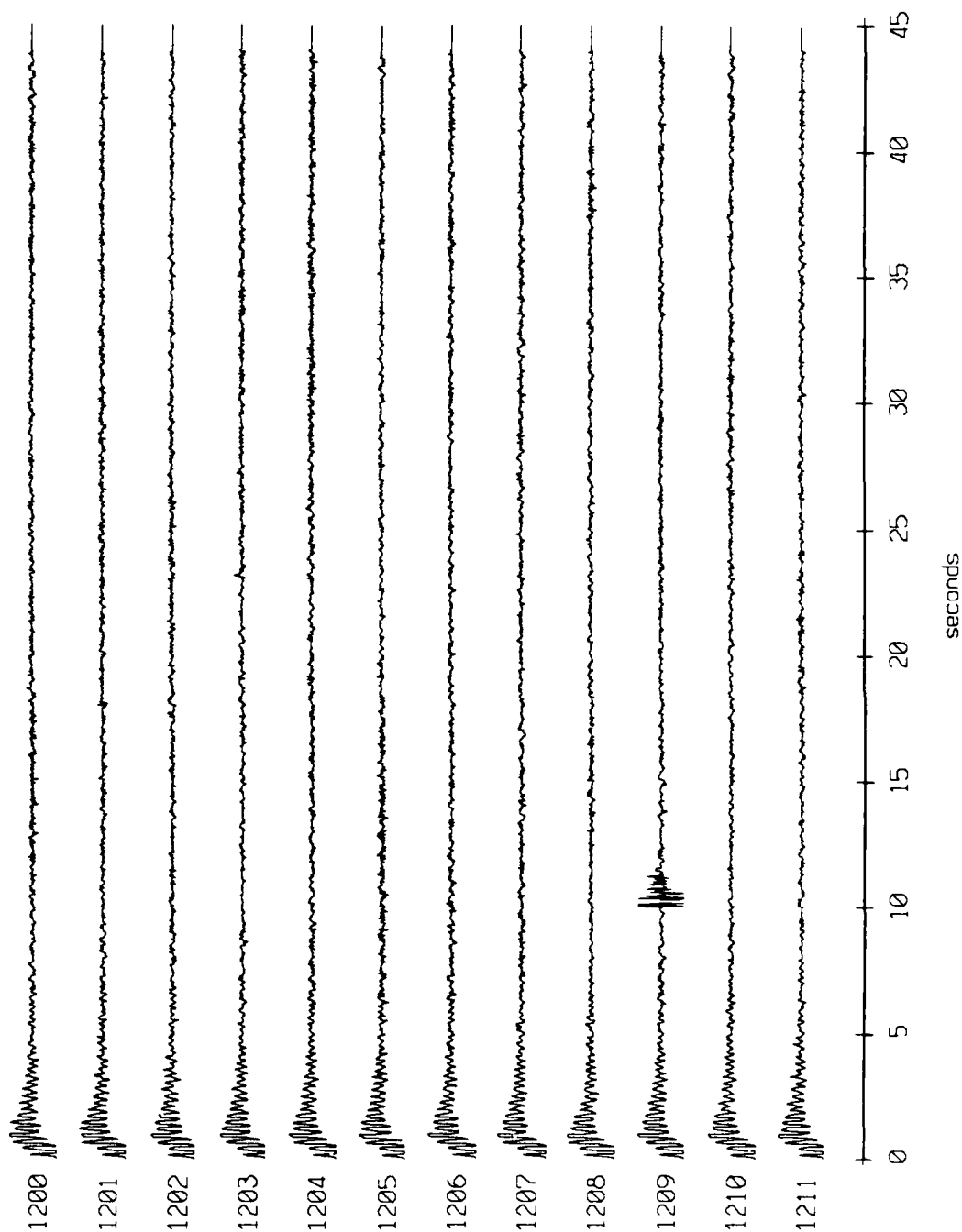
Floot 9, 1986 Deployment - records 1200 - 1211, (y-axis)
vertical axis scale is approx. -1.0 to 1.0 volts



930 corrected channel level (V)

Figure 2.5b

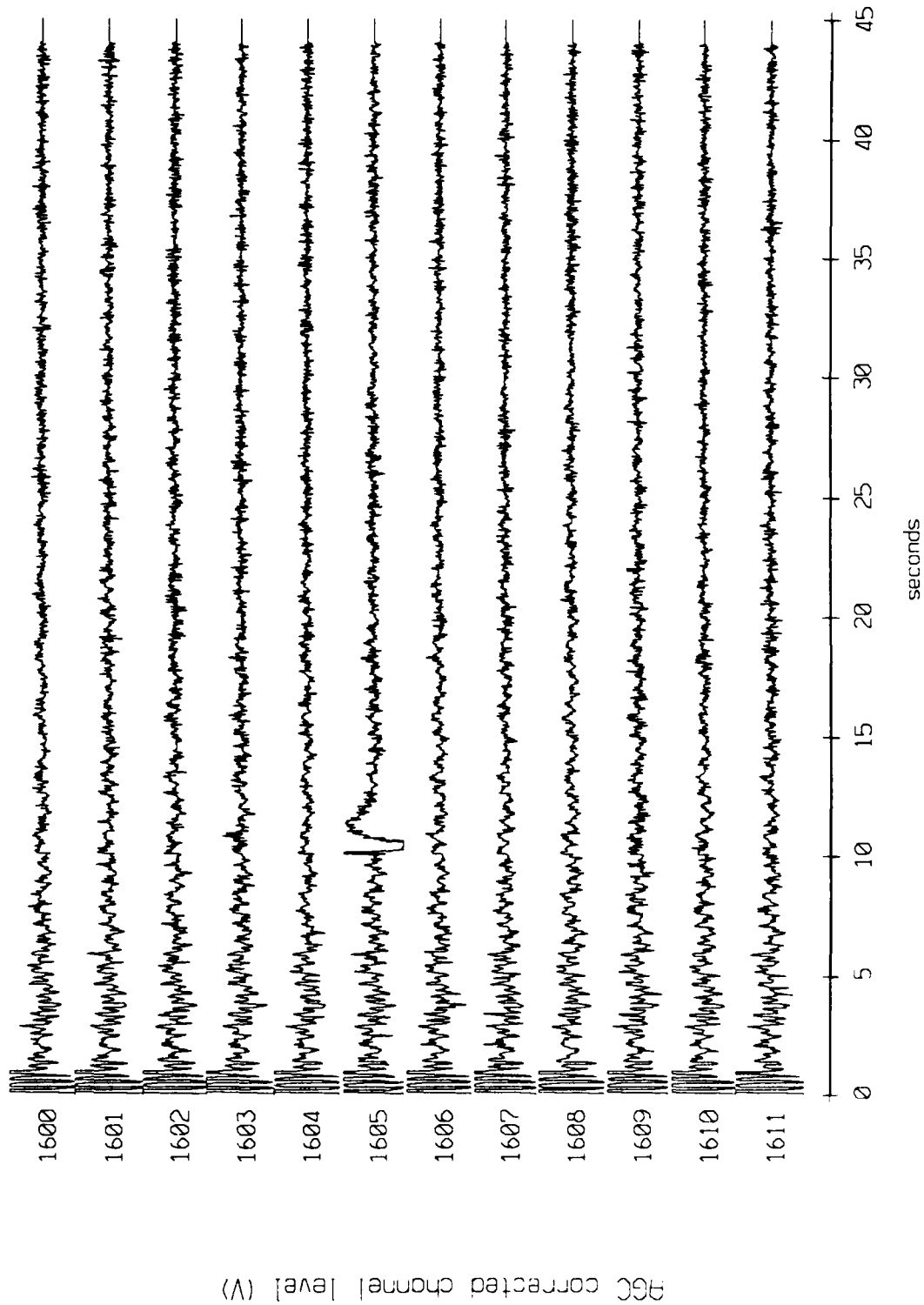
Float 9, 1986 Deployment - records 1200 - 1211, (z-axis)
vertical axis scale is approx. -1.0 to 1.0 volts



AGC corrected channel level (V)

Figure 2.5c

Floot 9, 1986 Deployment - records 1600 - 1611, (x-axis)
vertical axis scale is approx. -1.0 to 1.0 volts



9CC corrected channel level (V)

Figure 2.6a

Float 9, 1986 Deployment - records 1600 - 1611, (y-axis)
vertical axis scale is approx. -1.0 to 1.0 volts

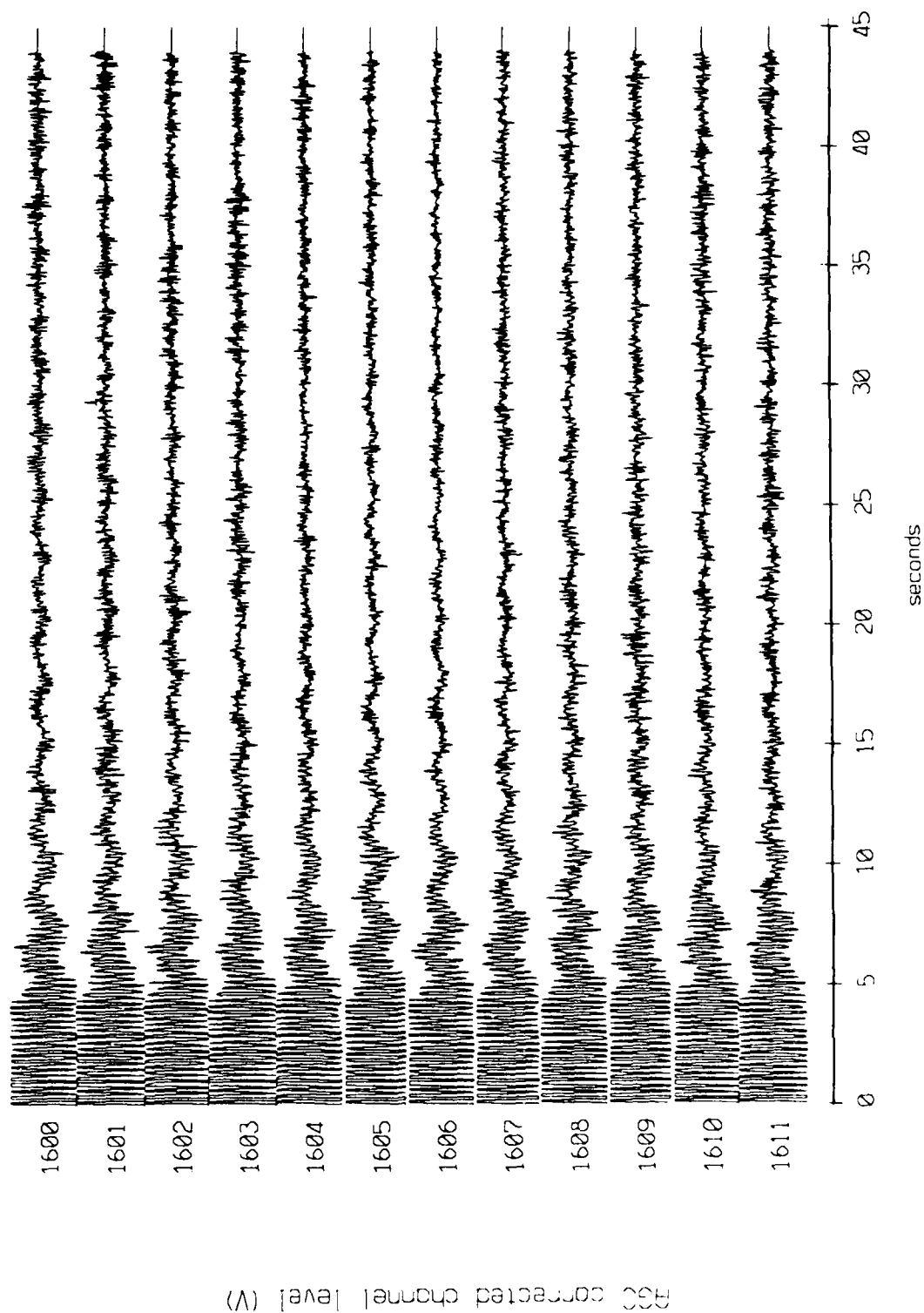
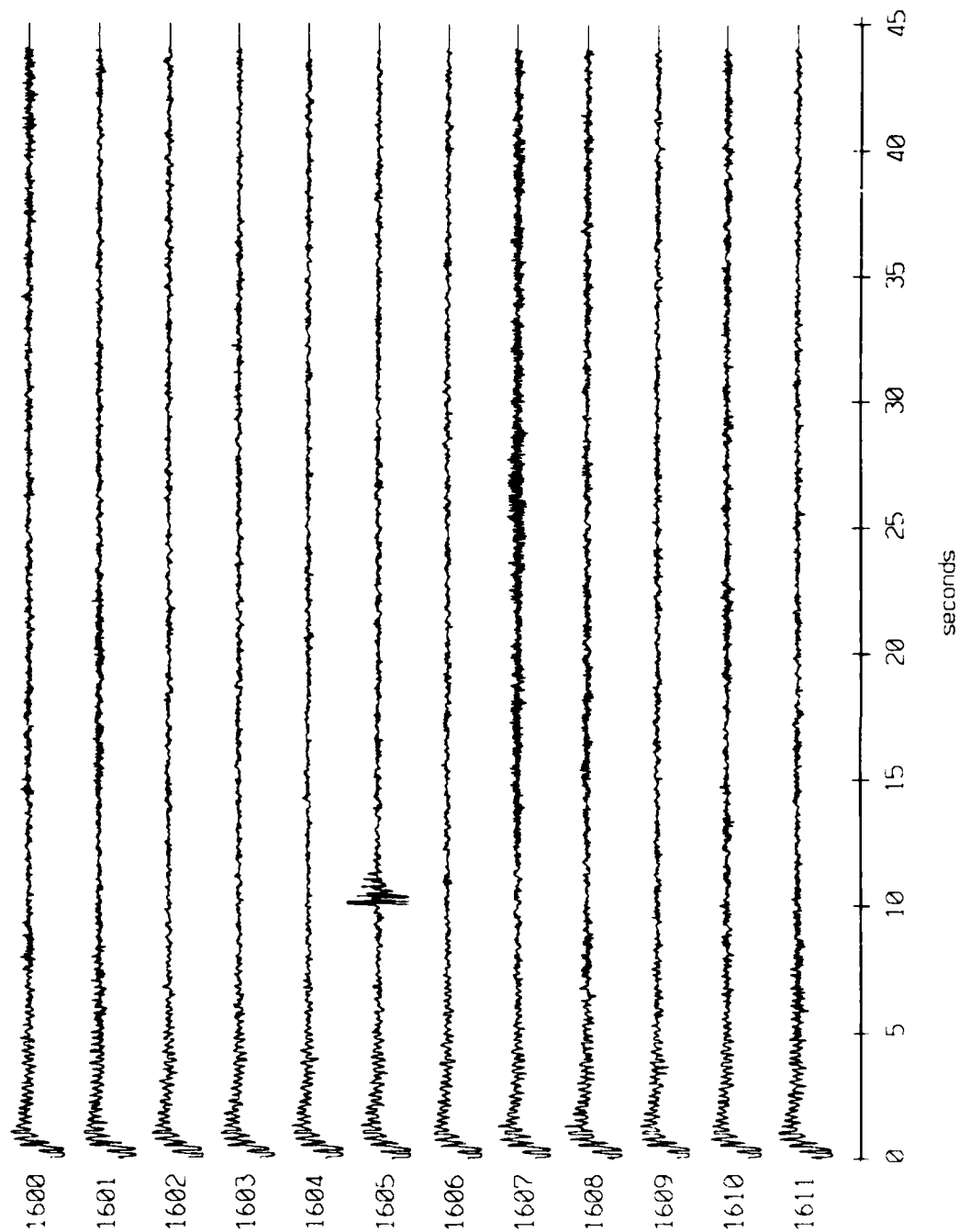


Figure 2.6b

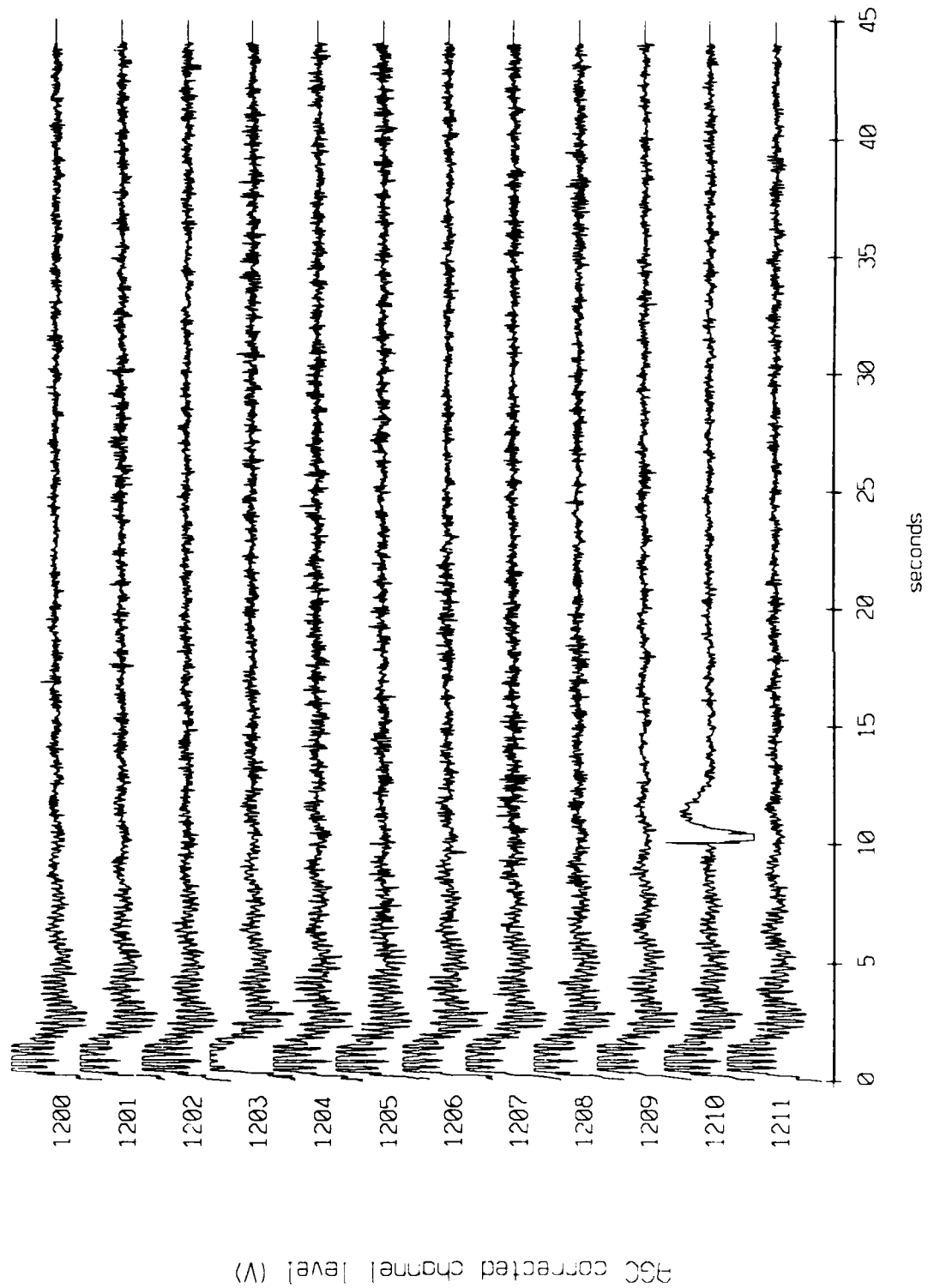
Float 9, 1986 Deployment - records 1600 - 1611, (z-axis)
vertical axis scale is approx. -1.0 to 1.0 volts



900 corrected channel level (V)

Figure 2.6c

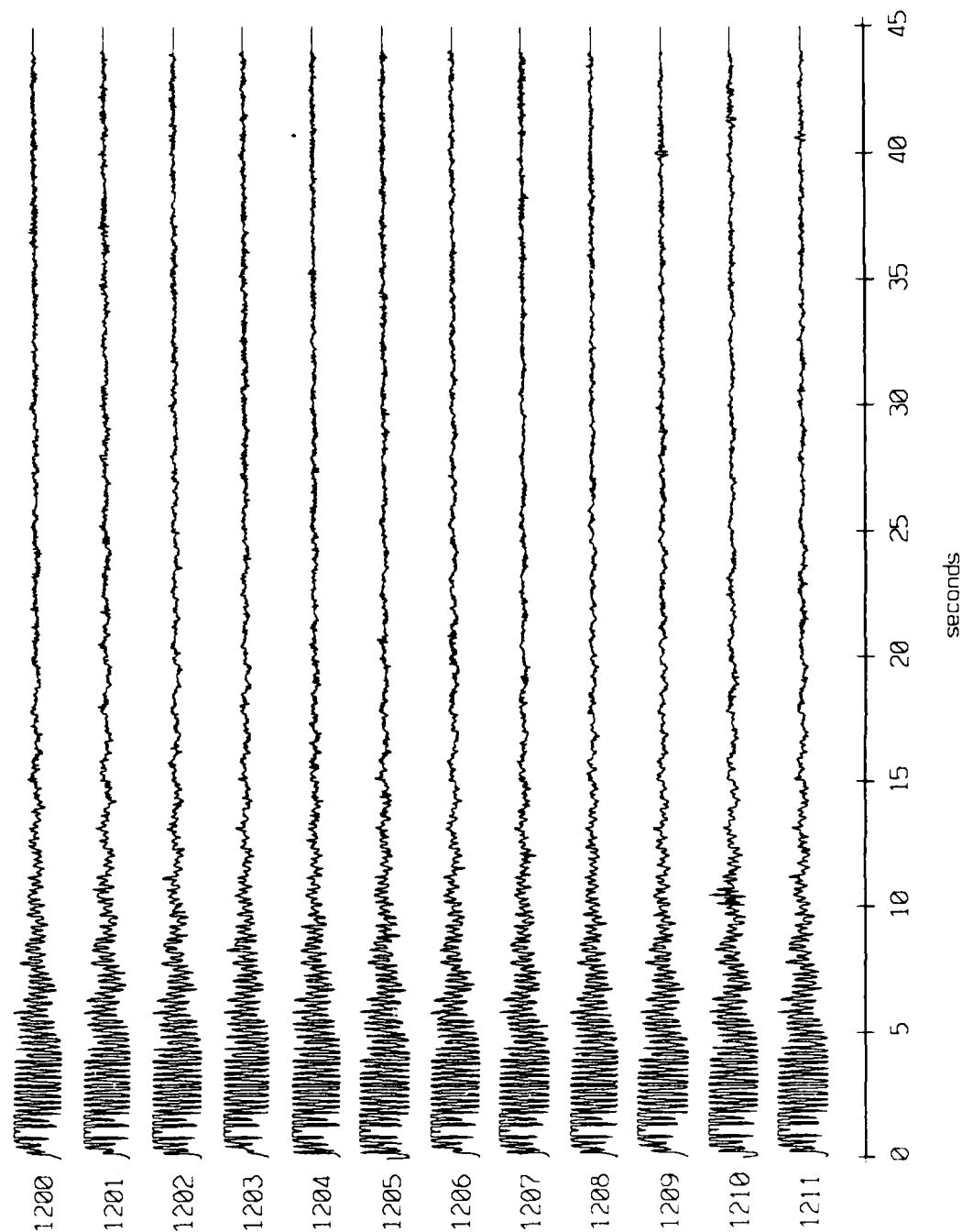
Floot 10, 1986 Deployment - records 1200 - 1211, (x-axis)
vertical axis scale is approx. -1.0 to 1.0 volts



PGC corrected channel level (V)

Figure 2.7a

Floot 10, 1986 Deployment - records 1200 - 1211, (y-axis)
vertical axis scale is approx. -2.0 to 2.0 volts



100 corrected channel level (V)

Figure 2.7b

Floot 10, 1986 Deployment - records 1200 - 1211, (z-axis)
vertical axis scale is approx. -1.0 to 1.0 volts

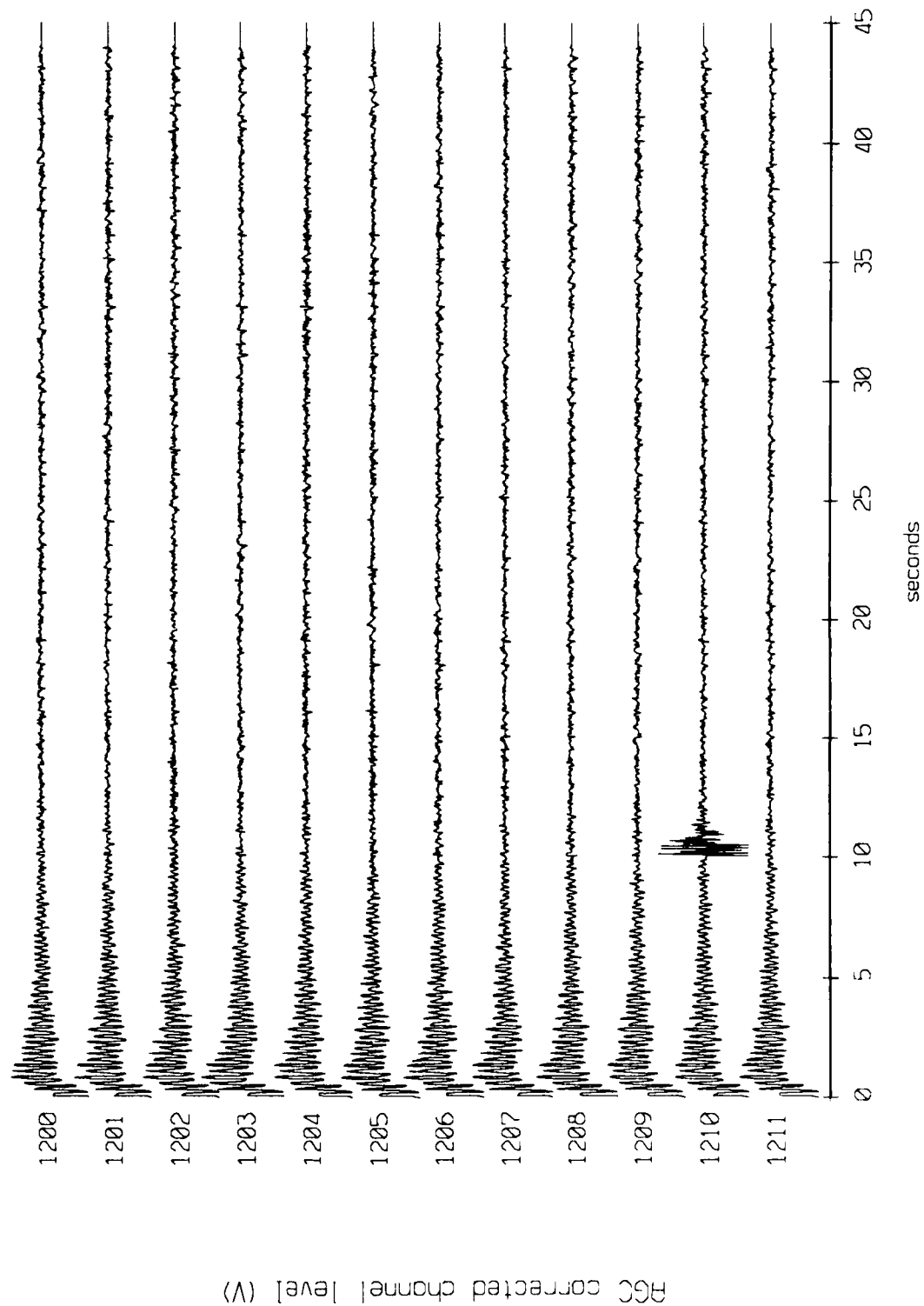


Figure 2.7c

Floot 10, 1986 Deployment - records 1600 - 1611, (x-axis)
vertical axis scale is approx. -1.0 to 1.0 volts

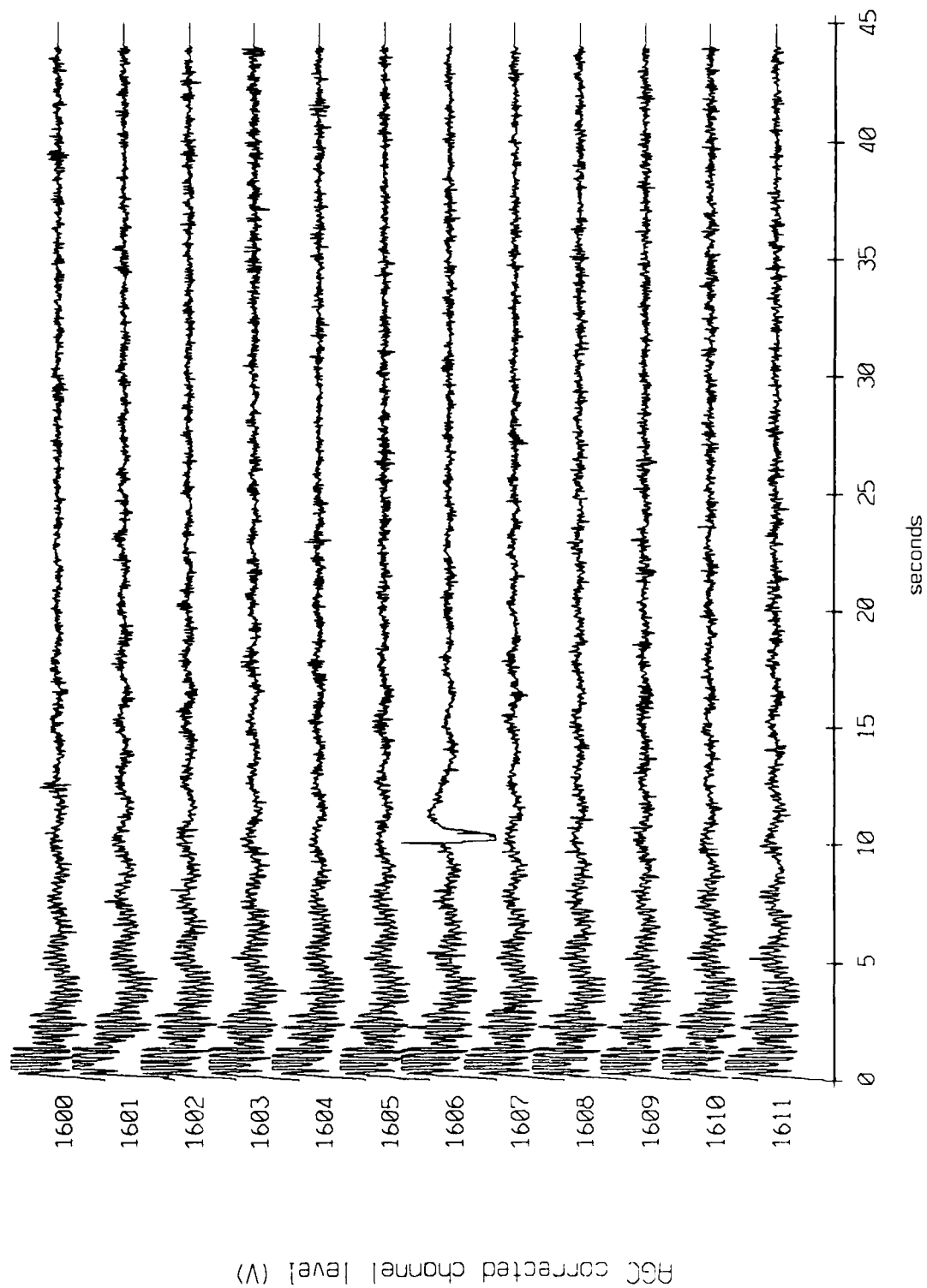


Figure 2.8a

AGC corrected channel level (V)

Floot 10, 1986 Deployment - records 1600 - 1611, (y-axis)
vertical axis scale is approx. -2.0 to 2.0 volts

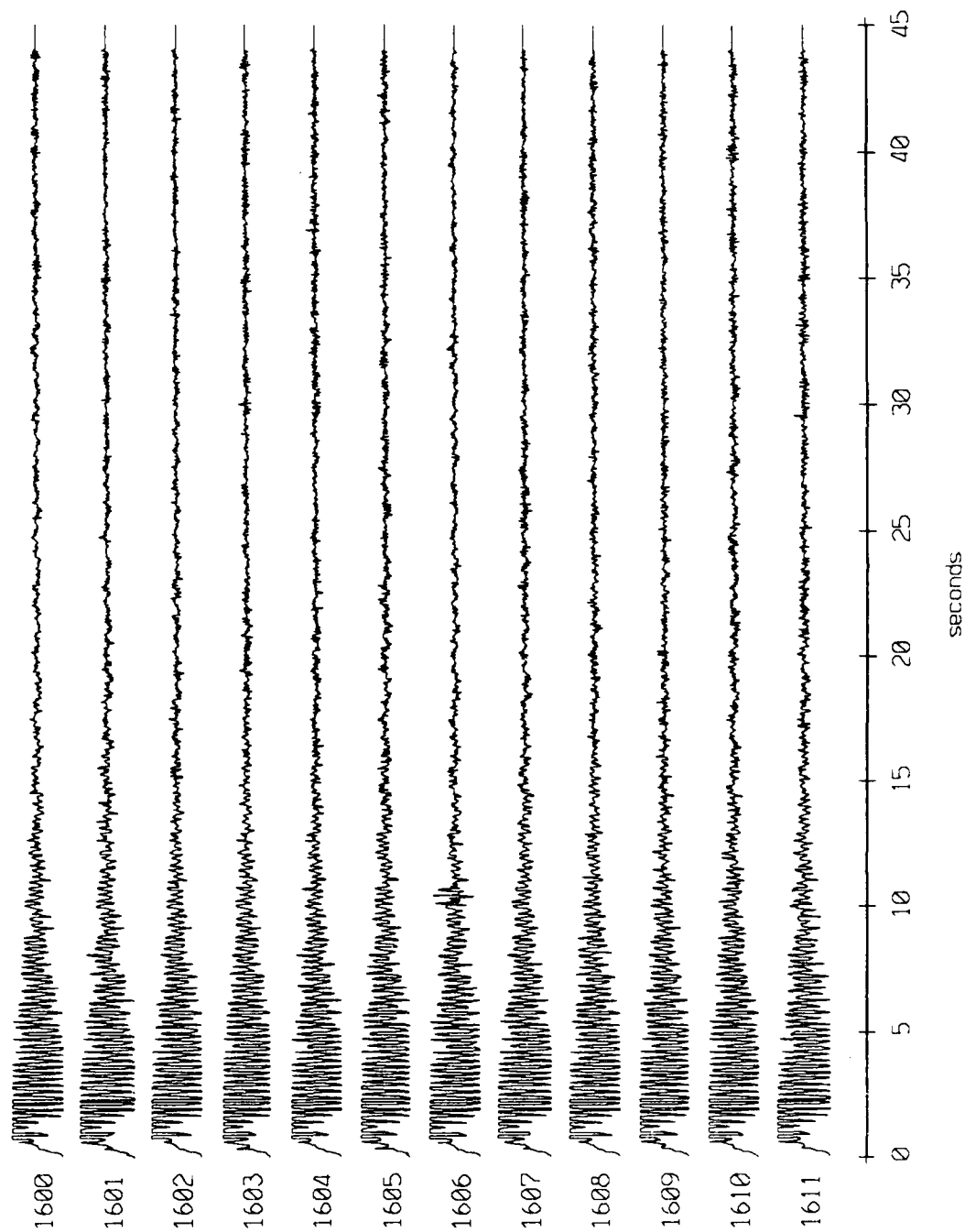
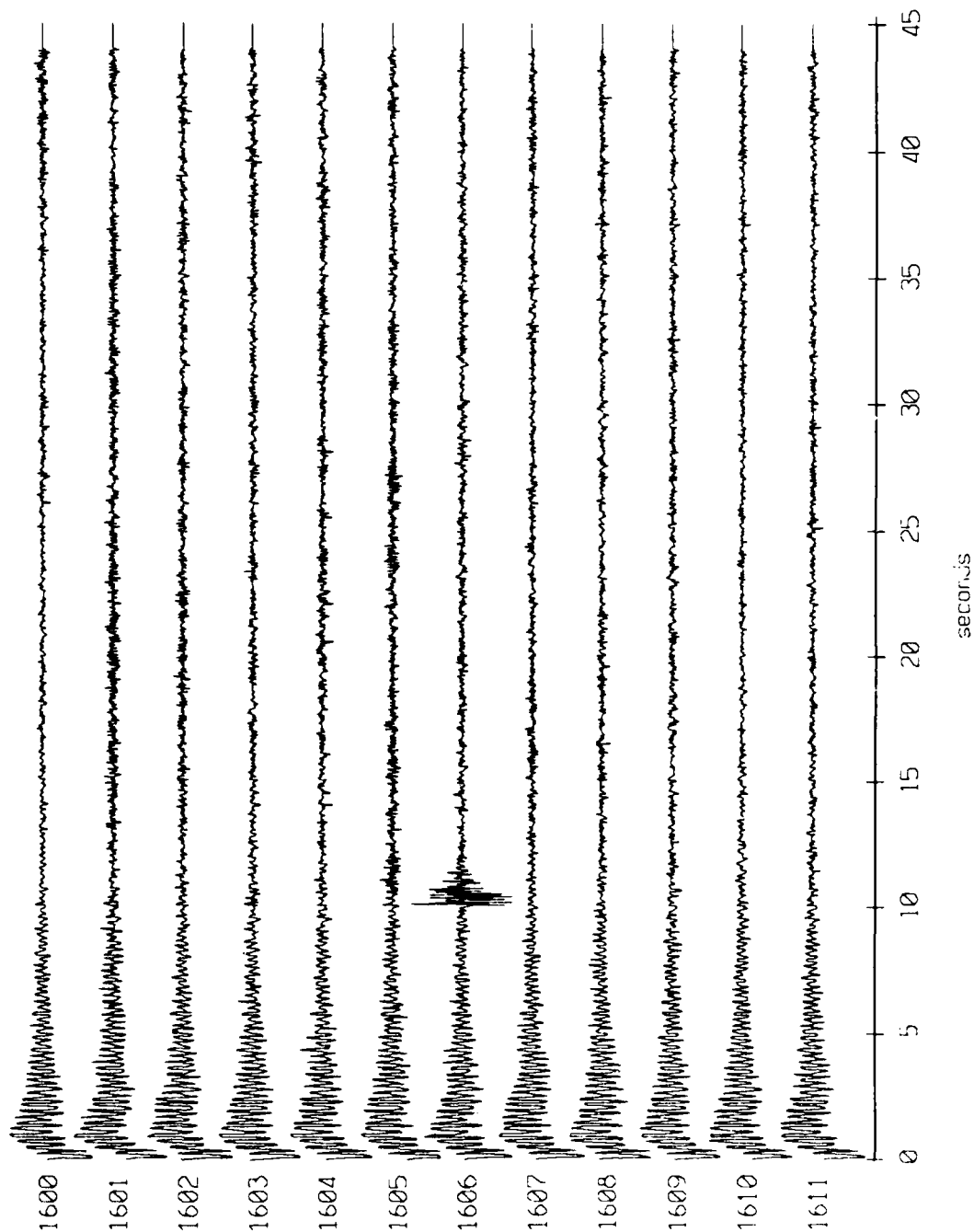


Figure 2.8b

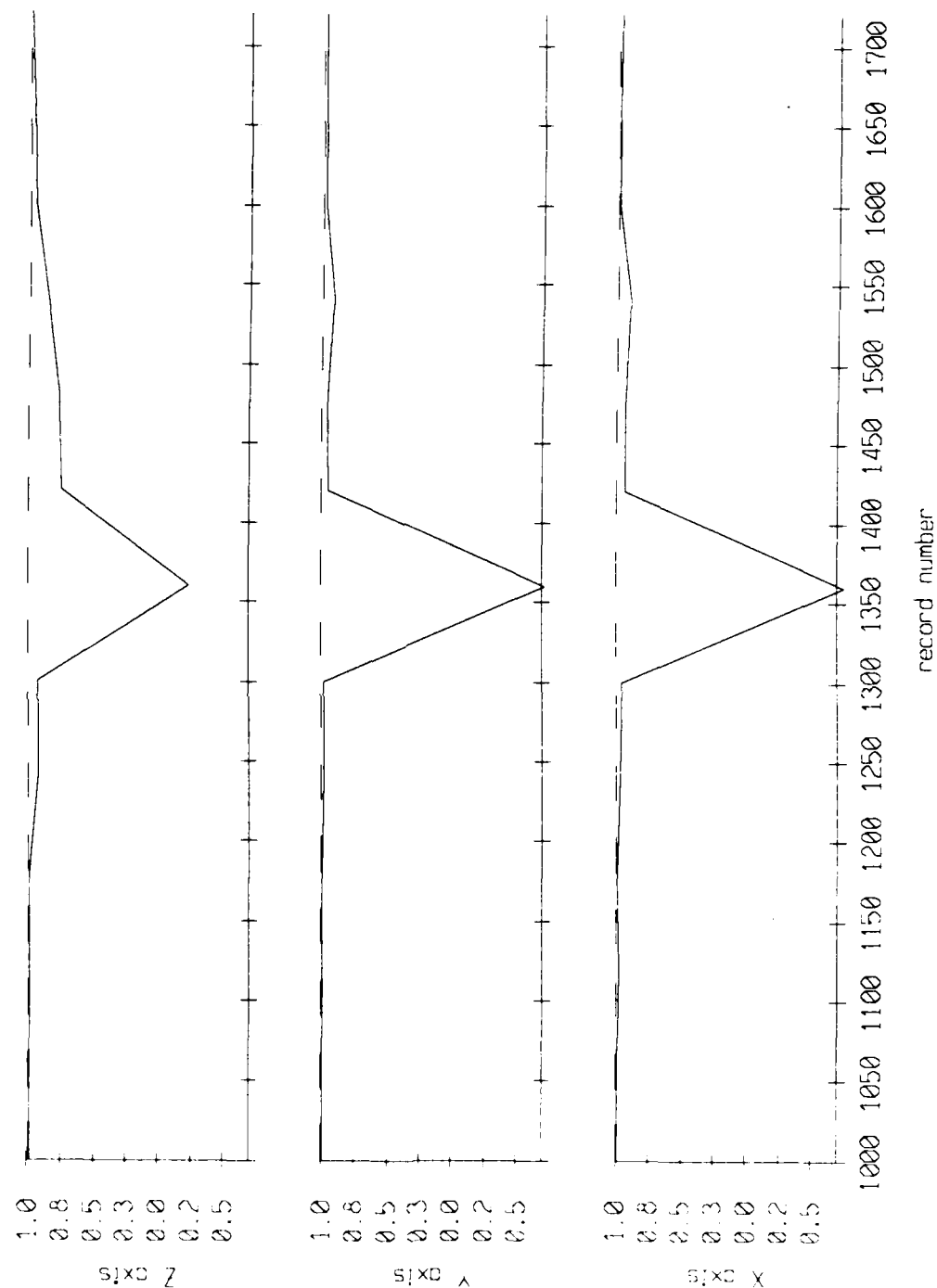
Float 10, 1986 Deployment - records 1600 - 1611, (z-axis)
vertical axis scale is approx. -1.0 to 1.0 volts



400 corrected channel level (V)

Figure 2.8c

Plot 3, September 1986 Trip
correlation coefficient between adjacent 60 record averages



correlation coefficient

Figure 4.1

Float 9, September 1986 Trip
correlation coefficient between adjacent 40 record averages

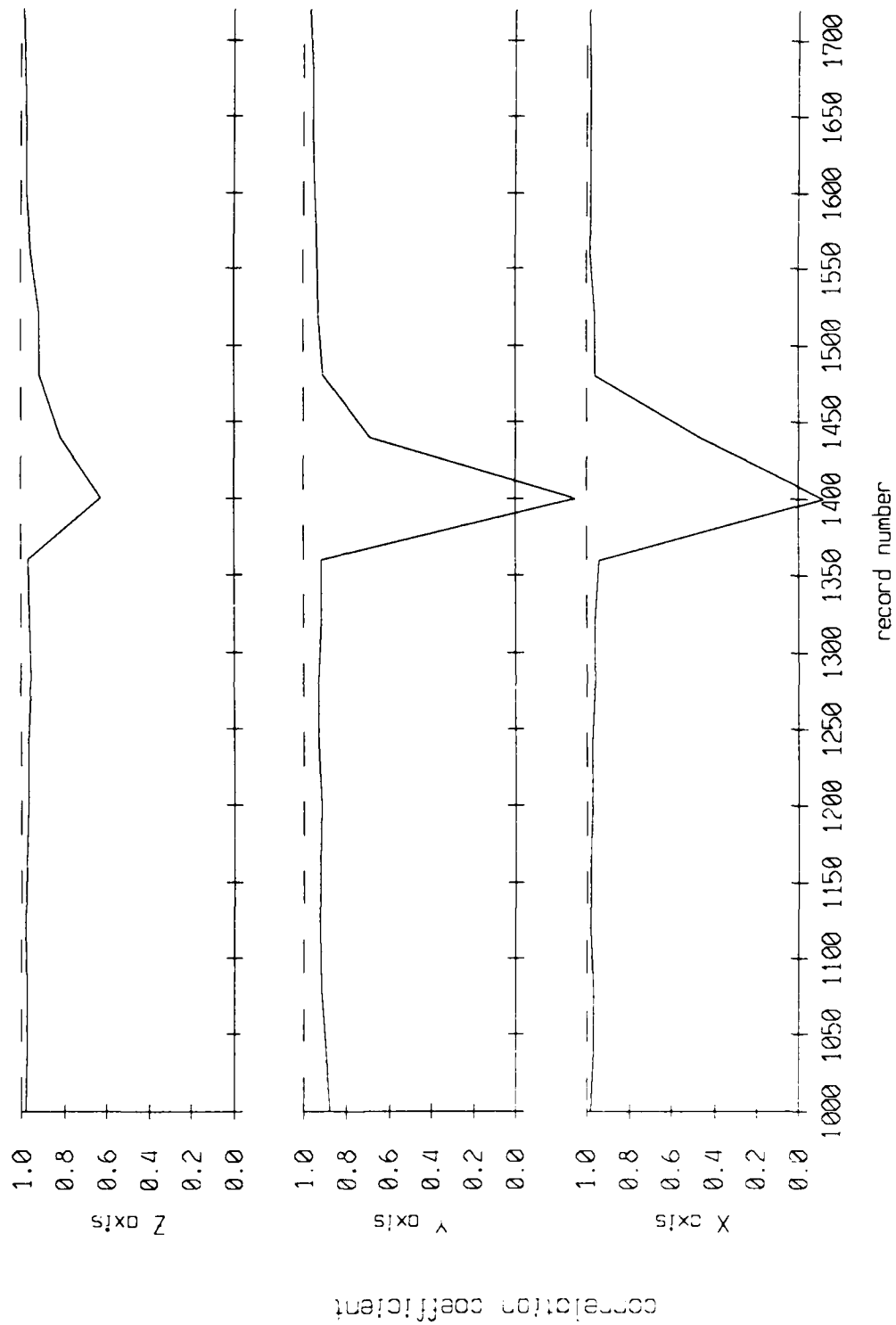


Figure 4.2

Float 10, September 1986 Trip
correlation coefficient between adjacent 40 record averages

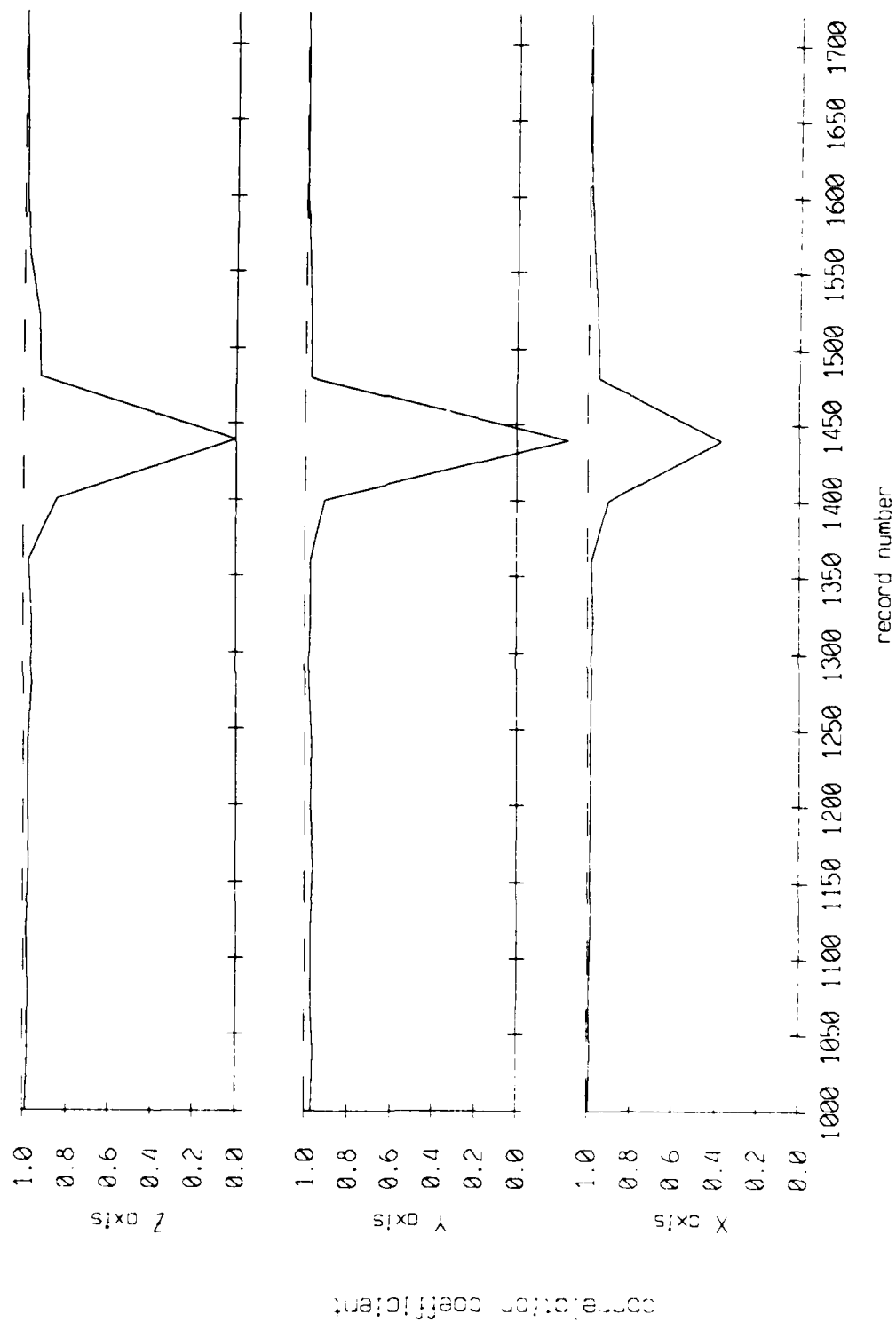


Figure 4.3

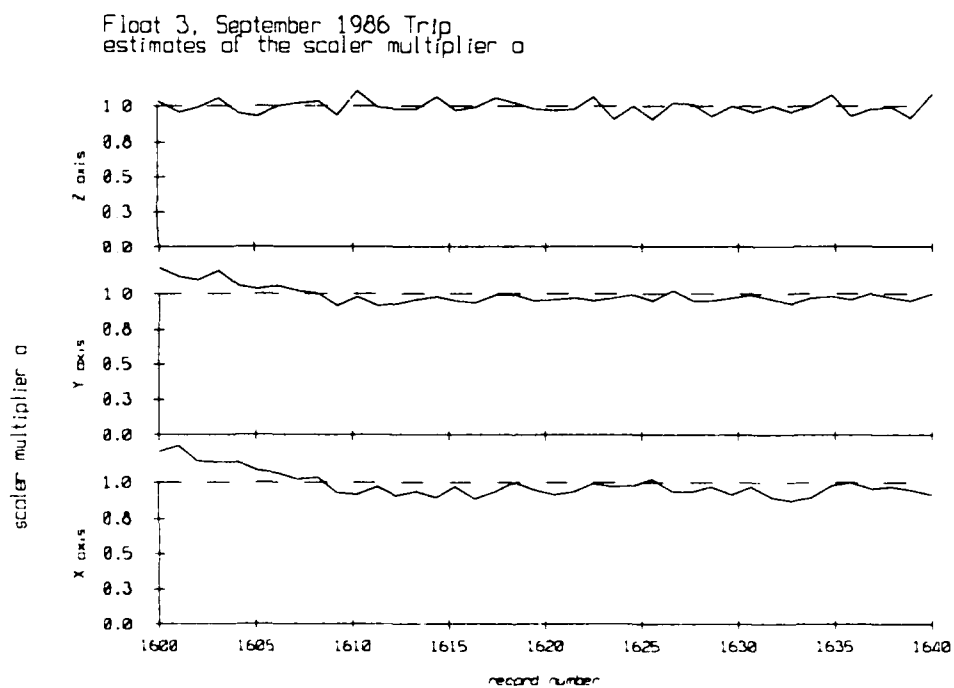
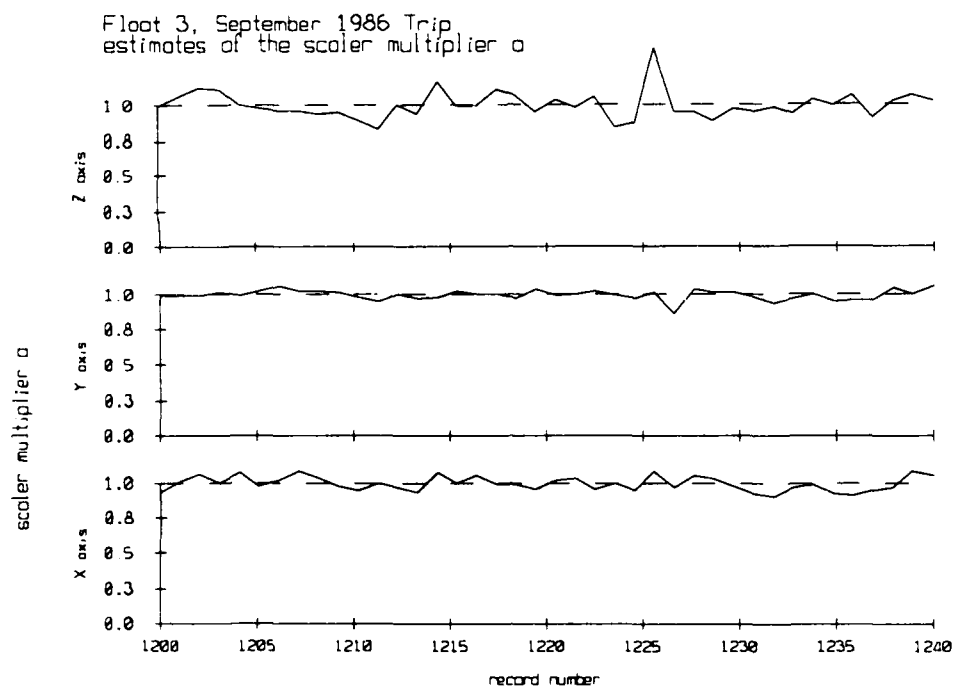
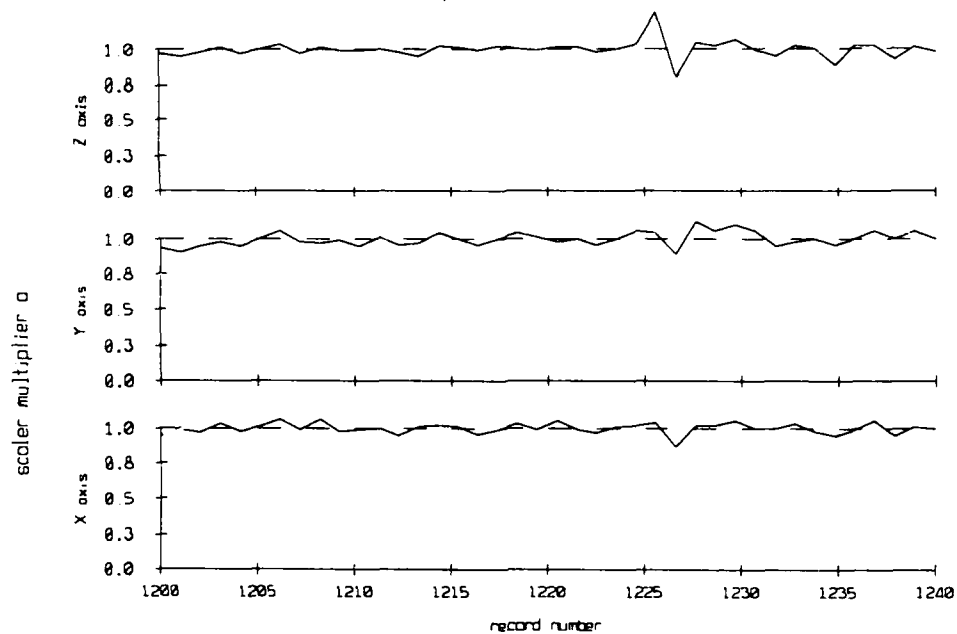


Figure 4.4

Float 9, September 1986 Trip
estimates of the scaler multiplier α



Float 9, September 1986 Trip
estimates of the scaler multiplier α

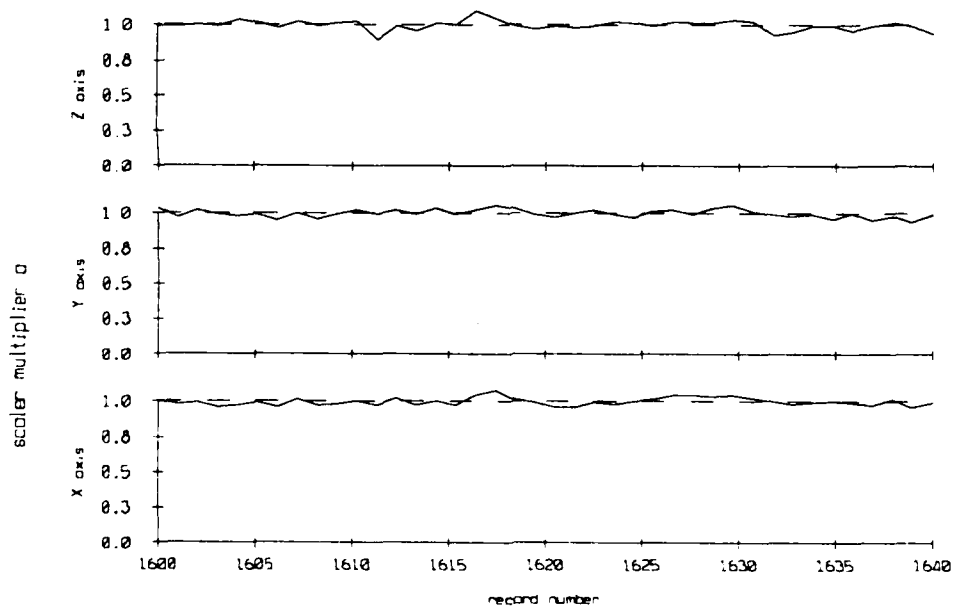
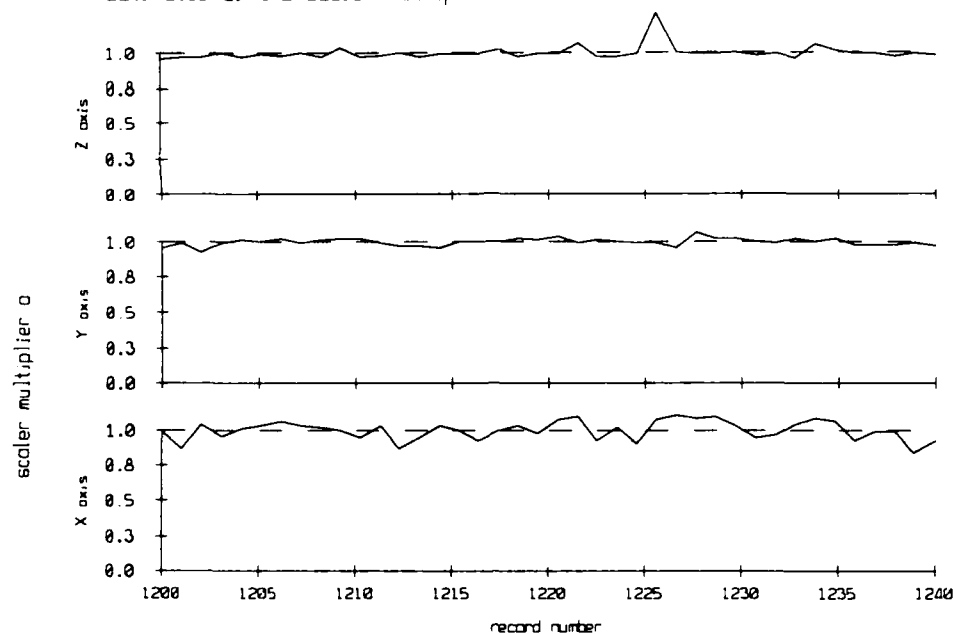


Figure 4.5

Float 10, September 1986 Trip
estimates of the scaler multiplier α



Float 10, September 1986 Trip
estimates of the scaler multiplier α

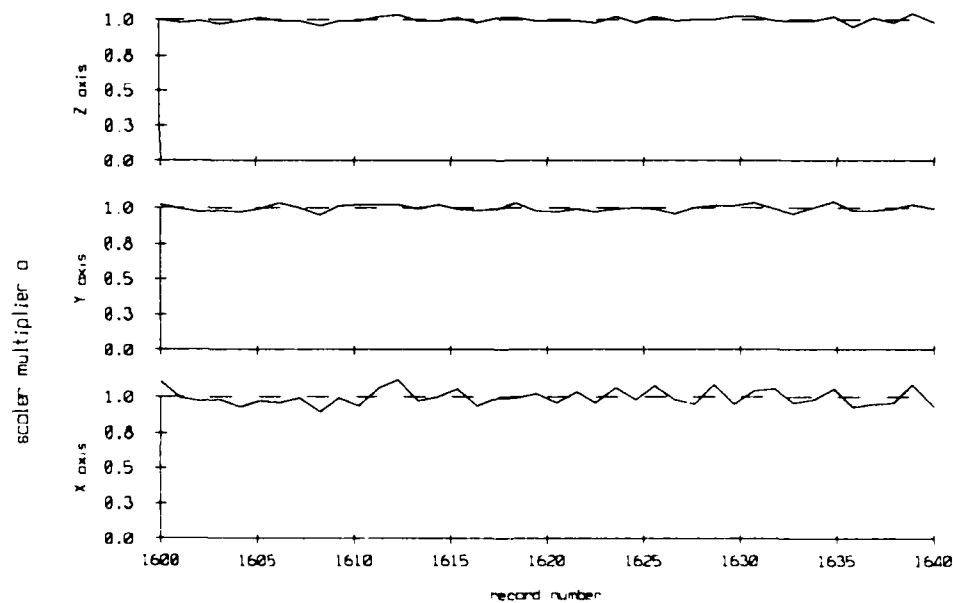


Figure 4.6

Float 3, September 1986 Trip
 record 1207 velocity time series

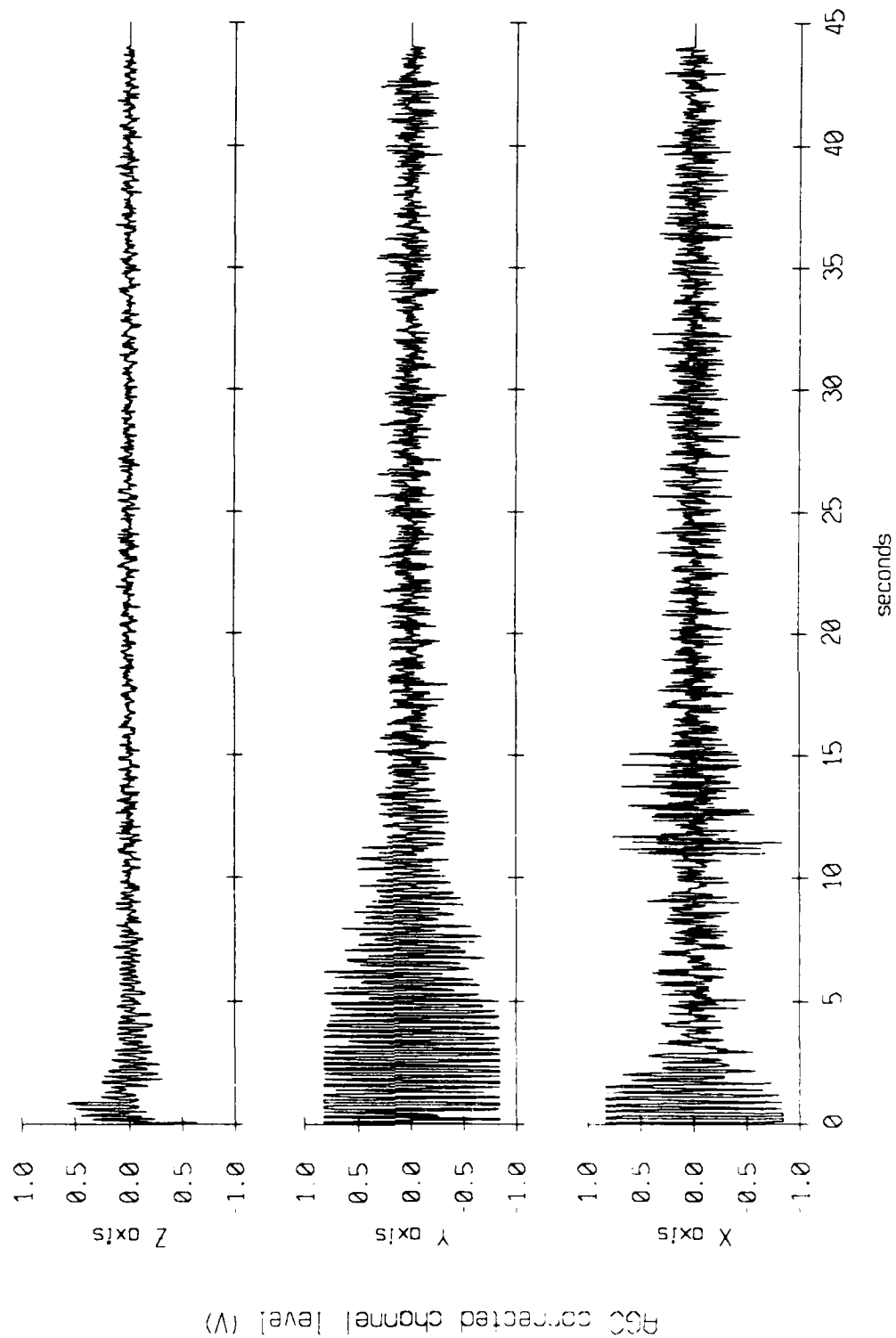


Figure 4.7a

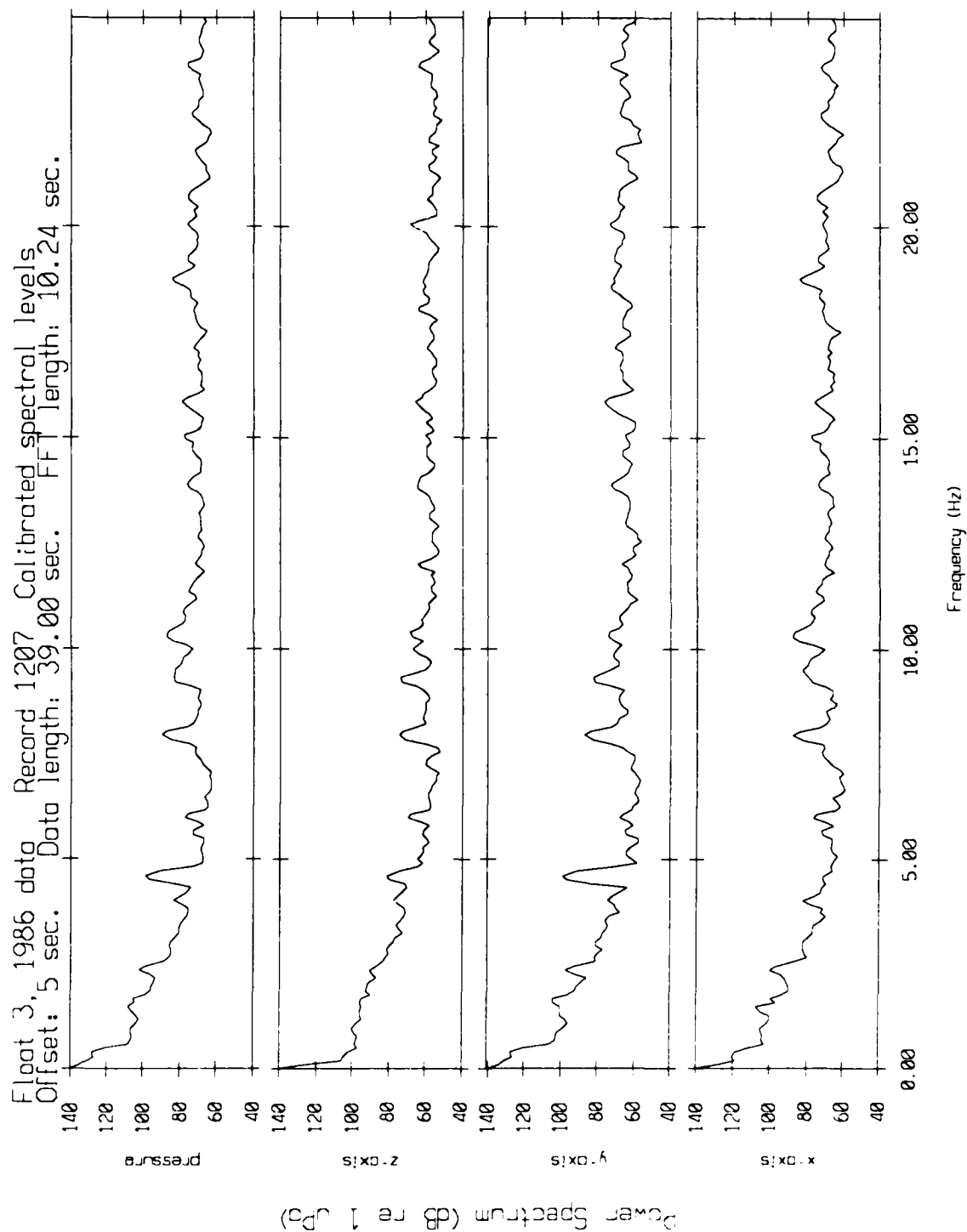


Figure 4.7b

Floot 3, September 1986 Trip
60 record average, starting with record 1201

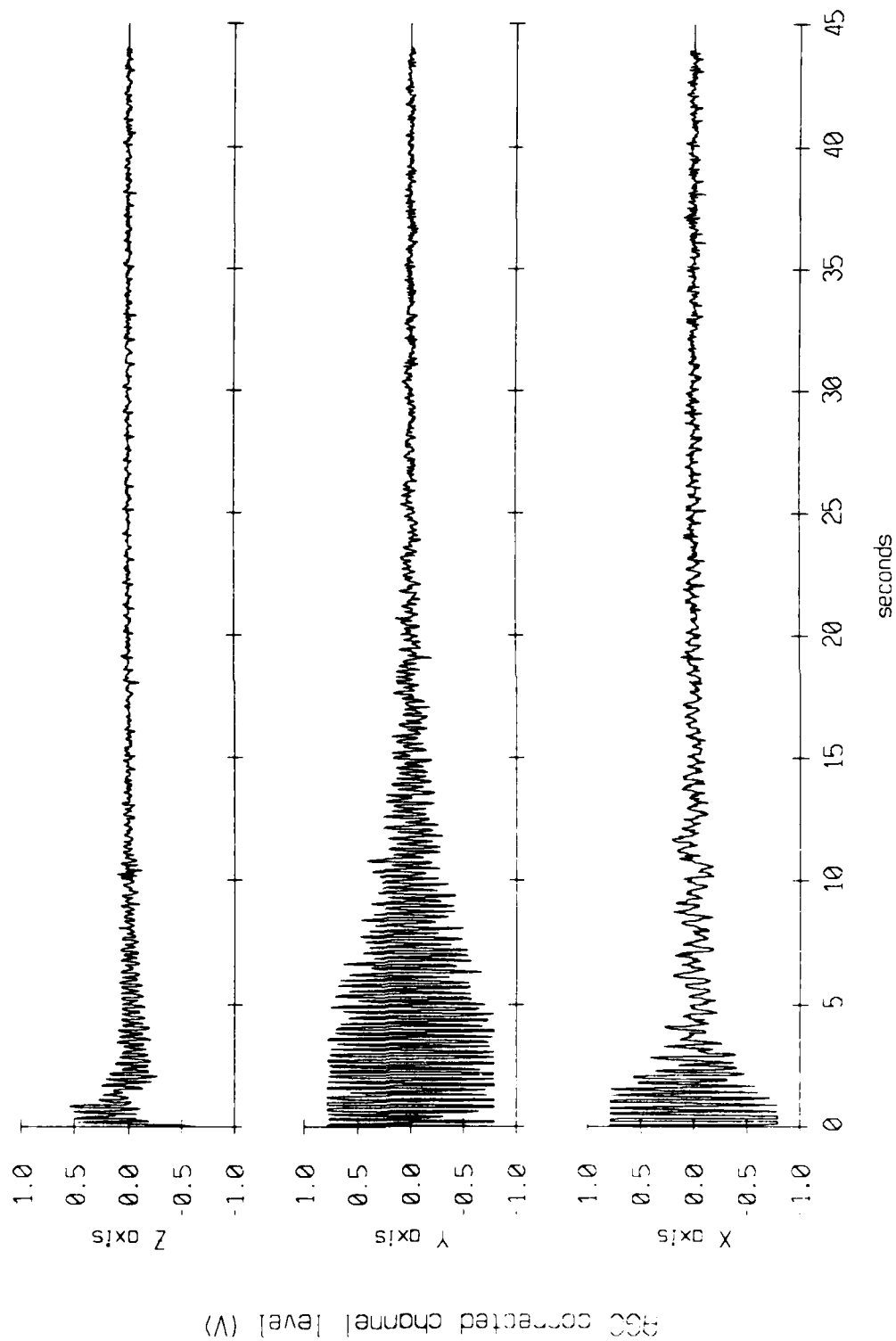


Figure 4.7c

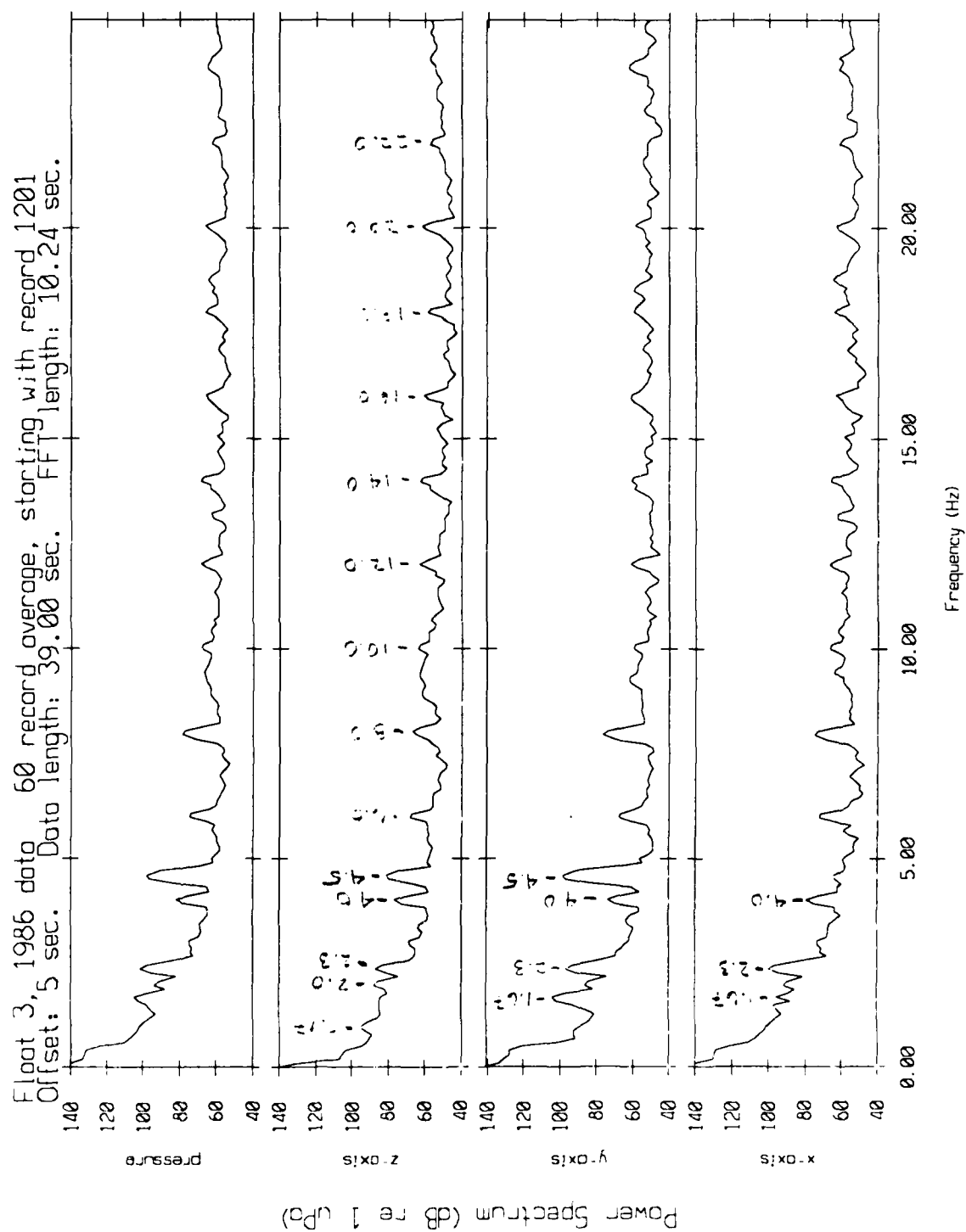


Figure 4.7d

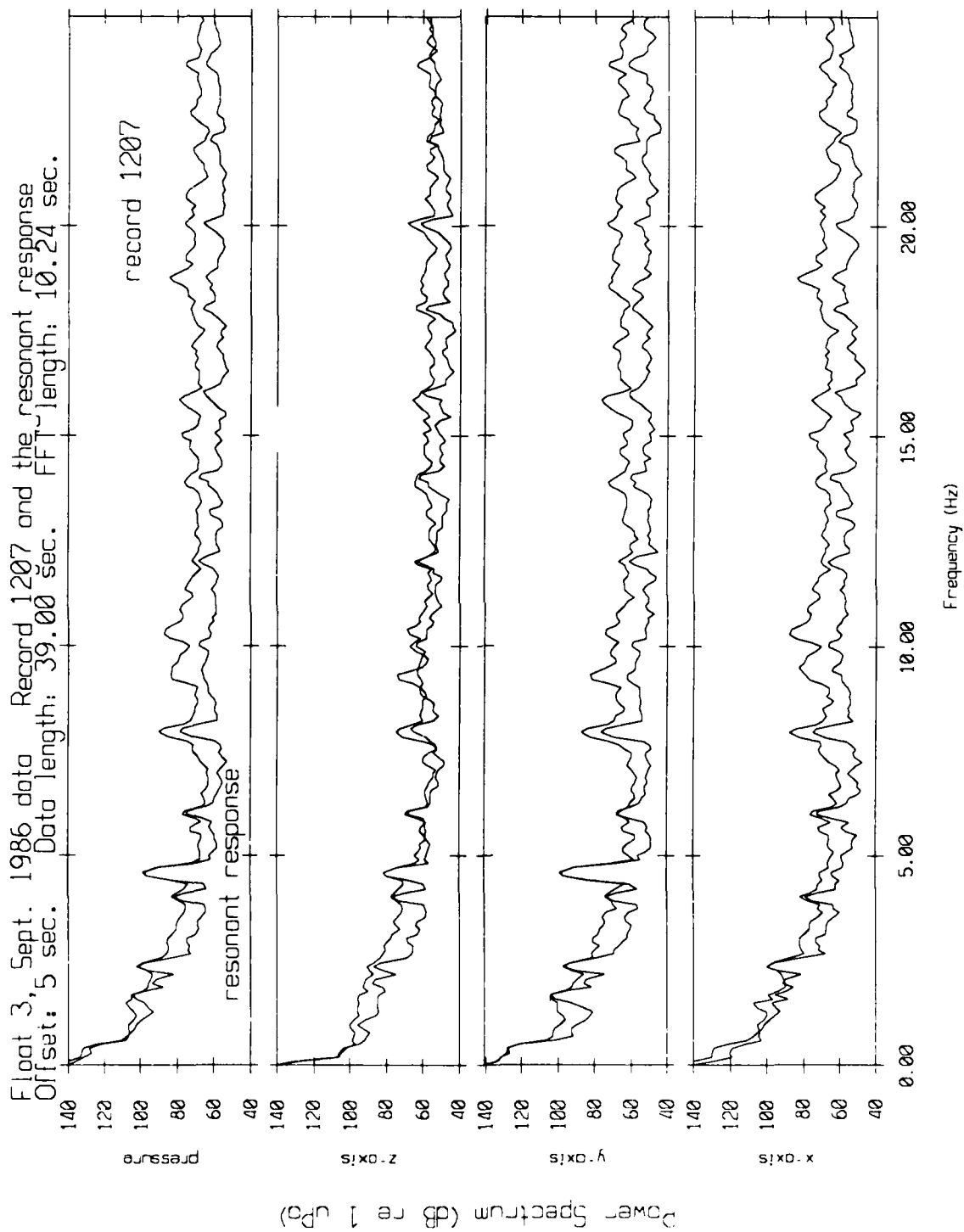


Figure 4.7e

Float 3 September 1986 Trip
 record 1207 with (1.0170 1.0548 0.95697) * r(n) subtracted

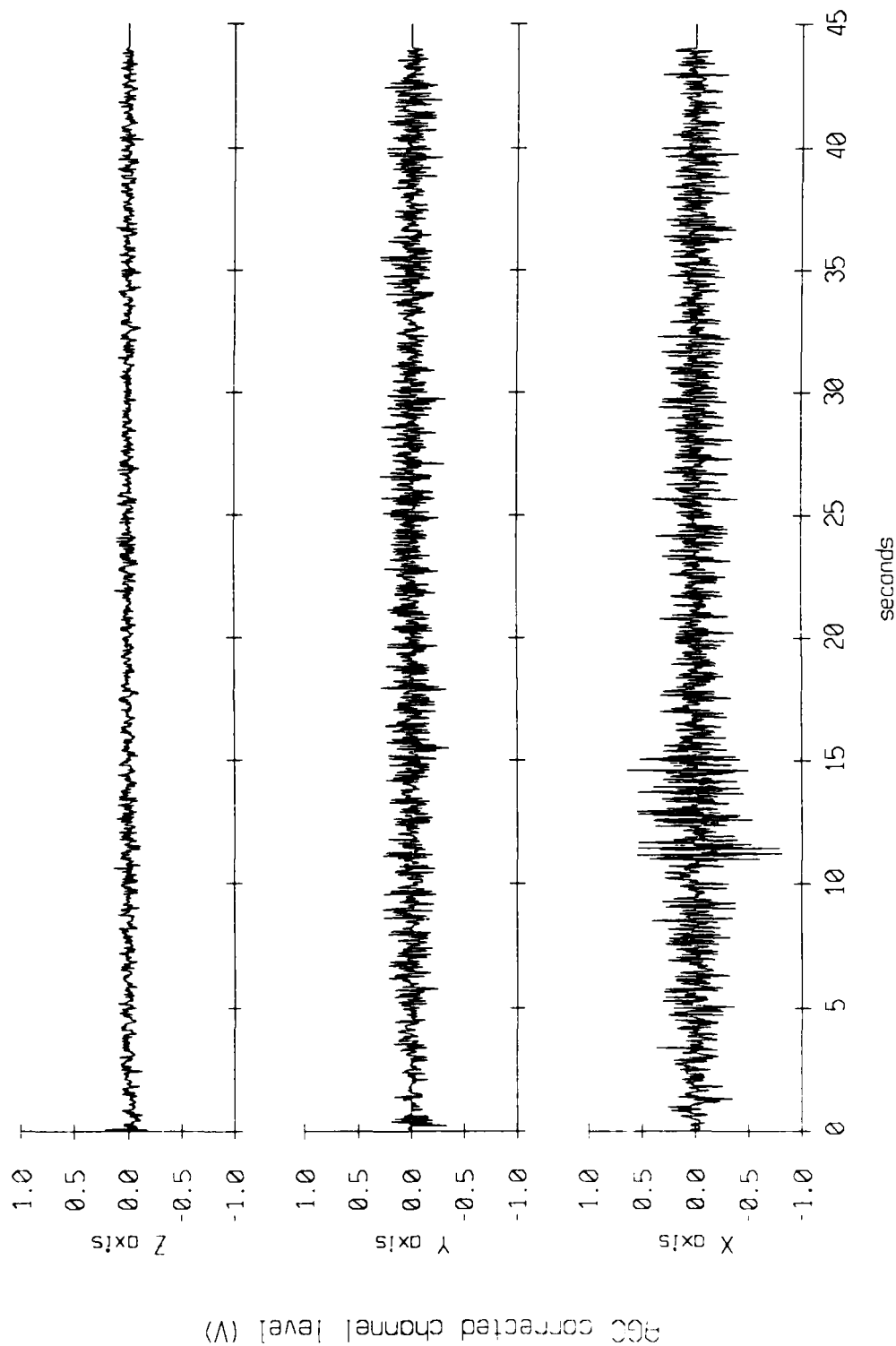


Figure 4.7f

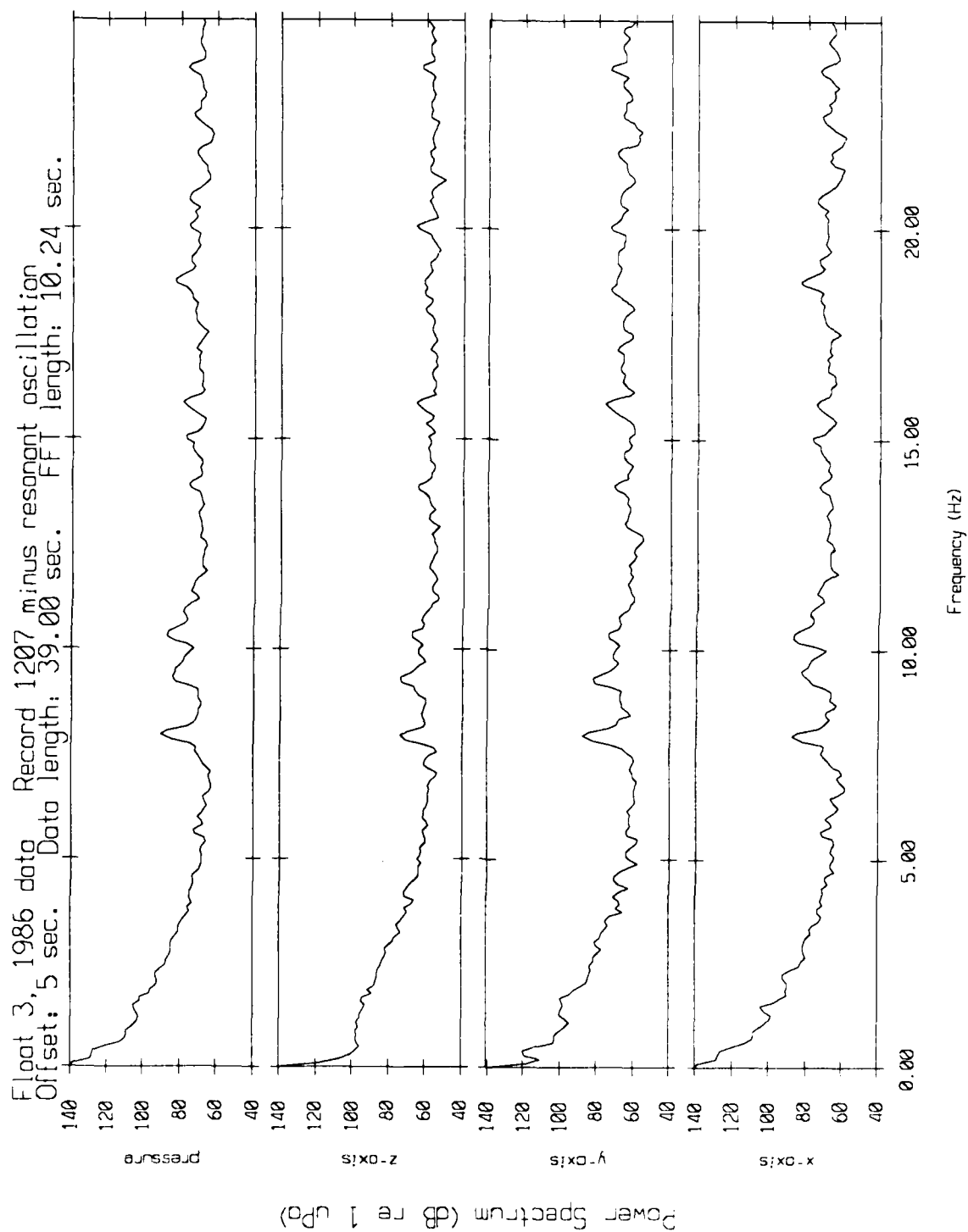


Figure 4.7g

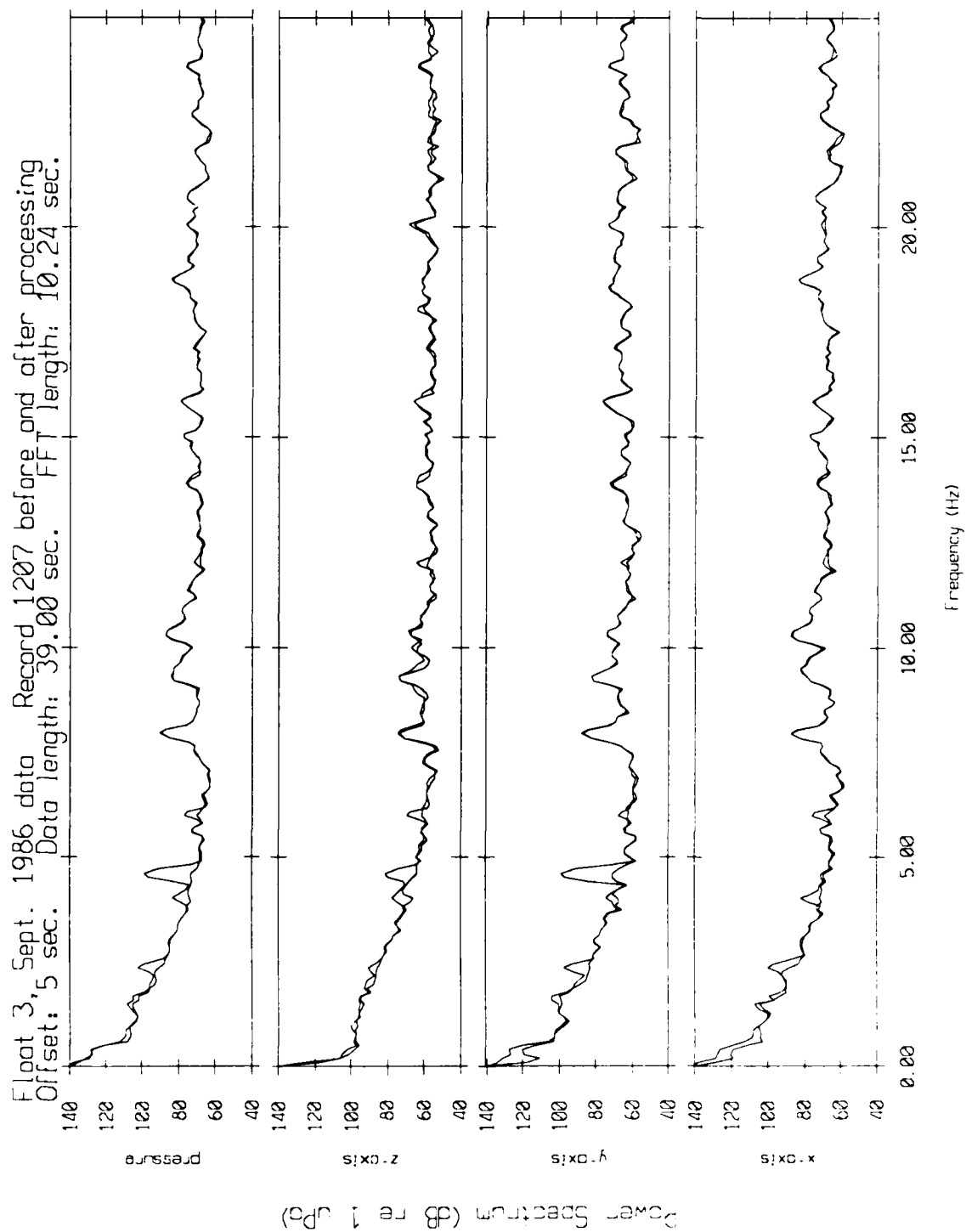
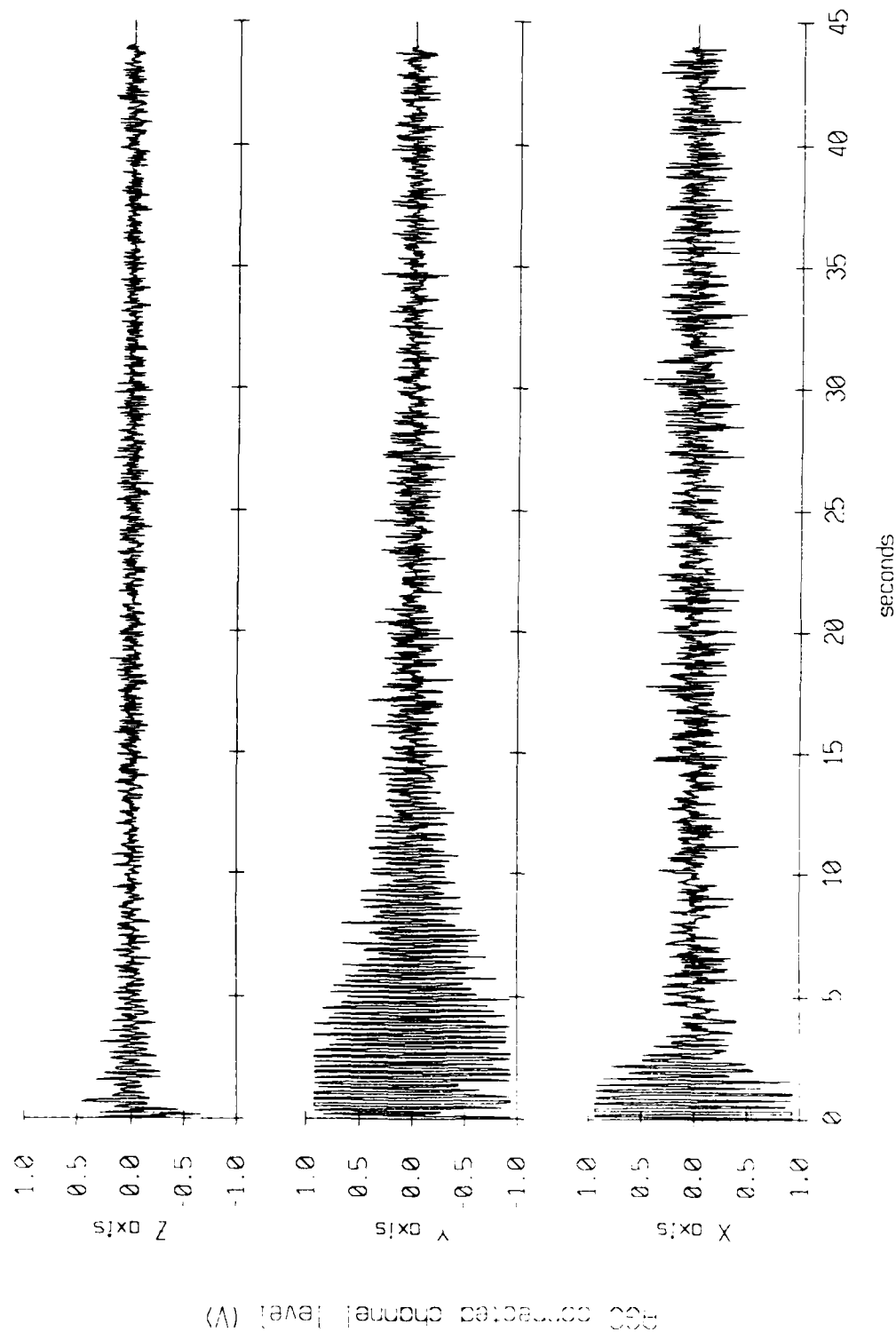


Figure 4.7h

Float 3, September 1986 Trip
 record 1607 velocity time series



PGC corrected channel level (V)

Figure 4.8a

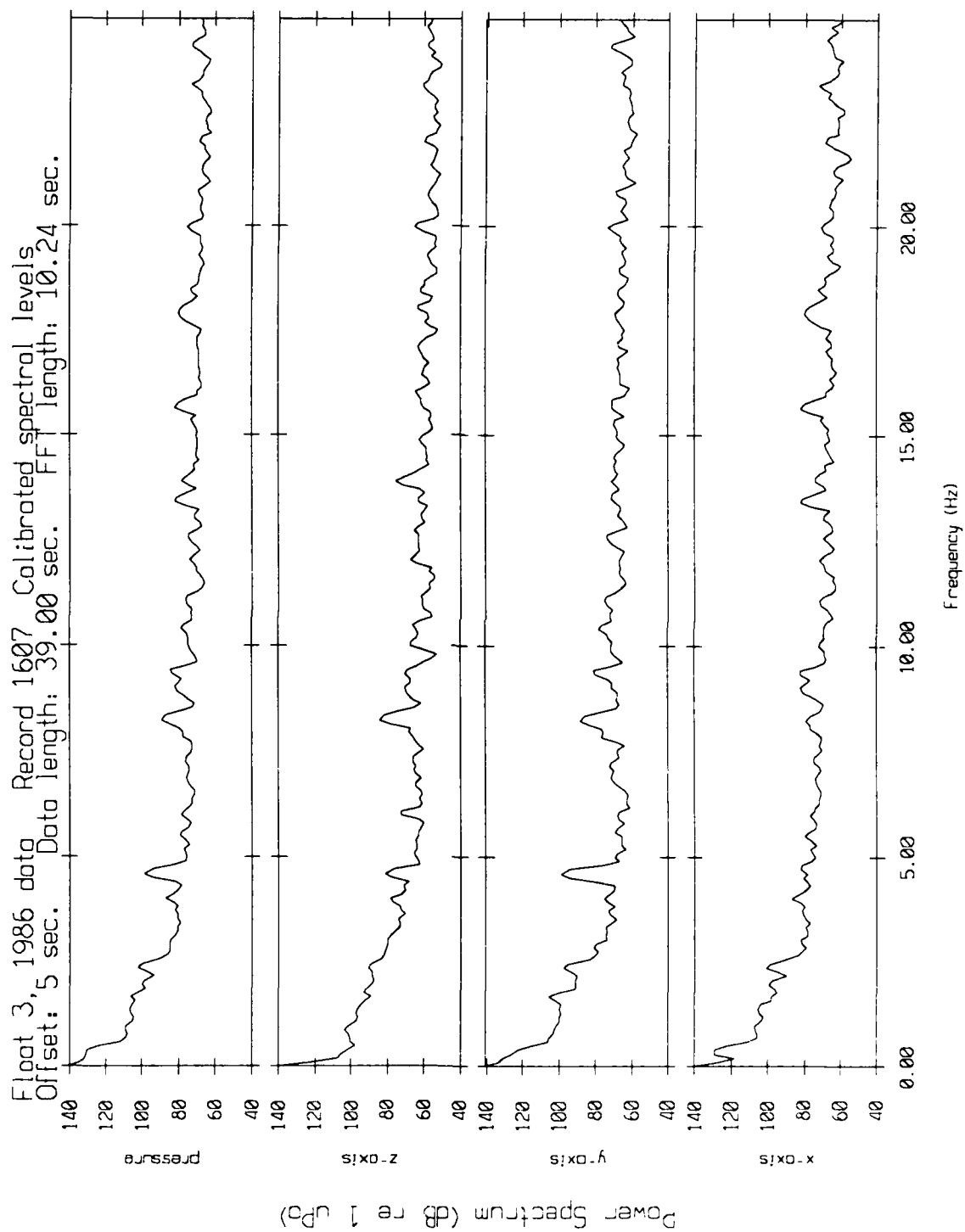
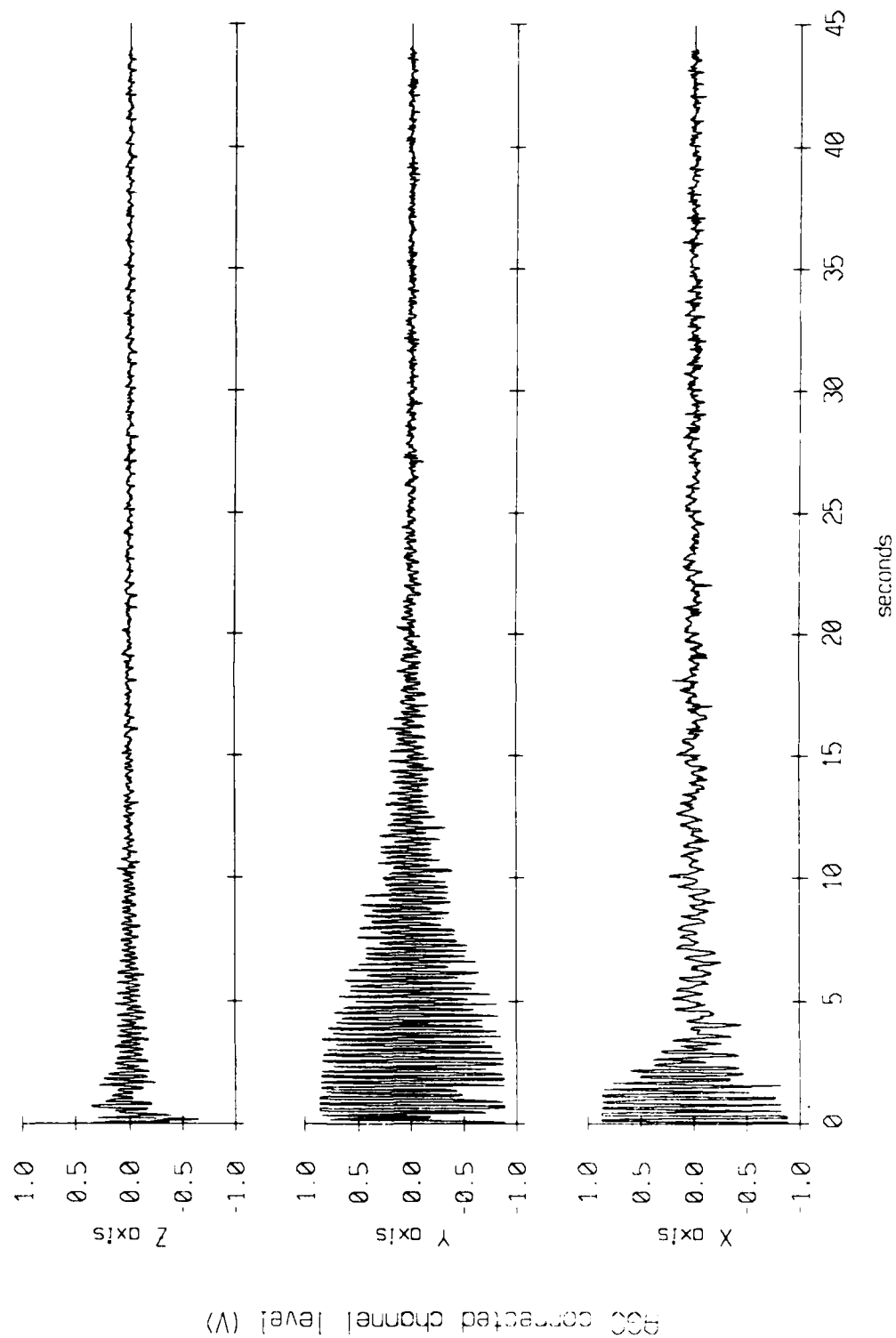


Figure 4.8b

Float 3, September 1986 Trip
60 record average, starting with record 1601



ADC connected channel level (V)

Figure 4.8c

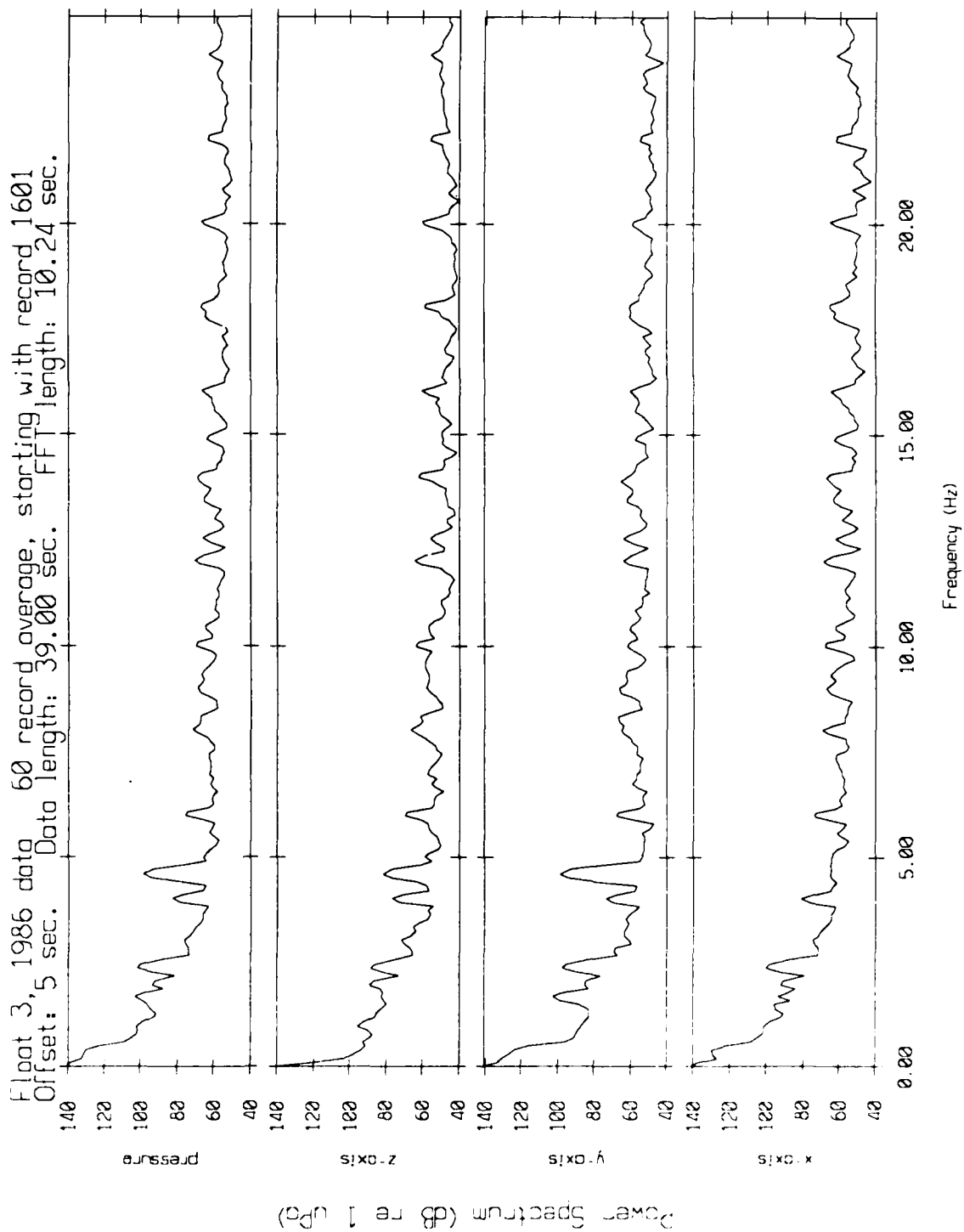


Figure 4.8d

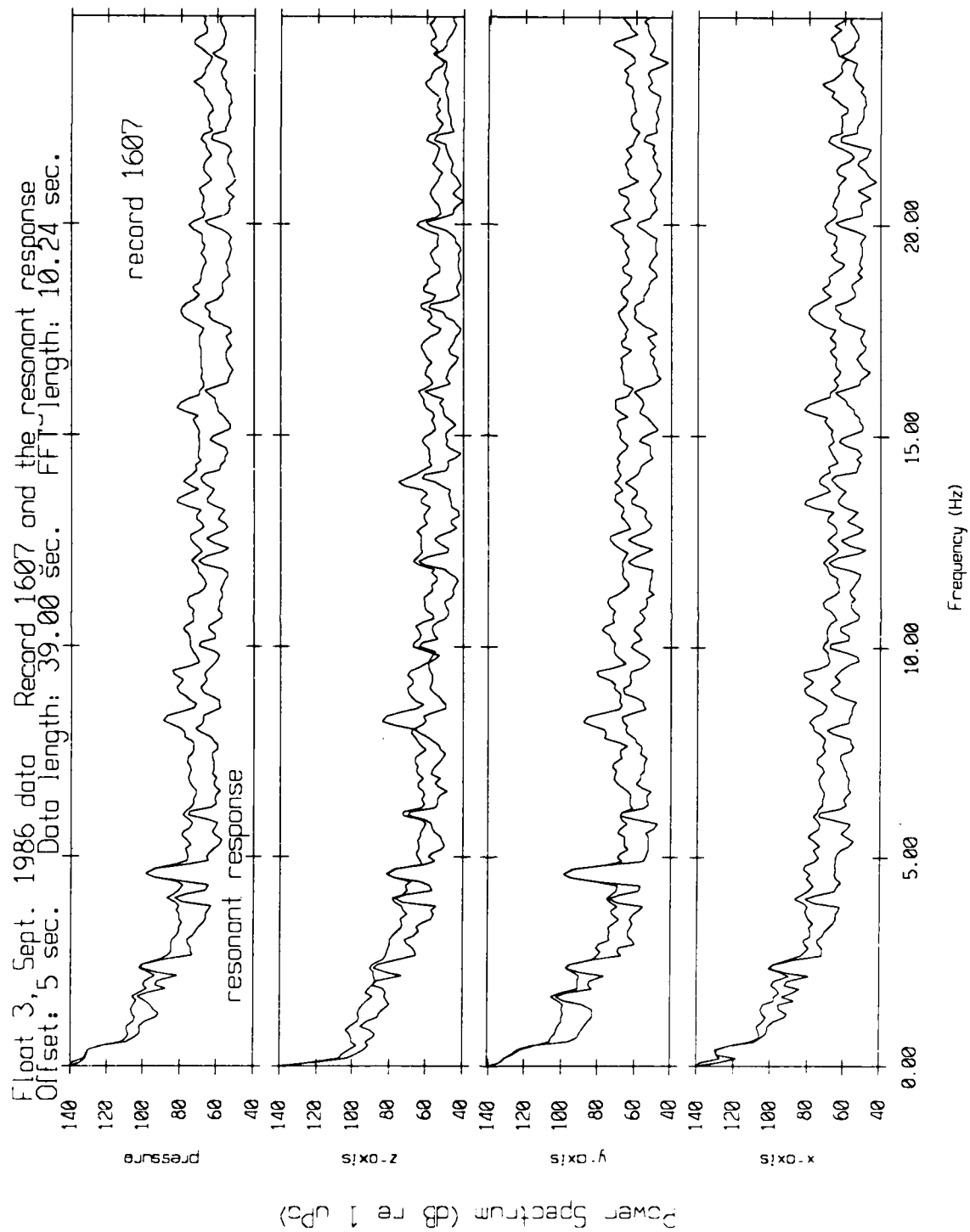
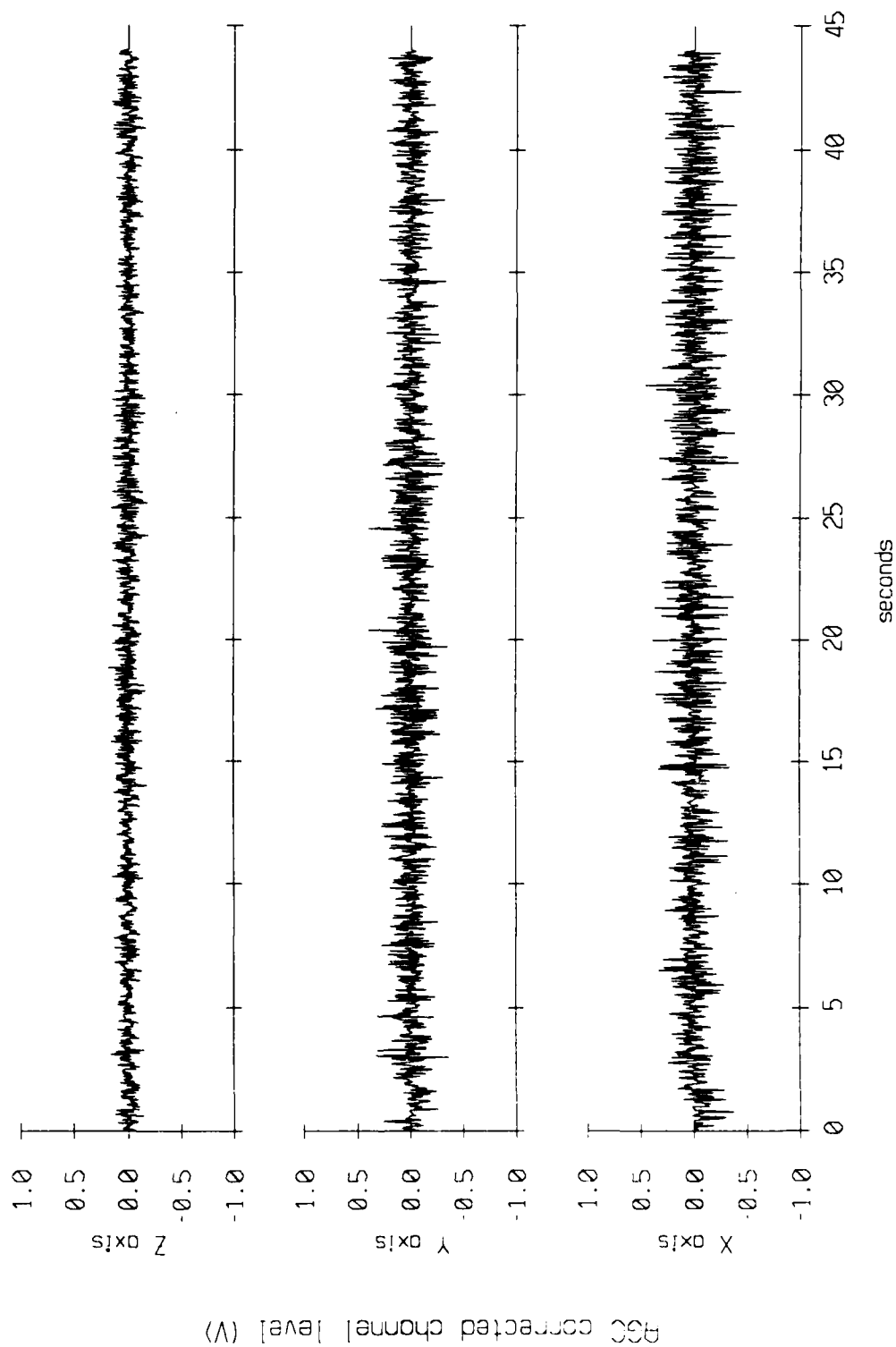


Figure 4.8e

Float 3 September 1986 Trip
 record 1607 with (1.0742 1.0537 1.0010) * r(n) subtracted



ASC corrected channel level (V)

Figure 4.8f

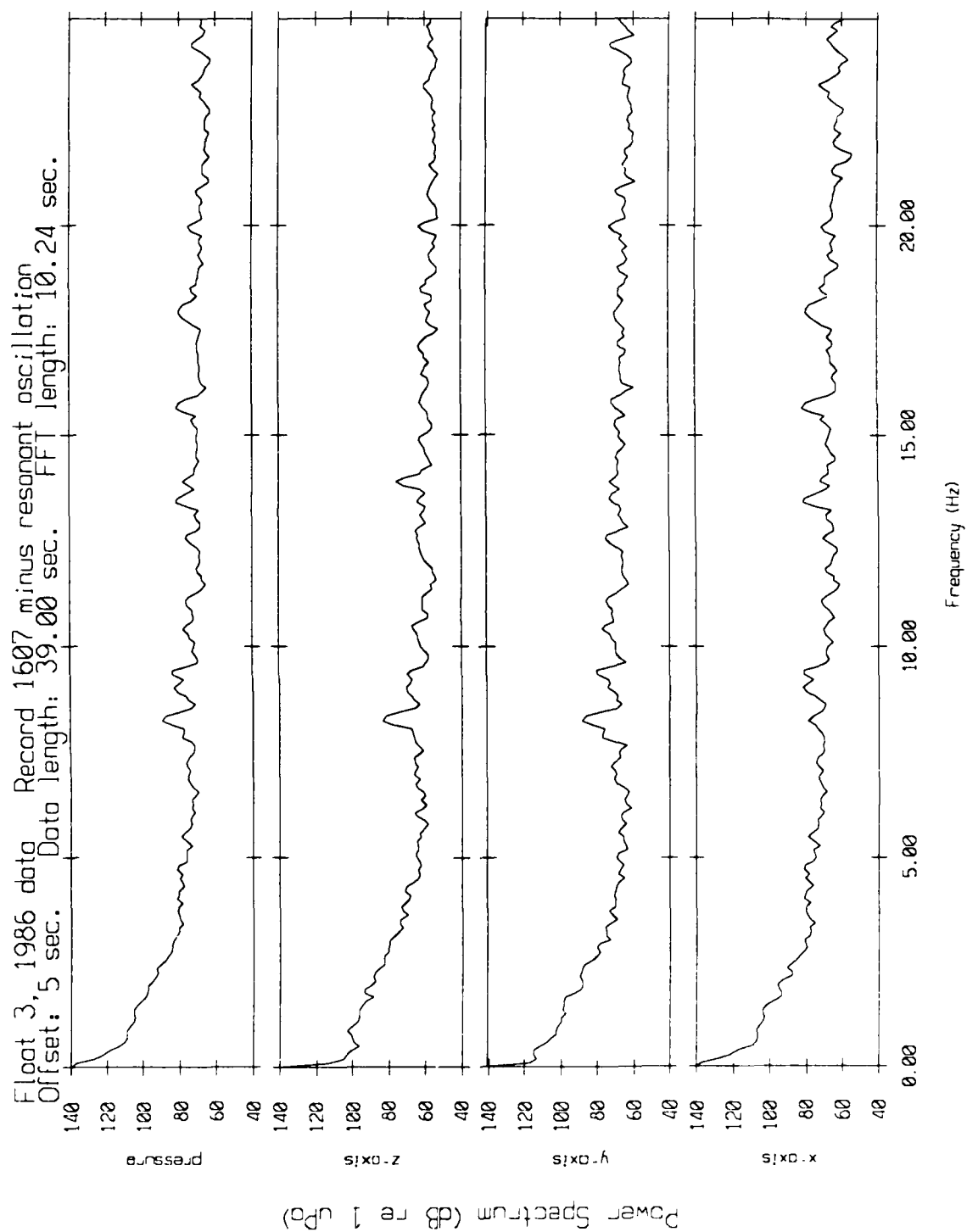


Figure 4.8g

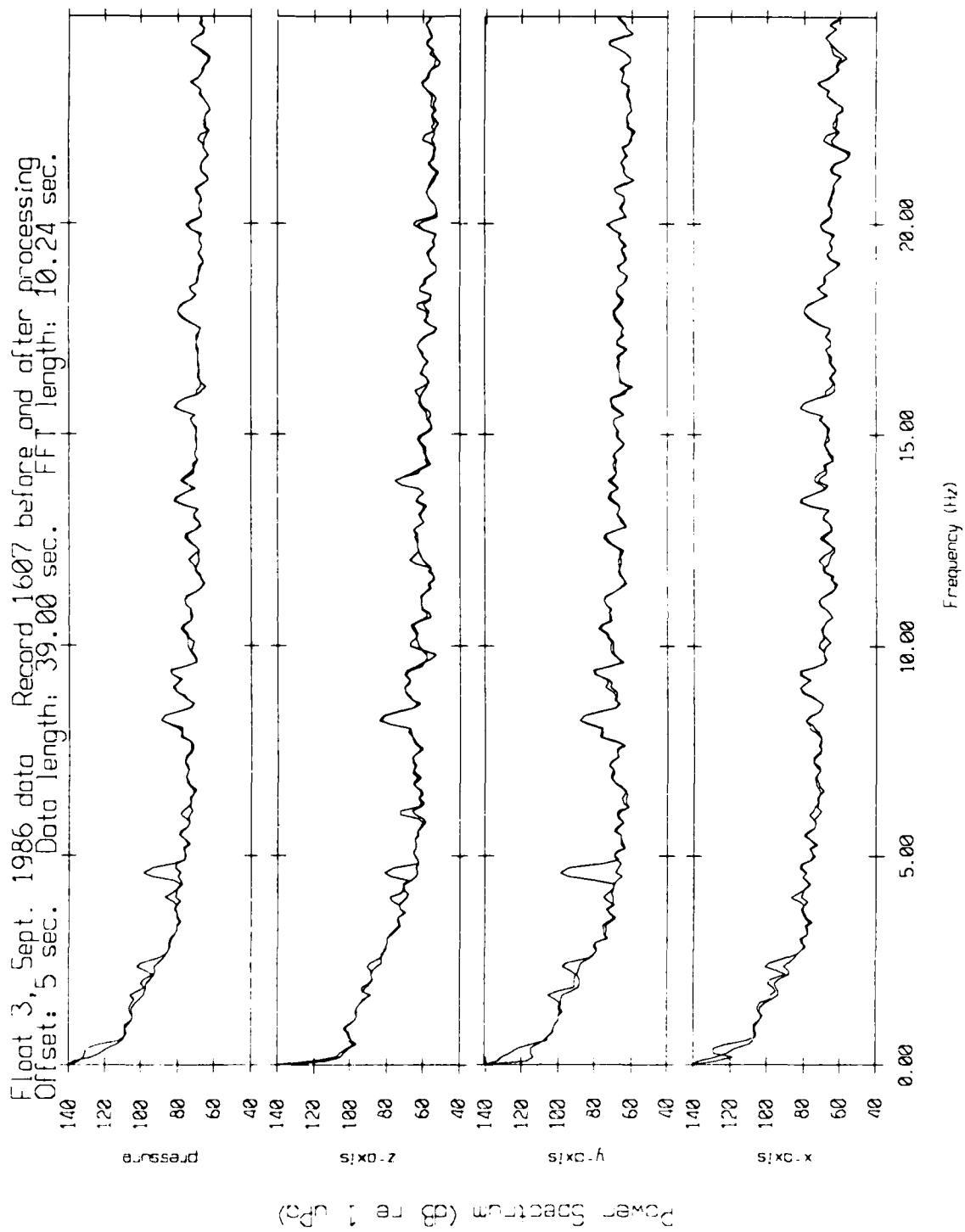


Figure 4.8h

Float 9, September 1986 Trip
 record 1207 velocity time series

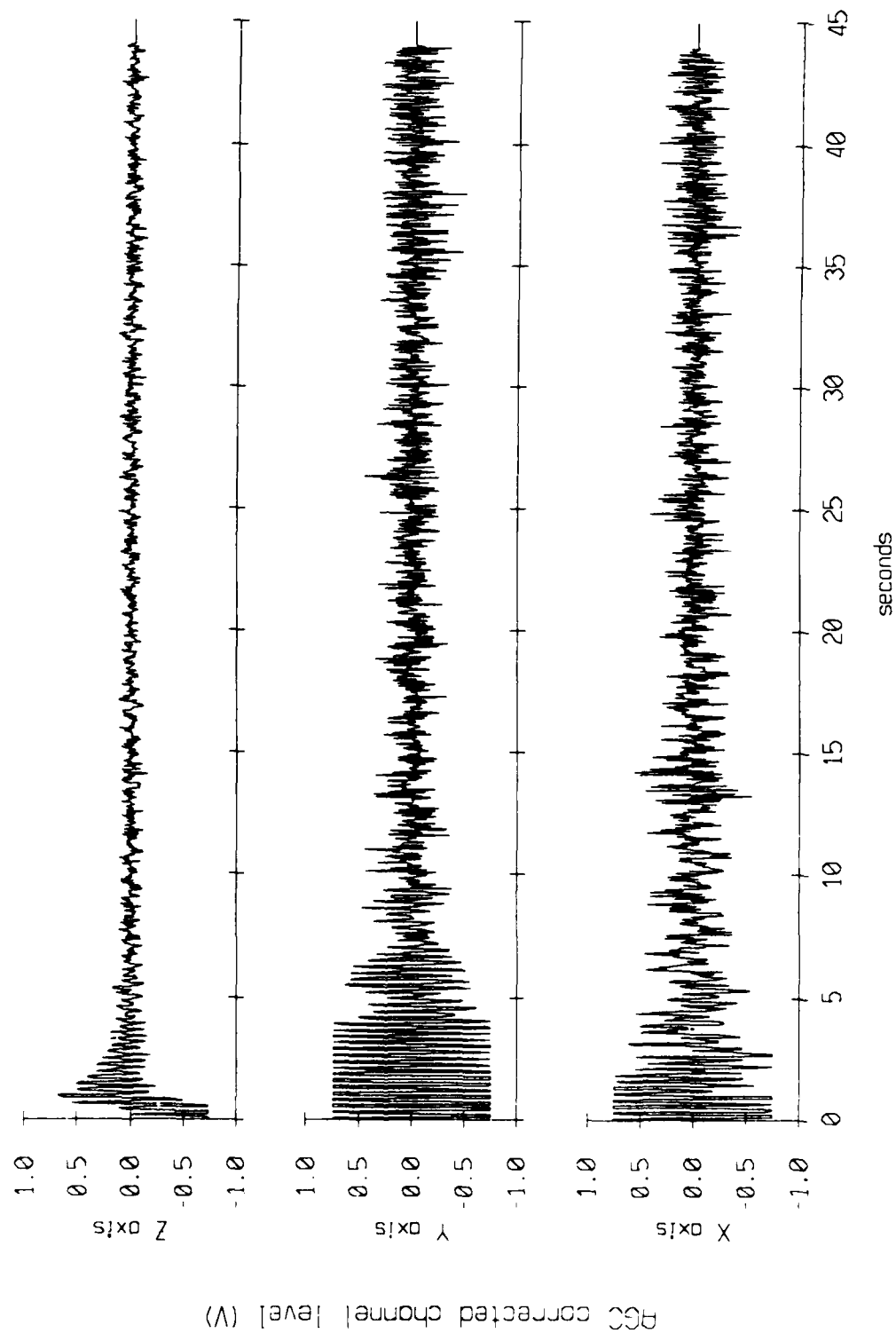


Figure 4.9a

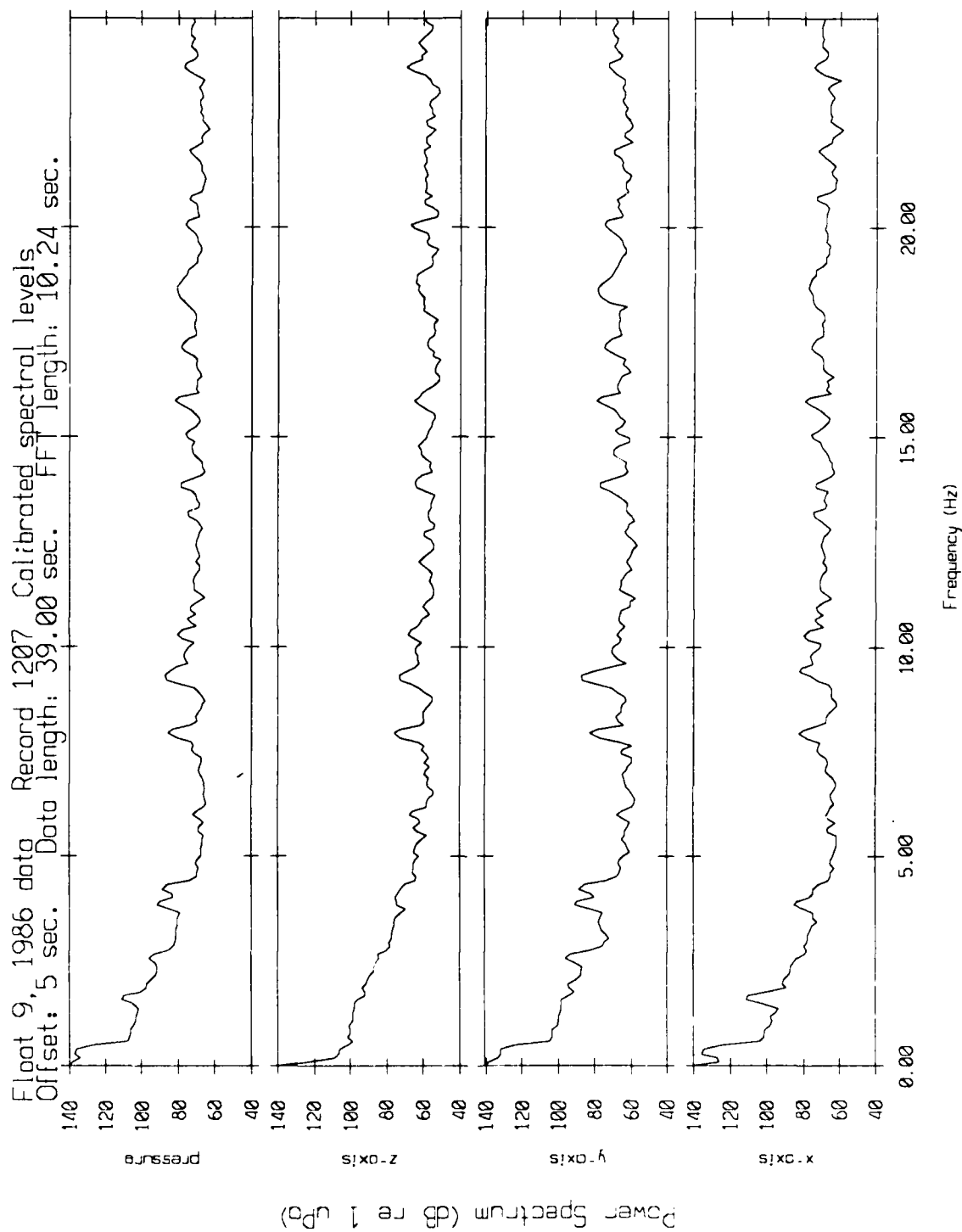


Figure 4.9b

Float 9, September 1986 Trip
40 record average, starting with record 1201

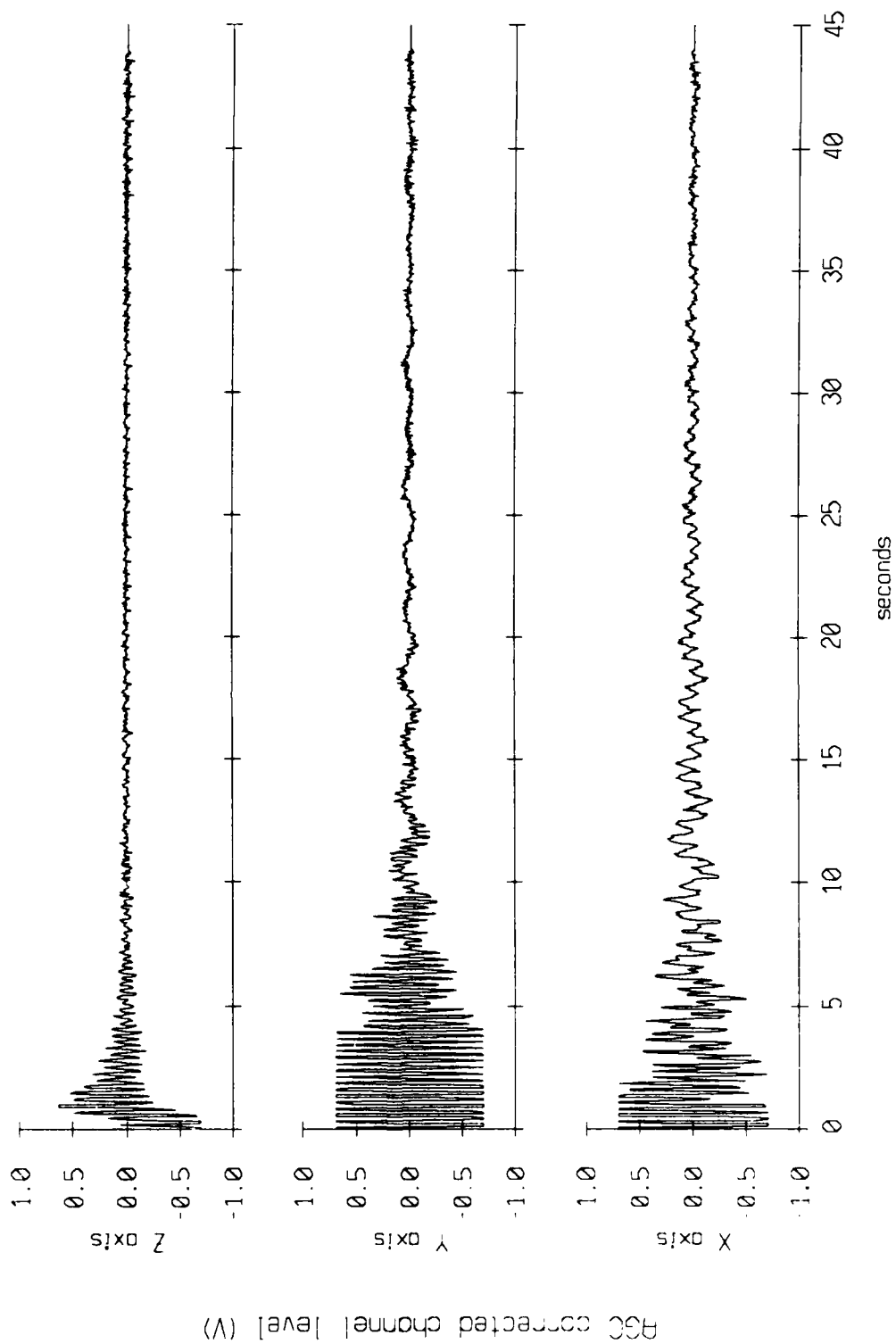


Figure 4.9c

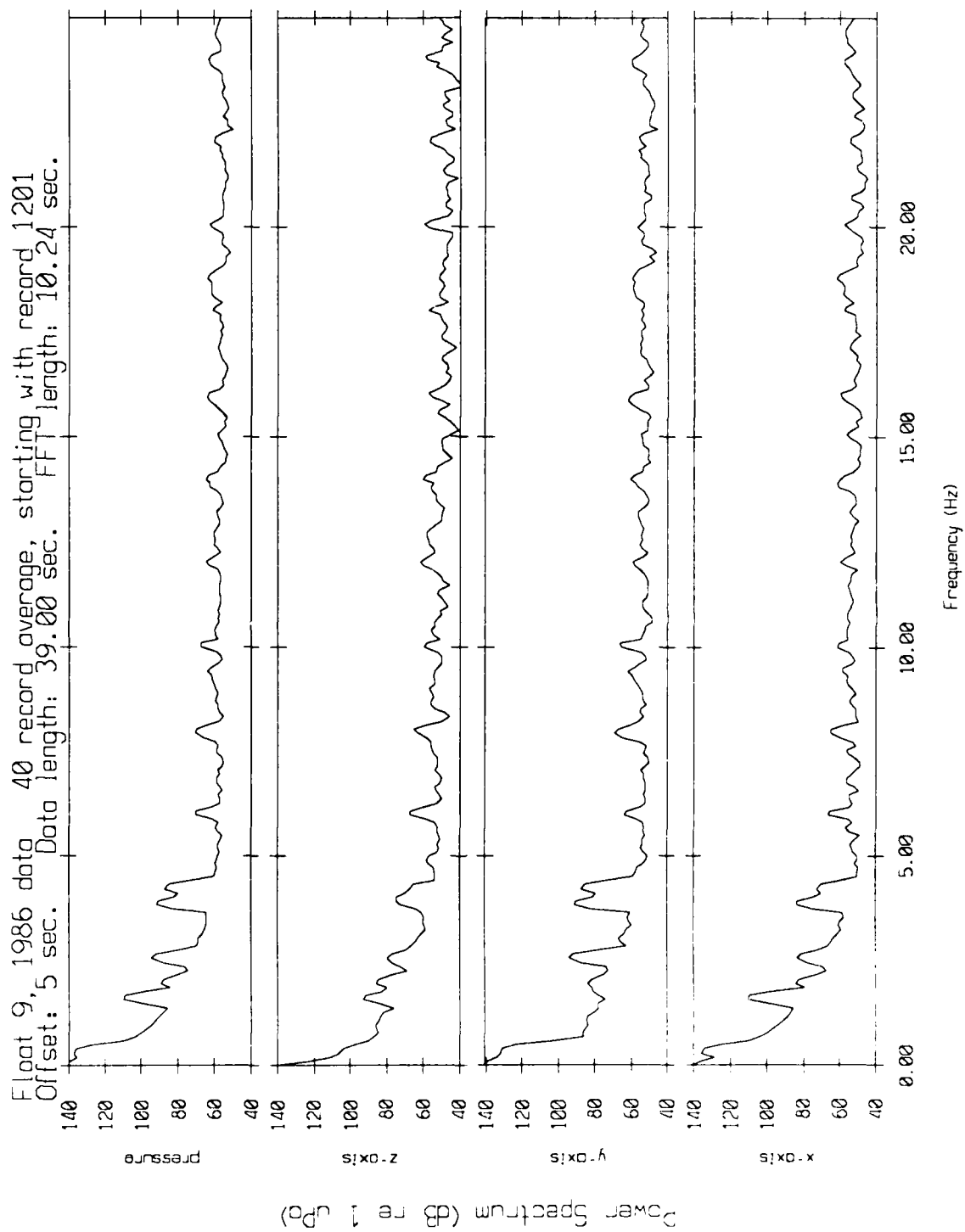


Figure 4.9d

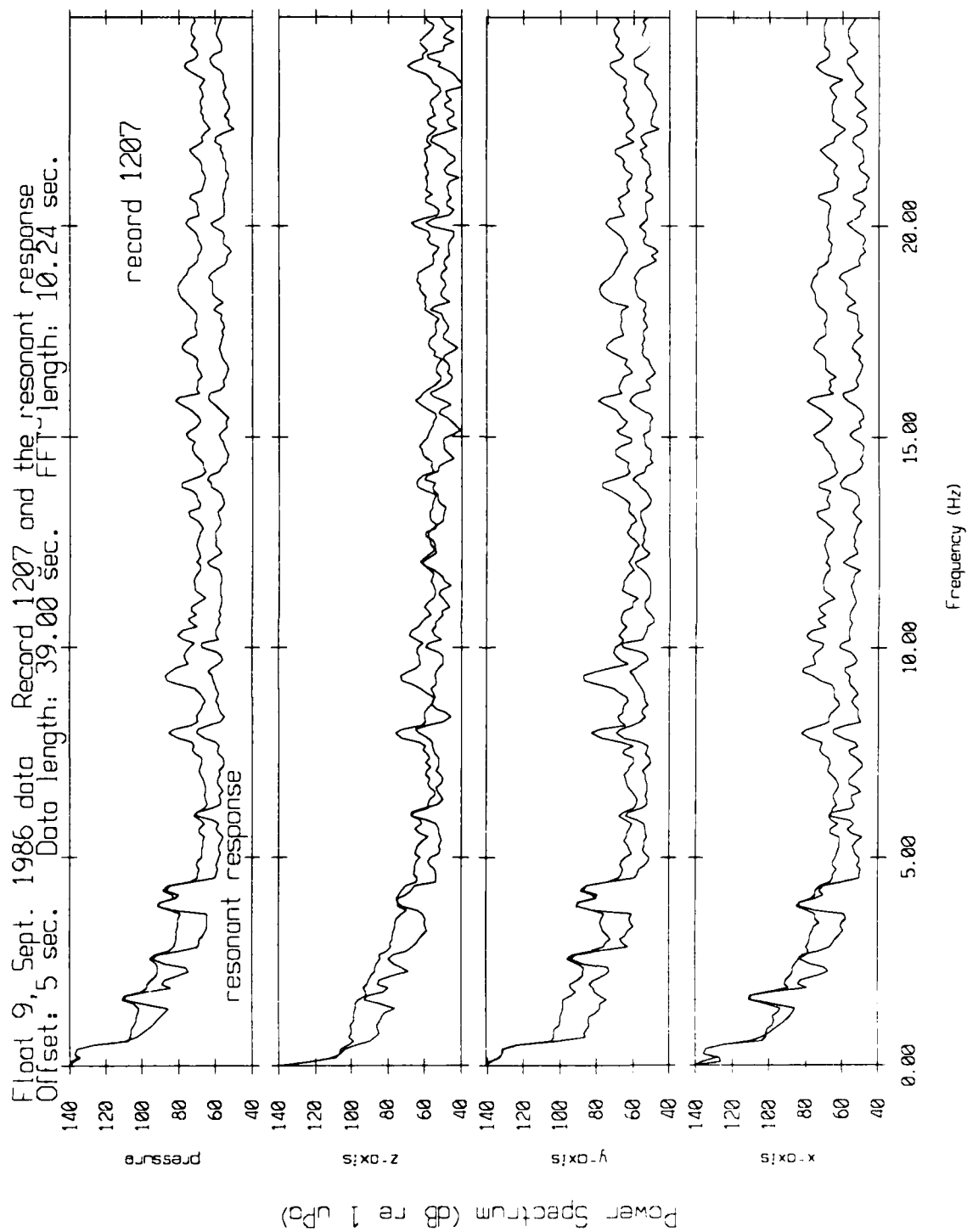


Figure 4.9e

Float 9, September 1986 Trip
 record 1207 with (1.0609 1.0510 1.0349) * r(n) subtracted

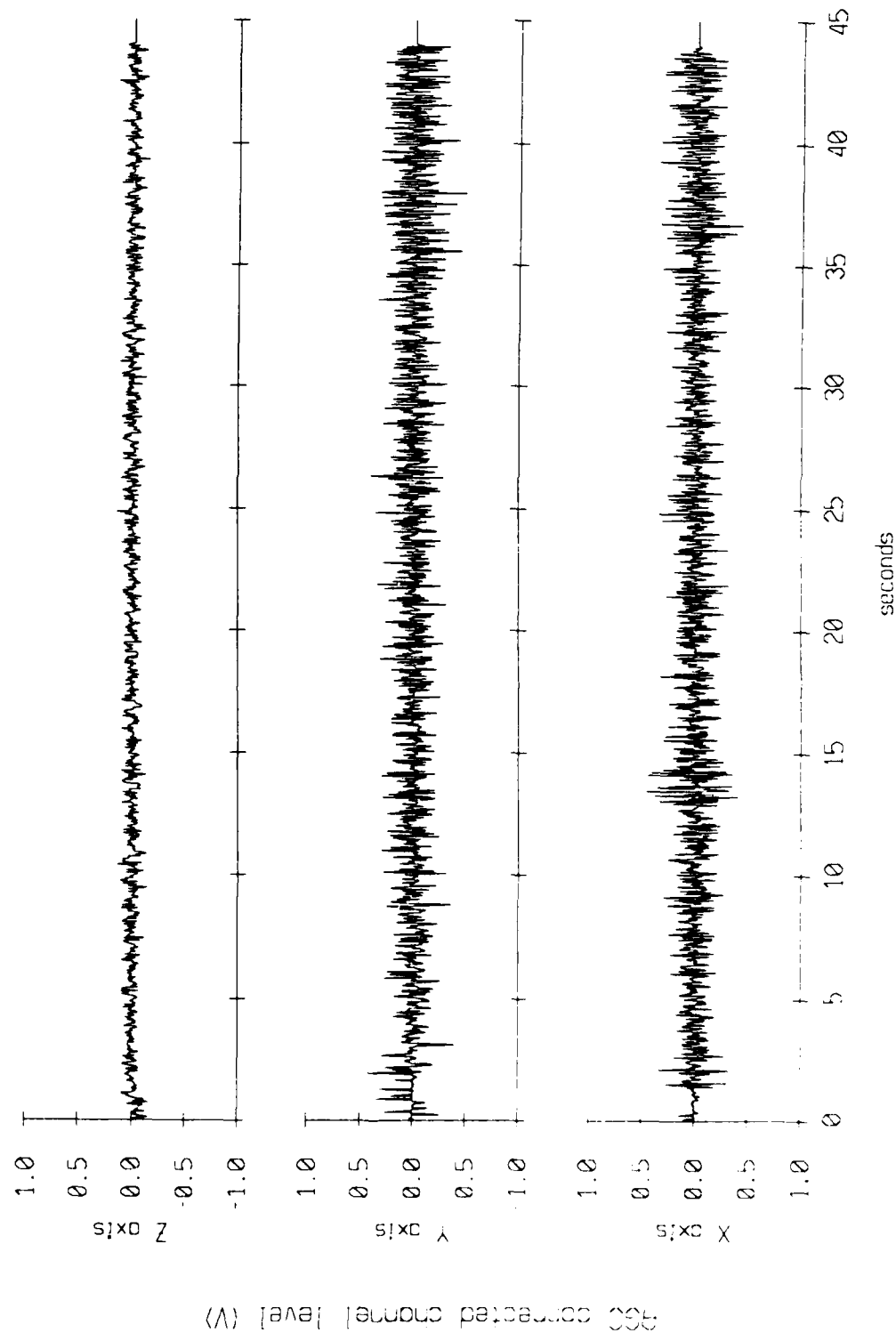


Figure 4.9f

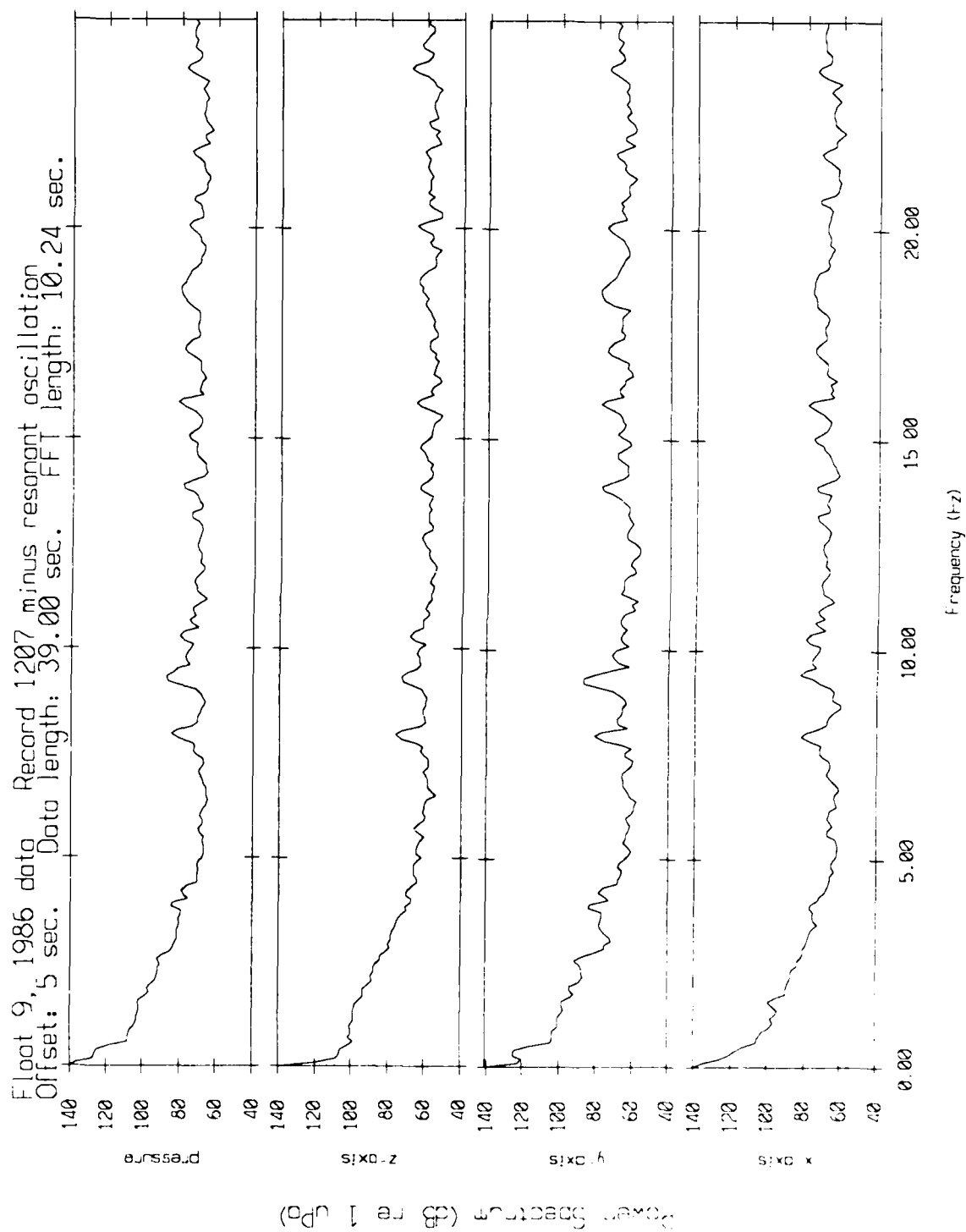


Figure 4.9g

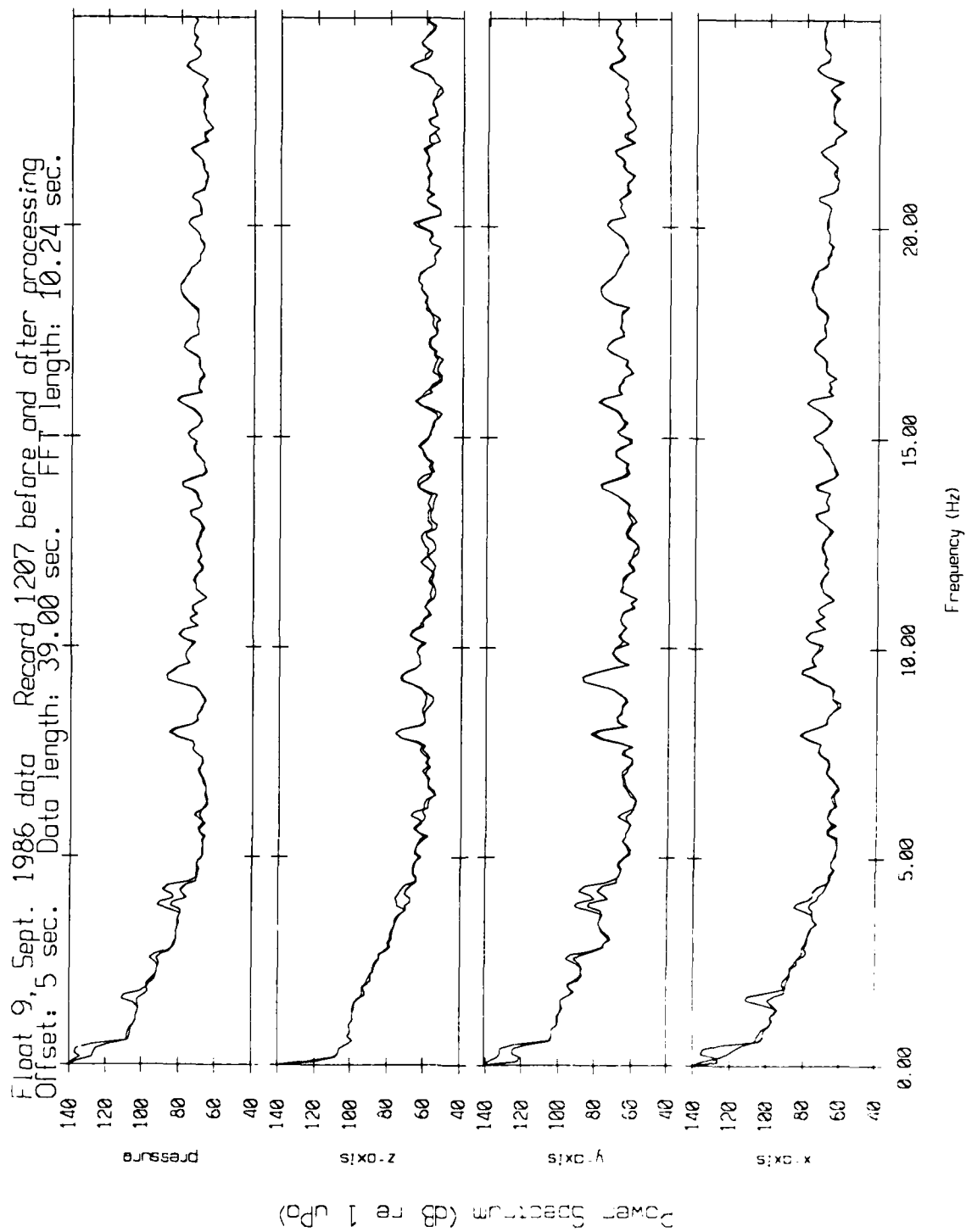


Figure 4.9h

August 9, September 1986 Trip
 record 1627 velocity time series

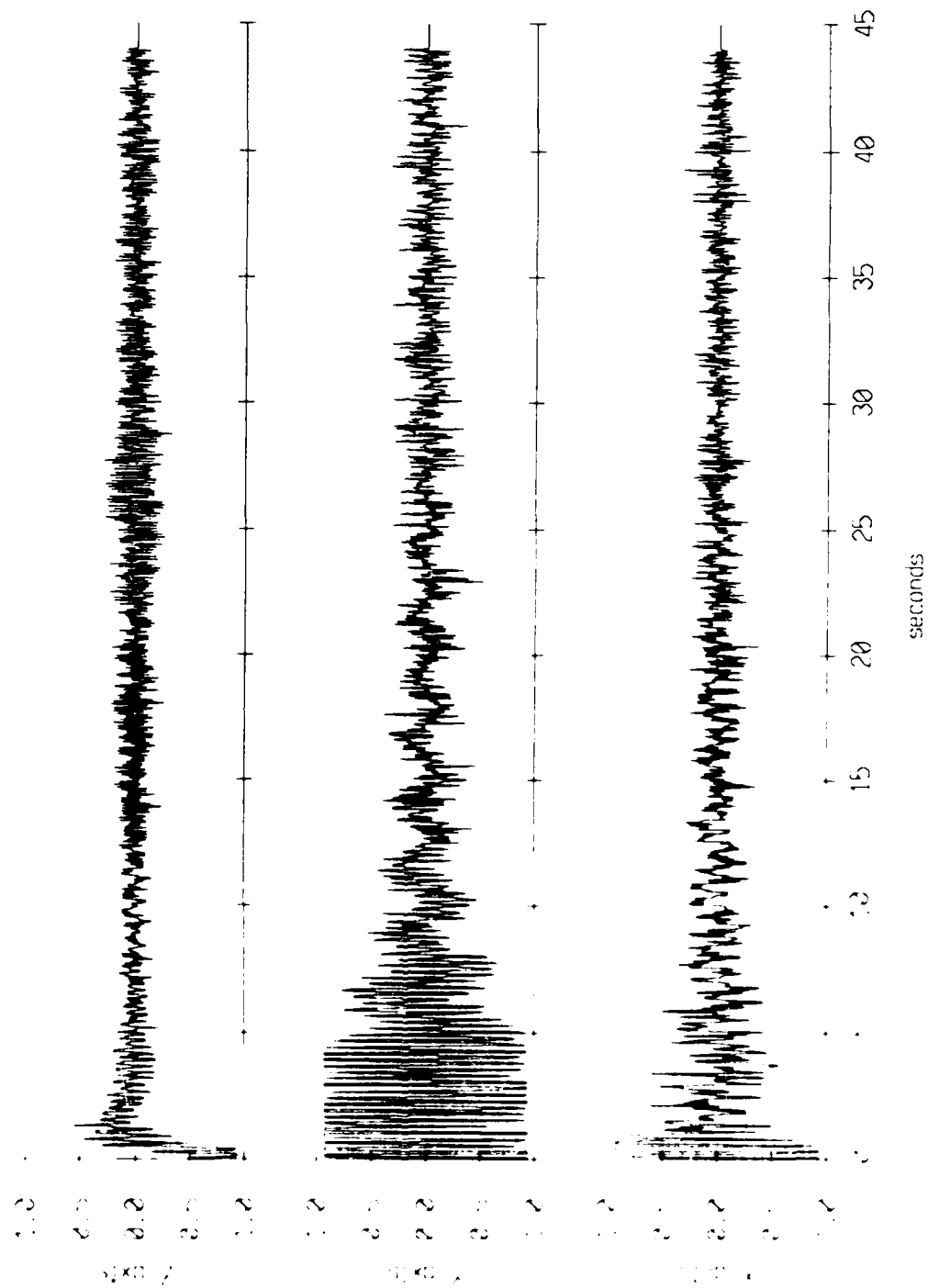


Figure 4.10a

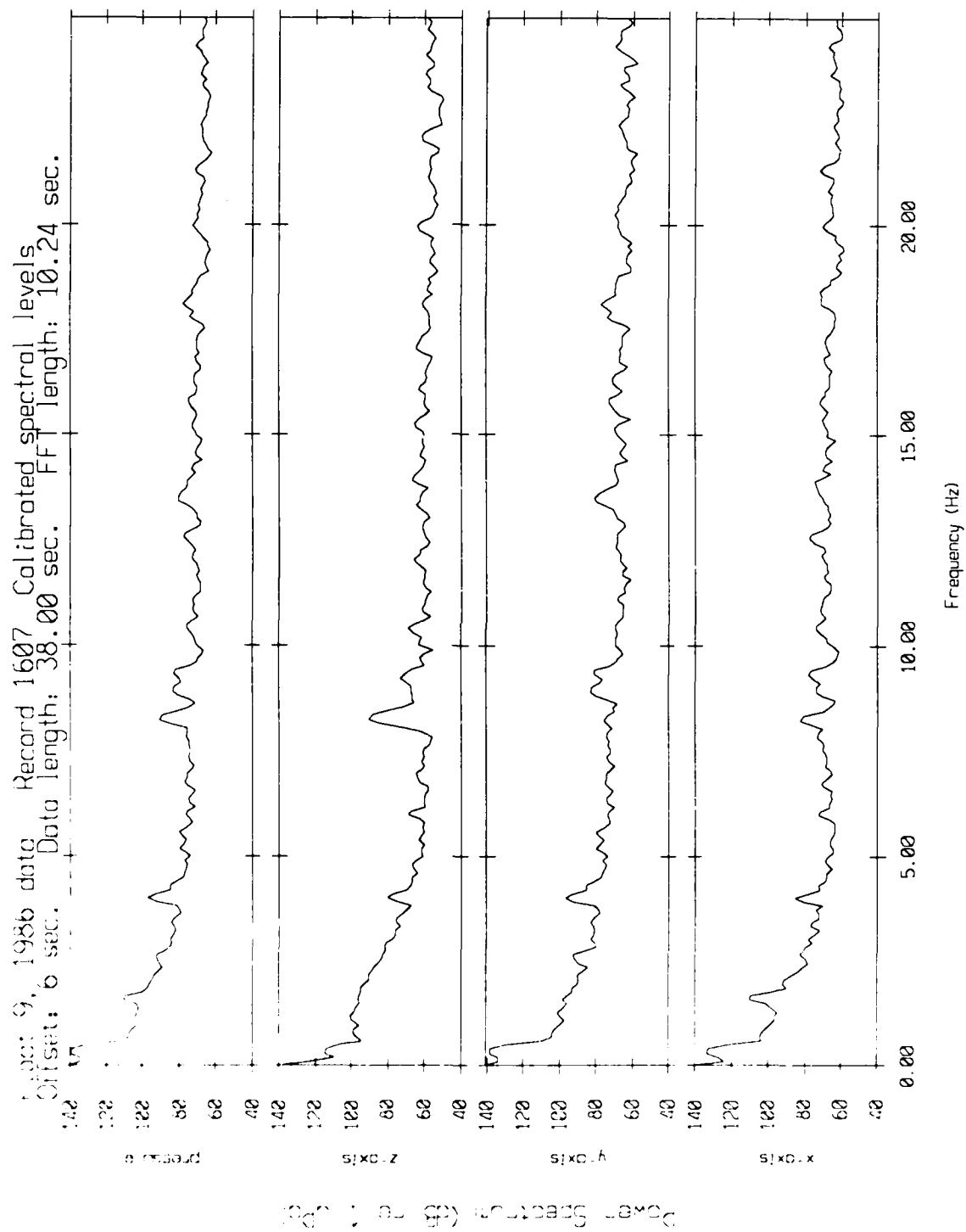


Figure 4.10b

Float 9, September 1986 Trip
40 record average, starting with record 1601

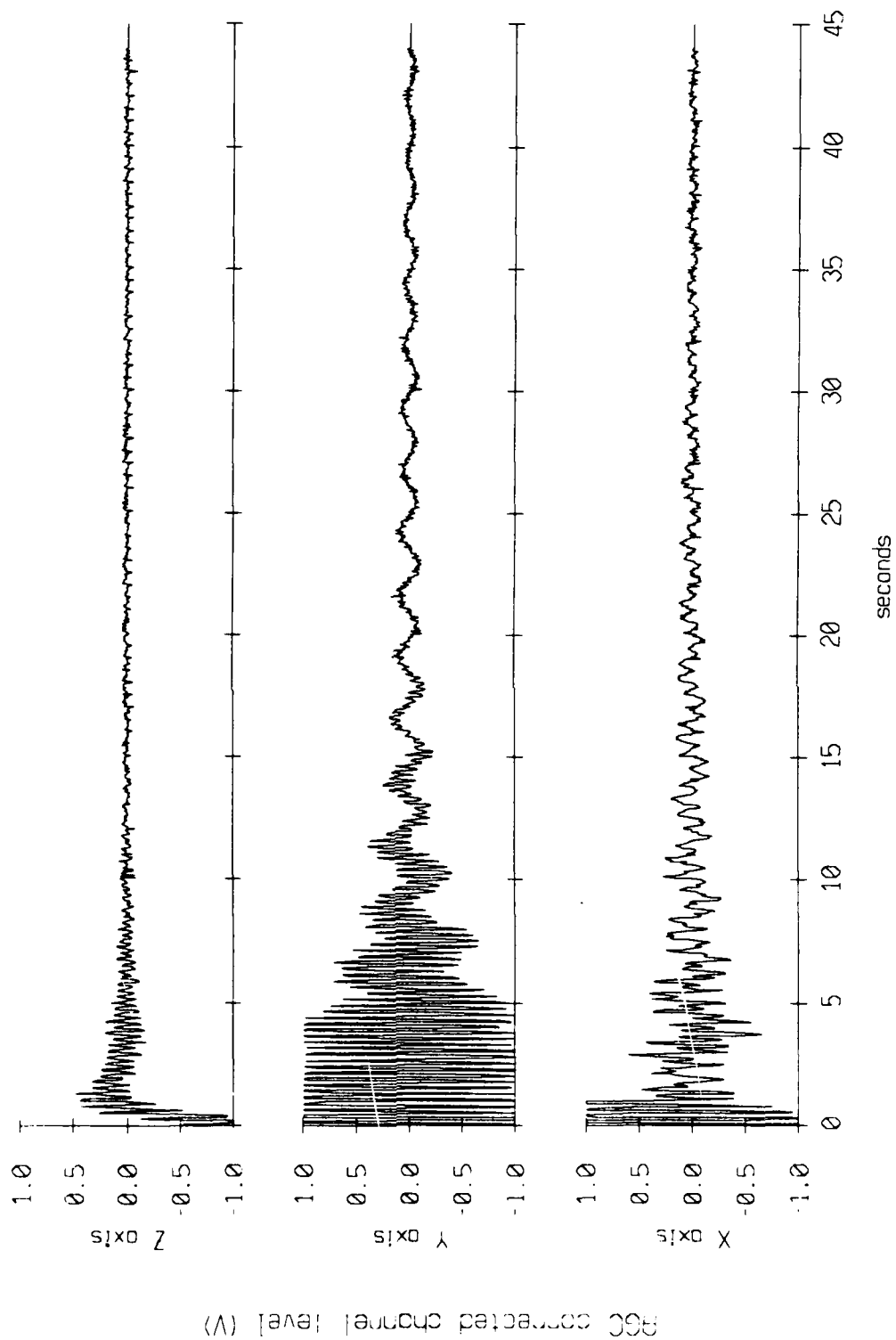


Figure 4.10c

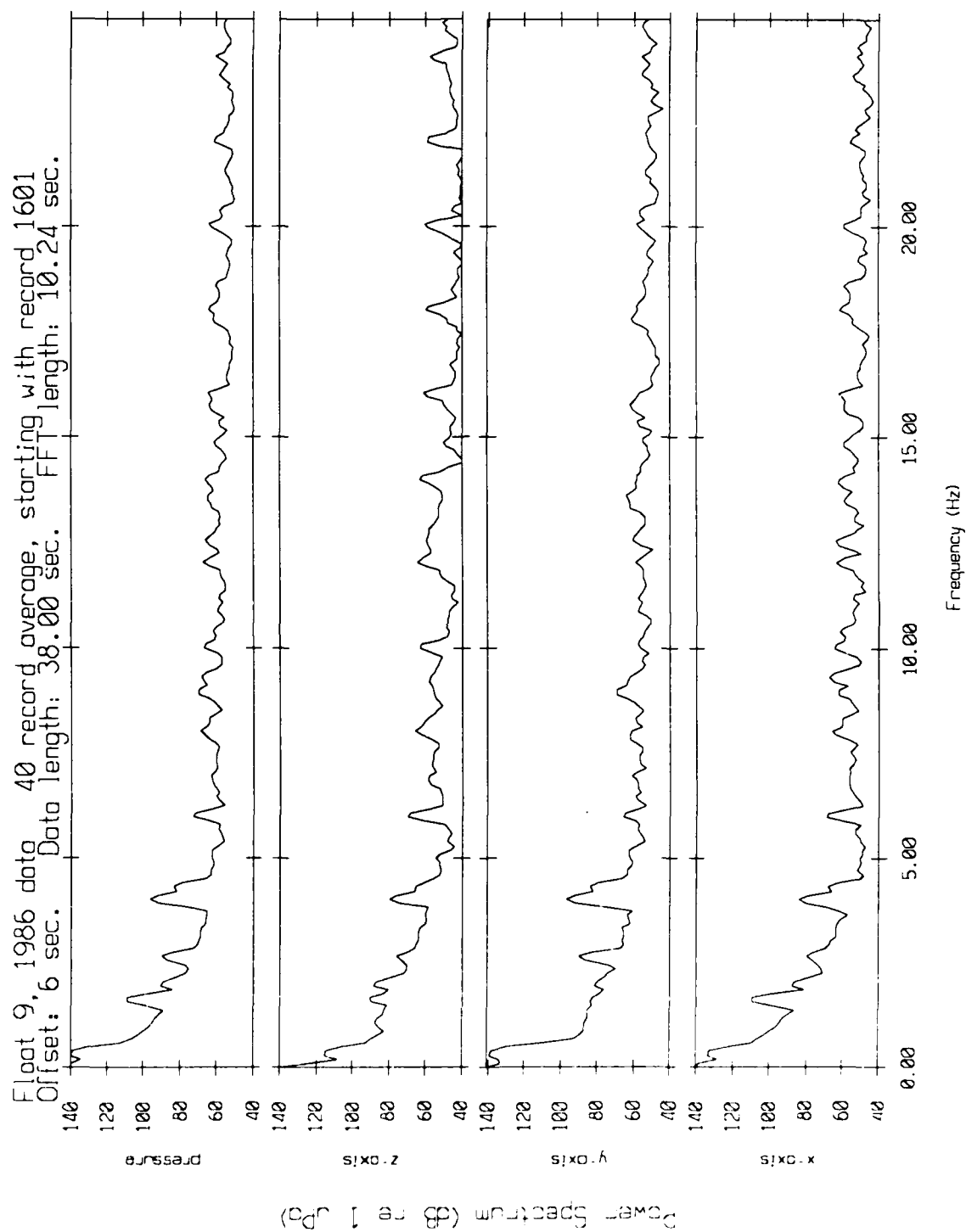


Figure 4.10d

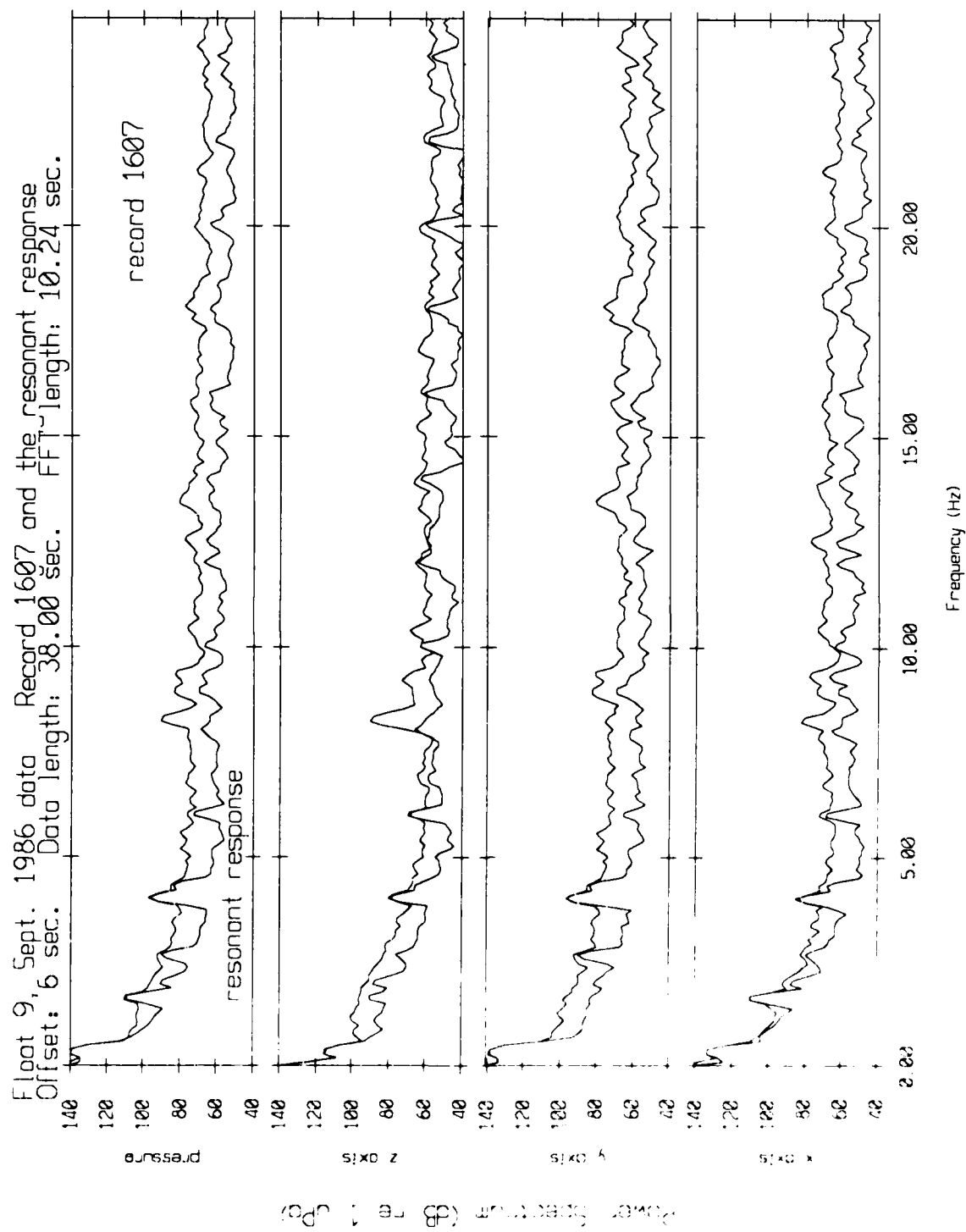


Figure 4.10e

about 9 September 1986 Trip
 record 1607 with (0.96009 0.95627 0.97934) * r(n) subtracted

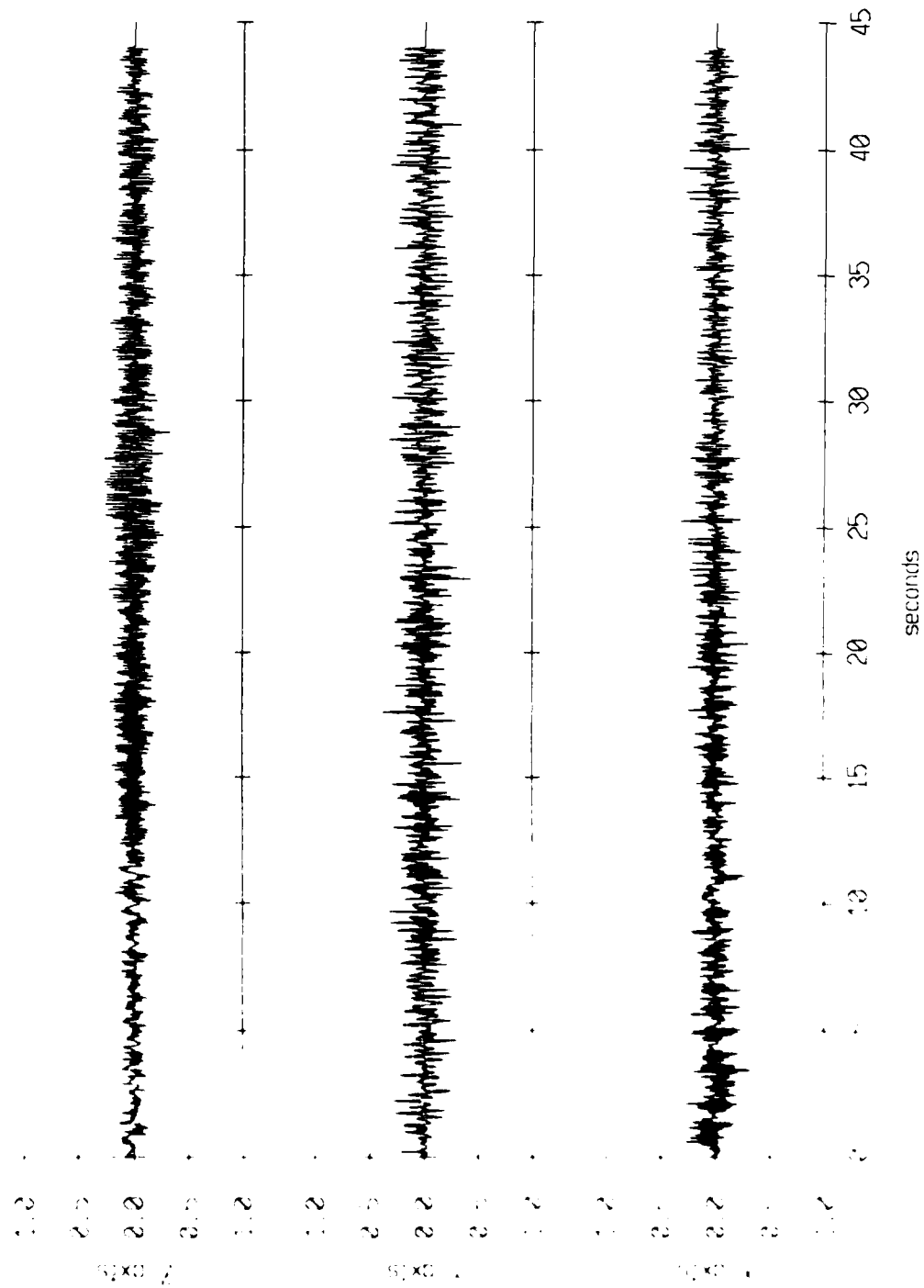


Figure 4.10f

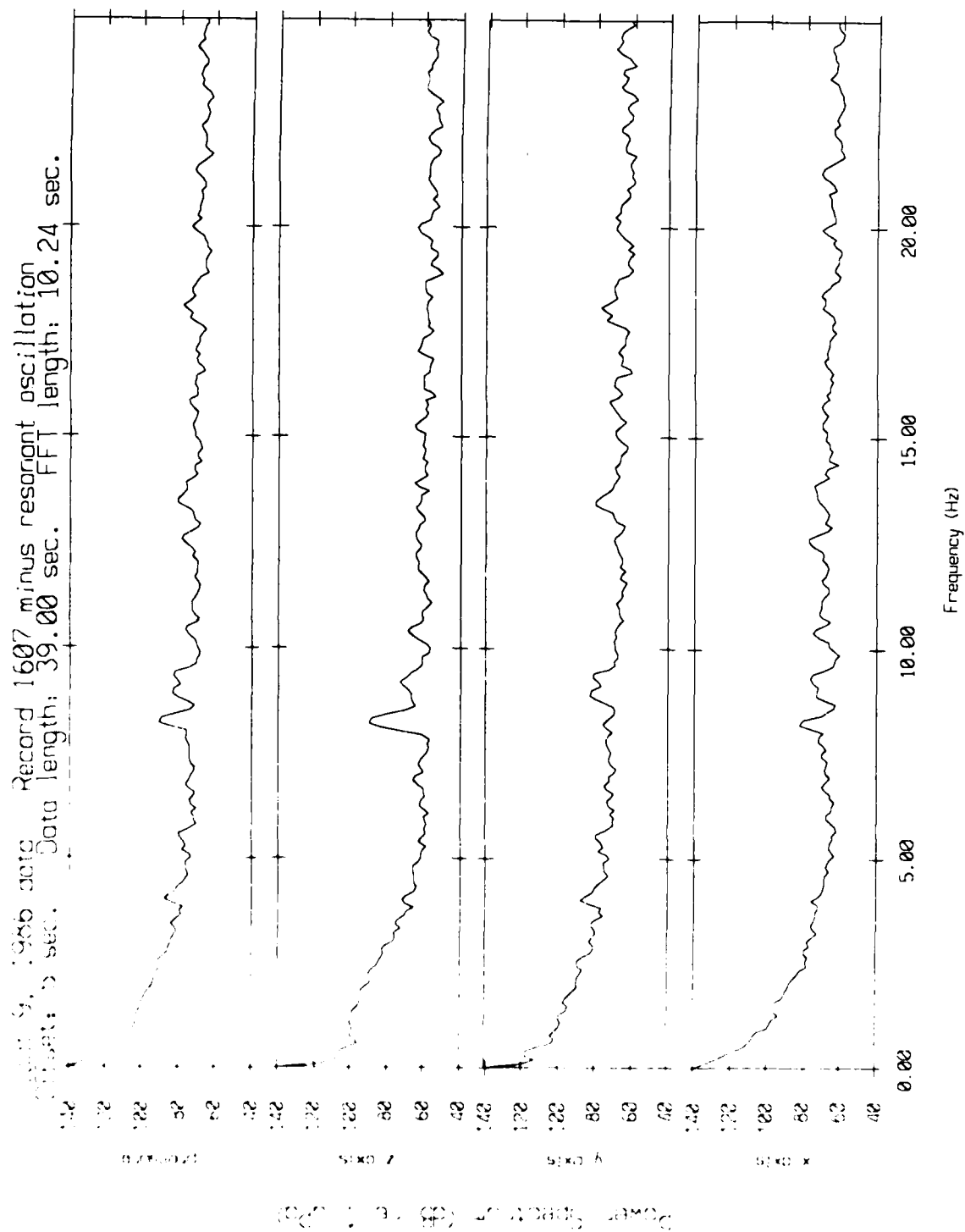


Figure 4.10g

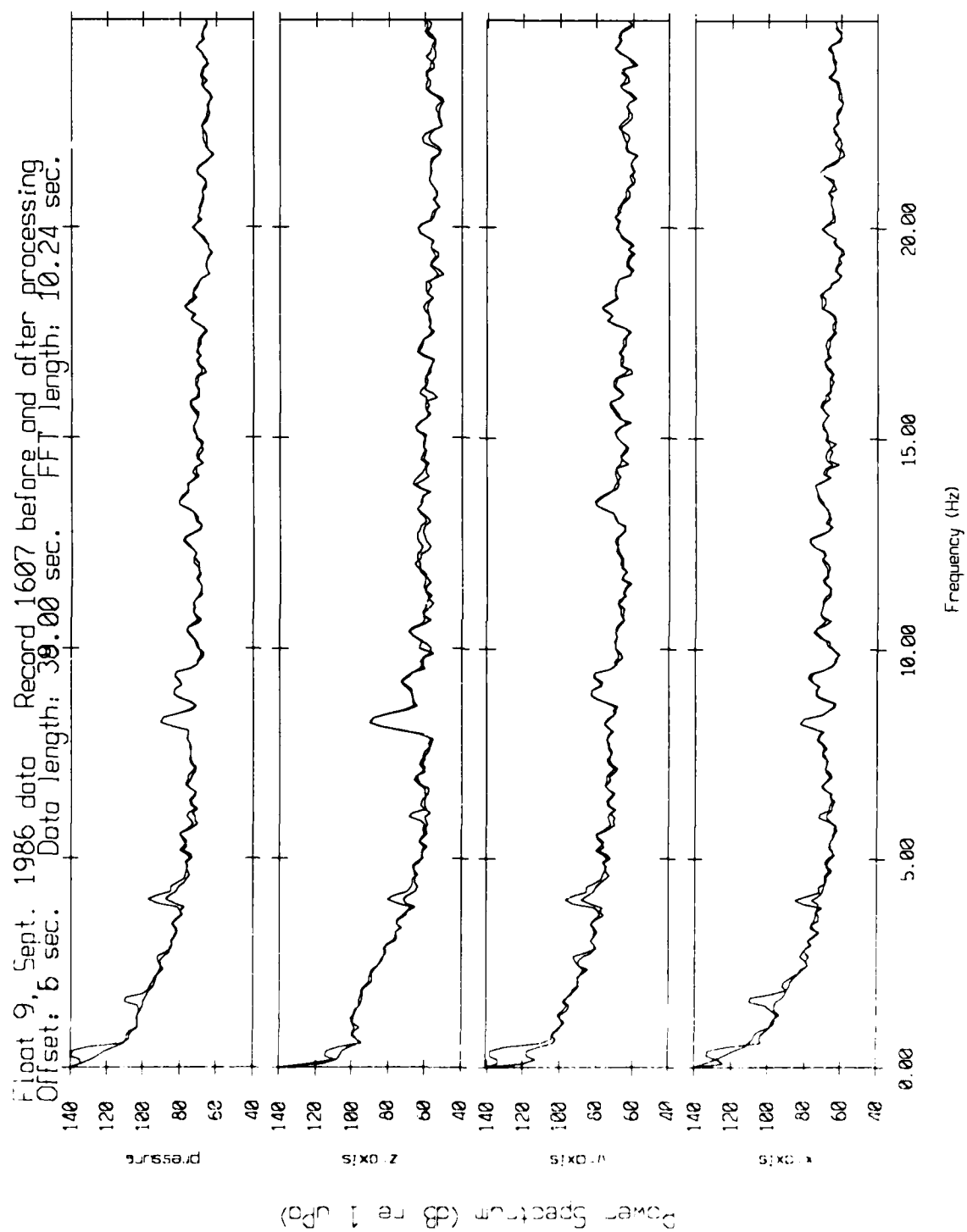


Figure 4.10h

Float 10, September 1986 Trip
 record 1207 velocity time series

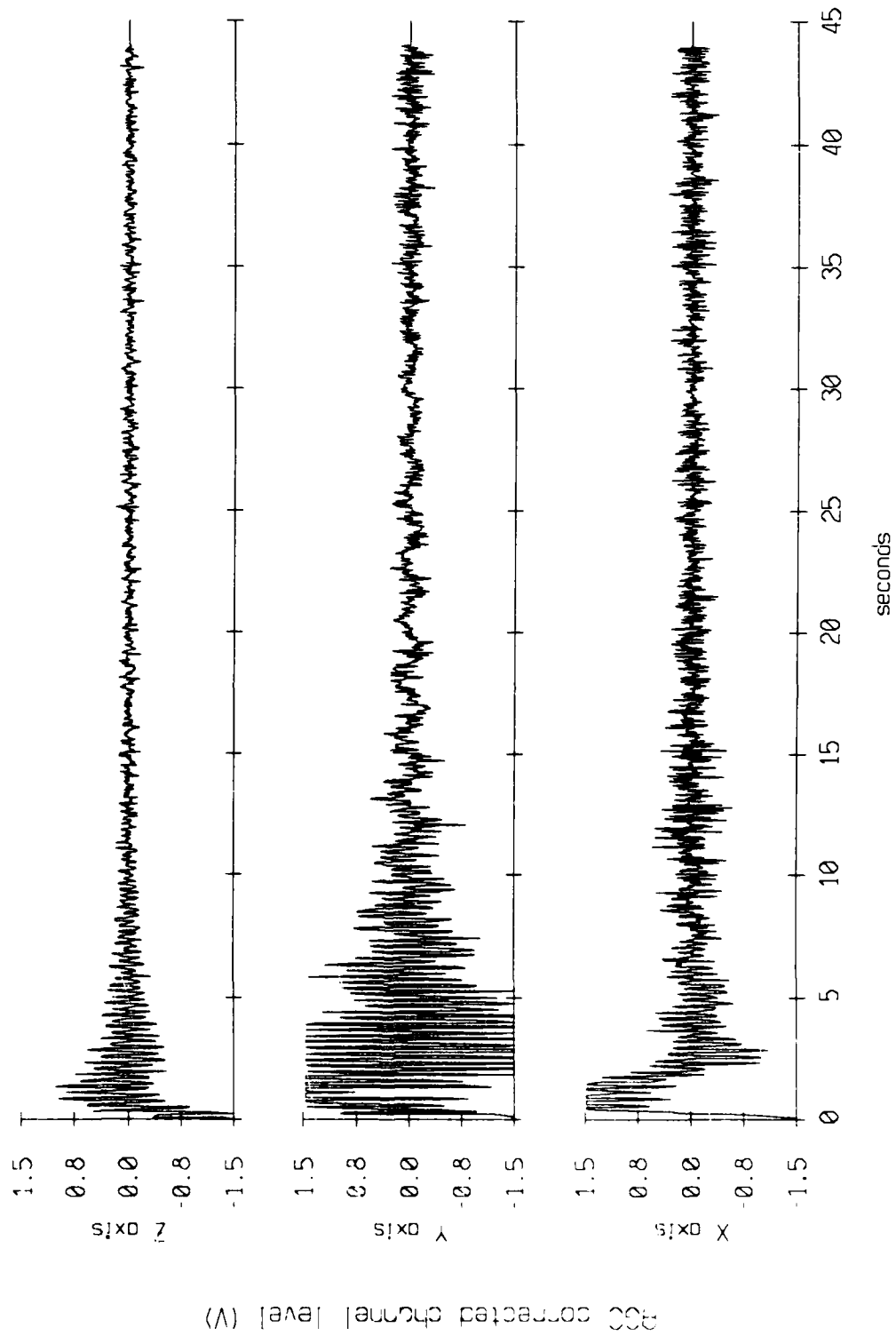


Figure 4.11a

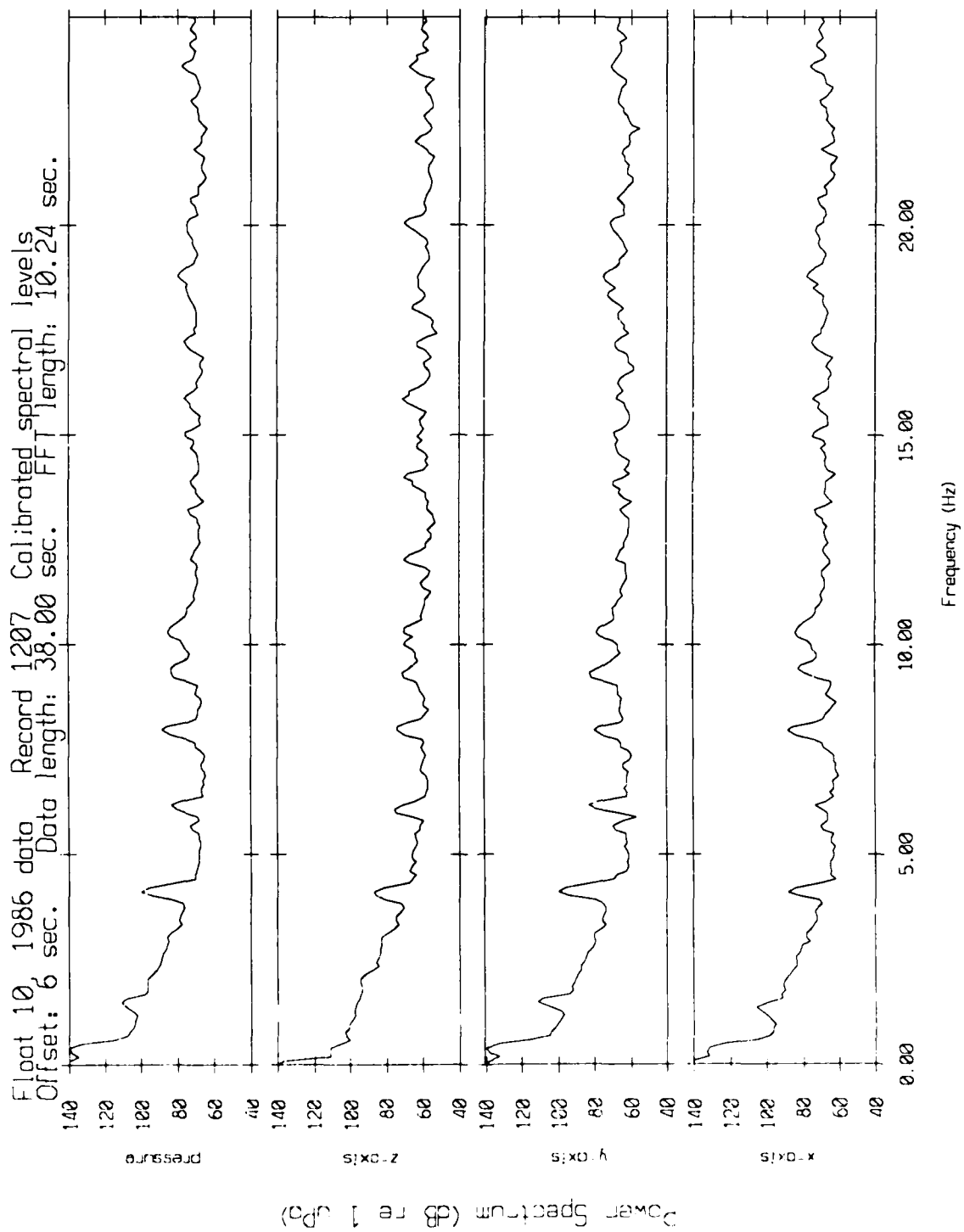


Figure 4.11b

Float 10, September 1986 Trip
 40 record average, starting with record 1201

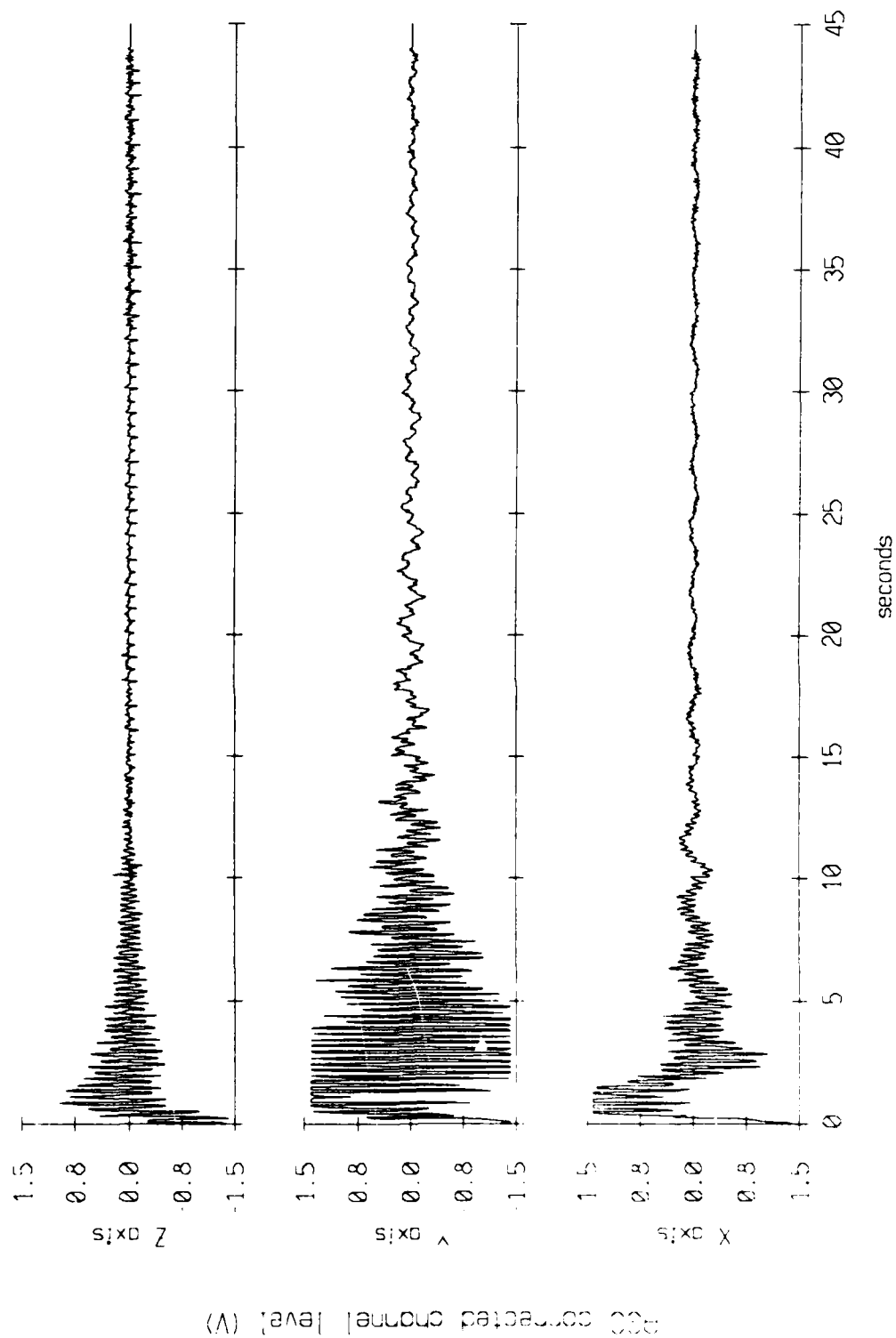


Figure 4.11c

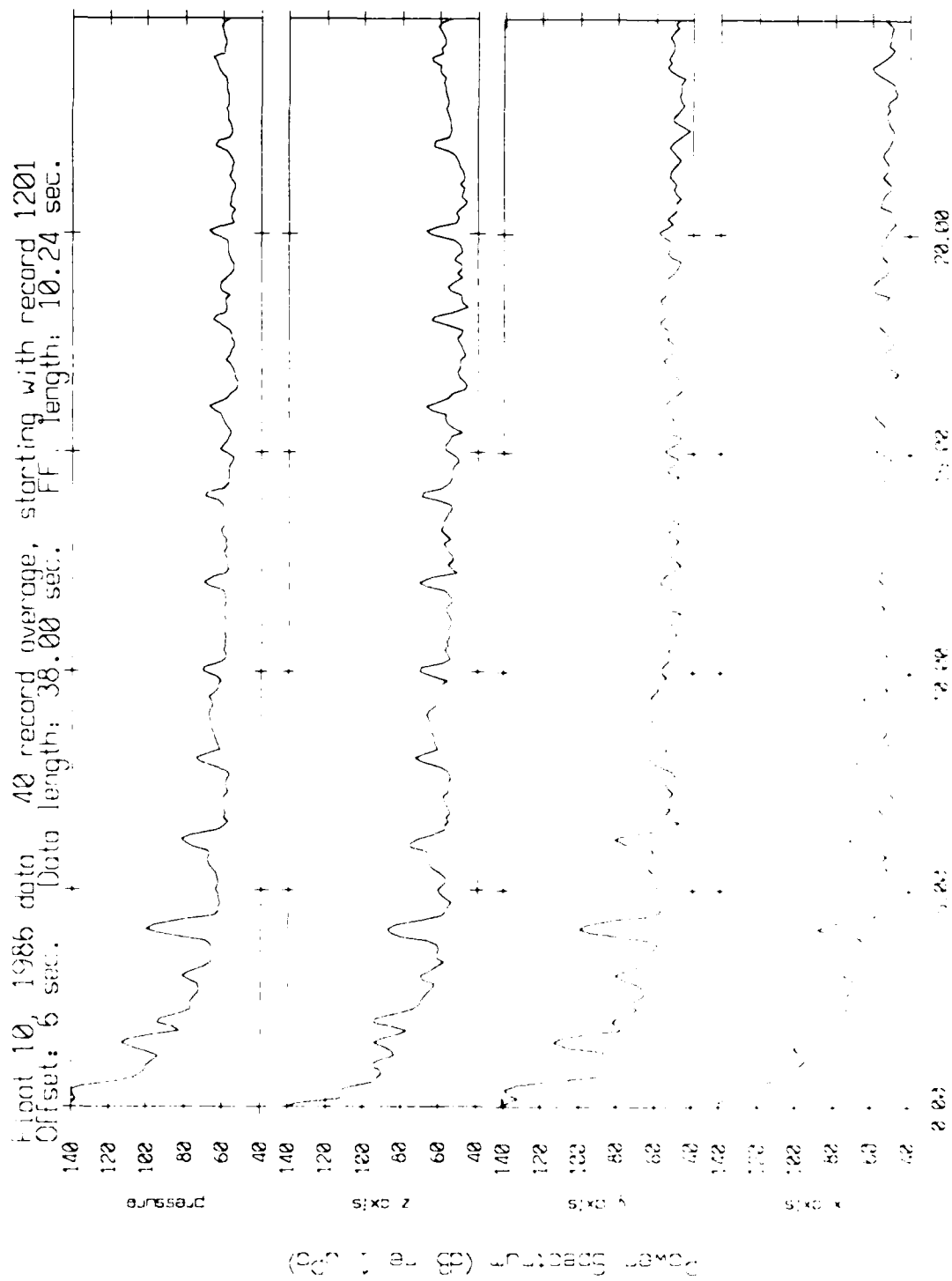


Figure 4.11d

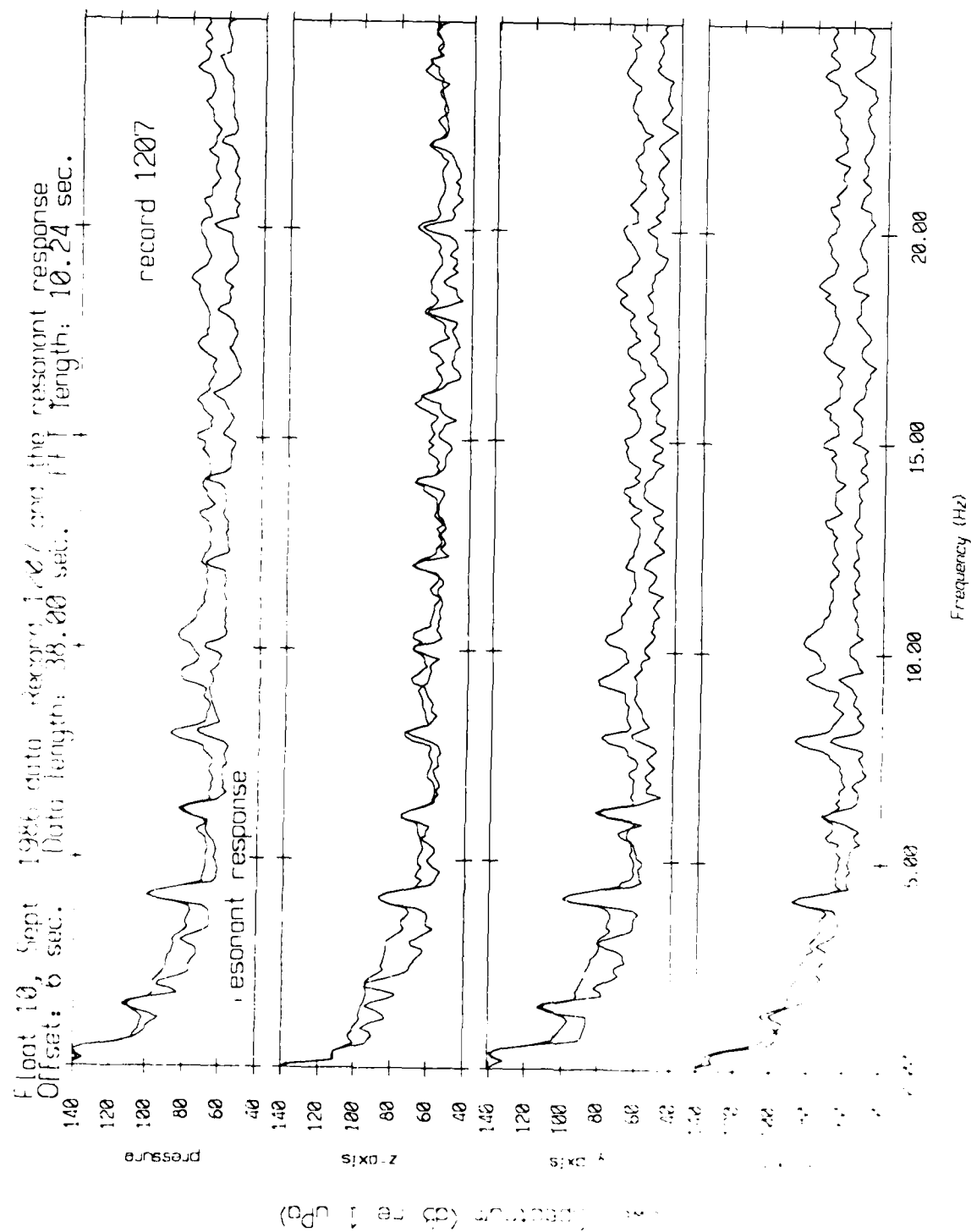


Figure 4.11e

AD-A188 895

REMOVING RESONANT OSCILLATION SIGNALS FROM SHALLOW
FLOAT DATA(U) SCRIPPS INSTITUTION OF OCEANOGRAPHY LA
JOLLA CA MARINE PHYSIC. R L CULVER ET AL. MAY 87

2/2

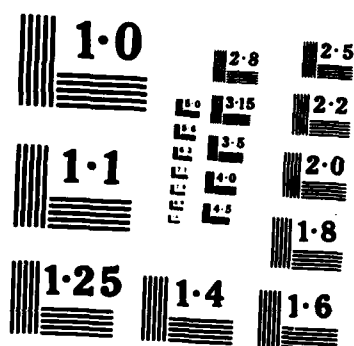
UNCLASSIFIED

MPL-TN-395 N00014-87-K-0010

F/G 20/1

NL





Floot 10, September 1986 Trip
 record 1207 with (1.0621 1.0256 0.98087) * r(n) subtracted

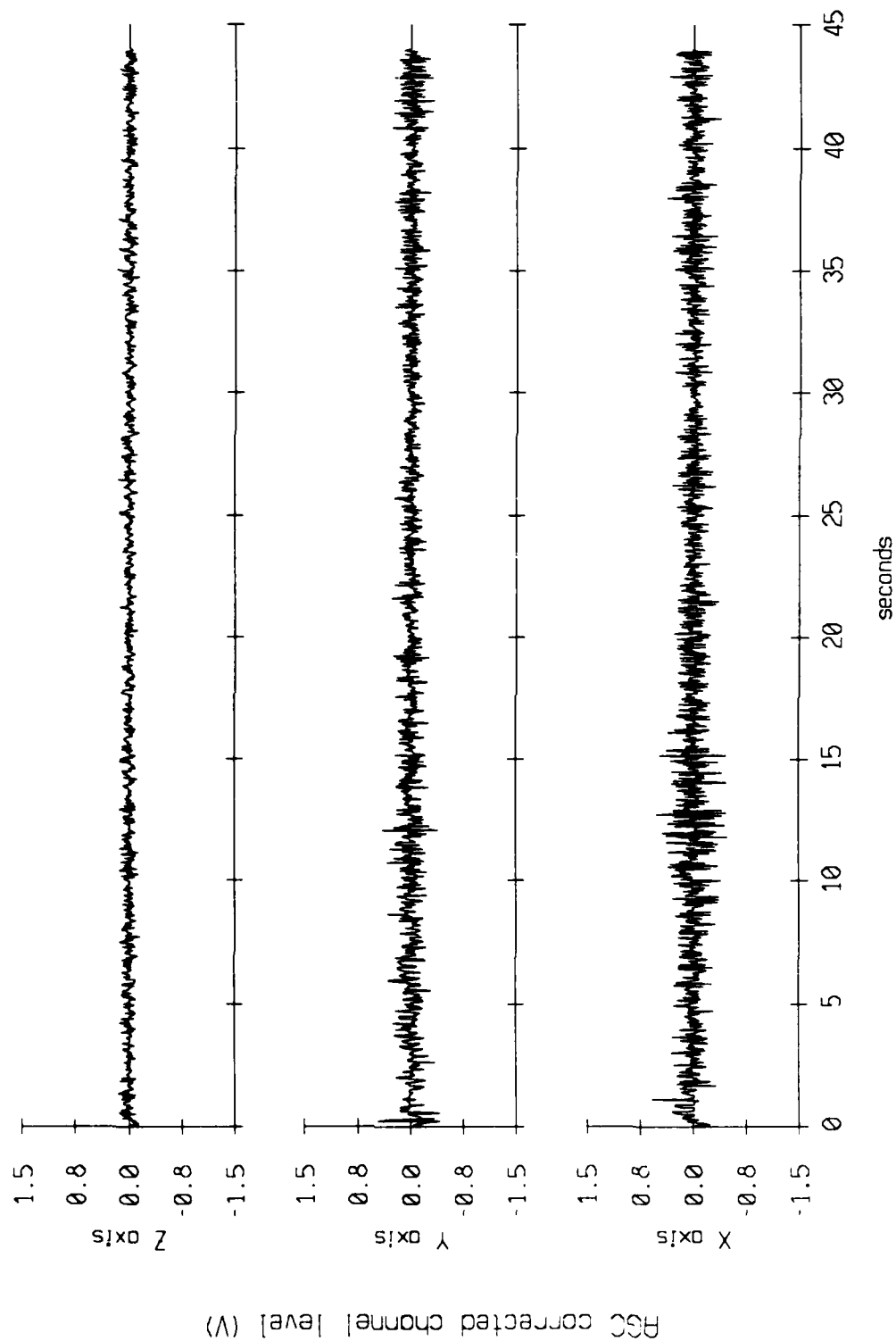


Figure 4.11f

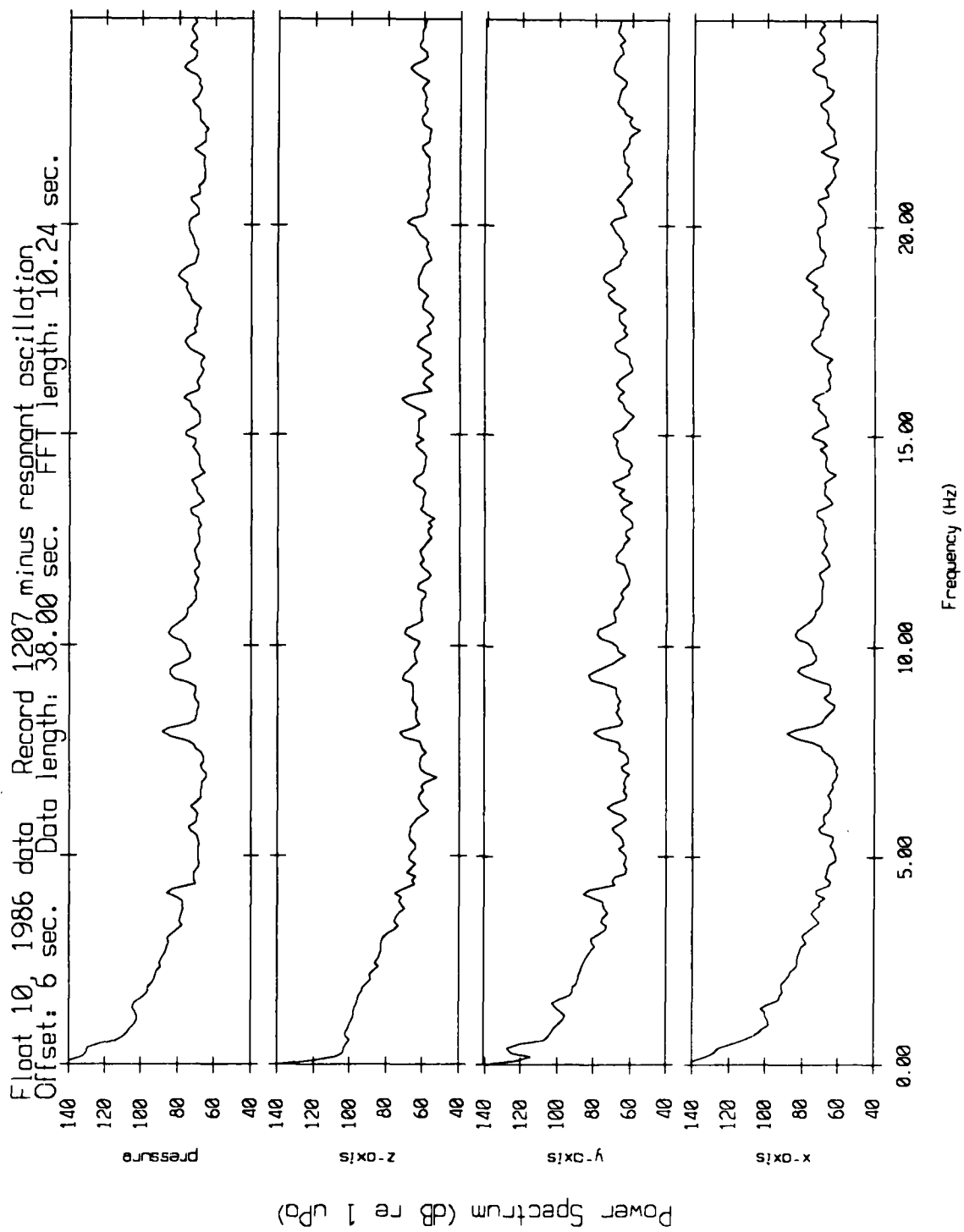


Figure 4.11g

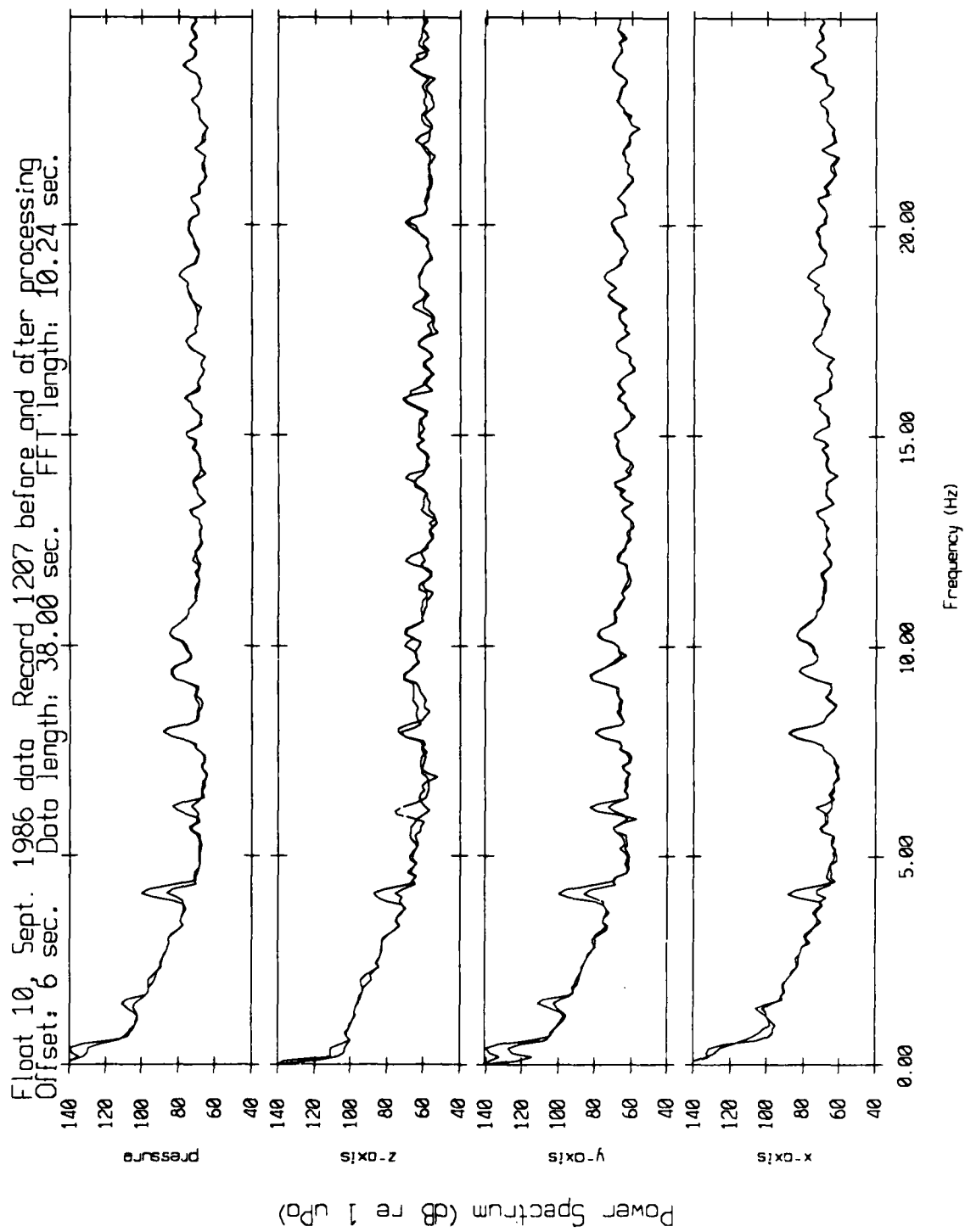


Figure 4.11h

Floot 10, September 1986 Trip
 record 1607 velocity time series

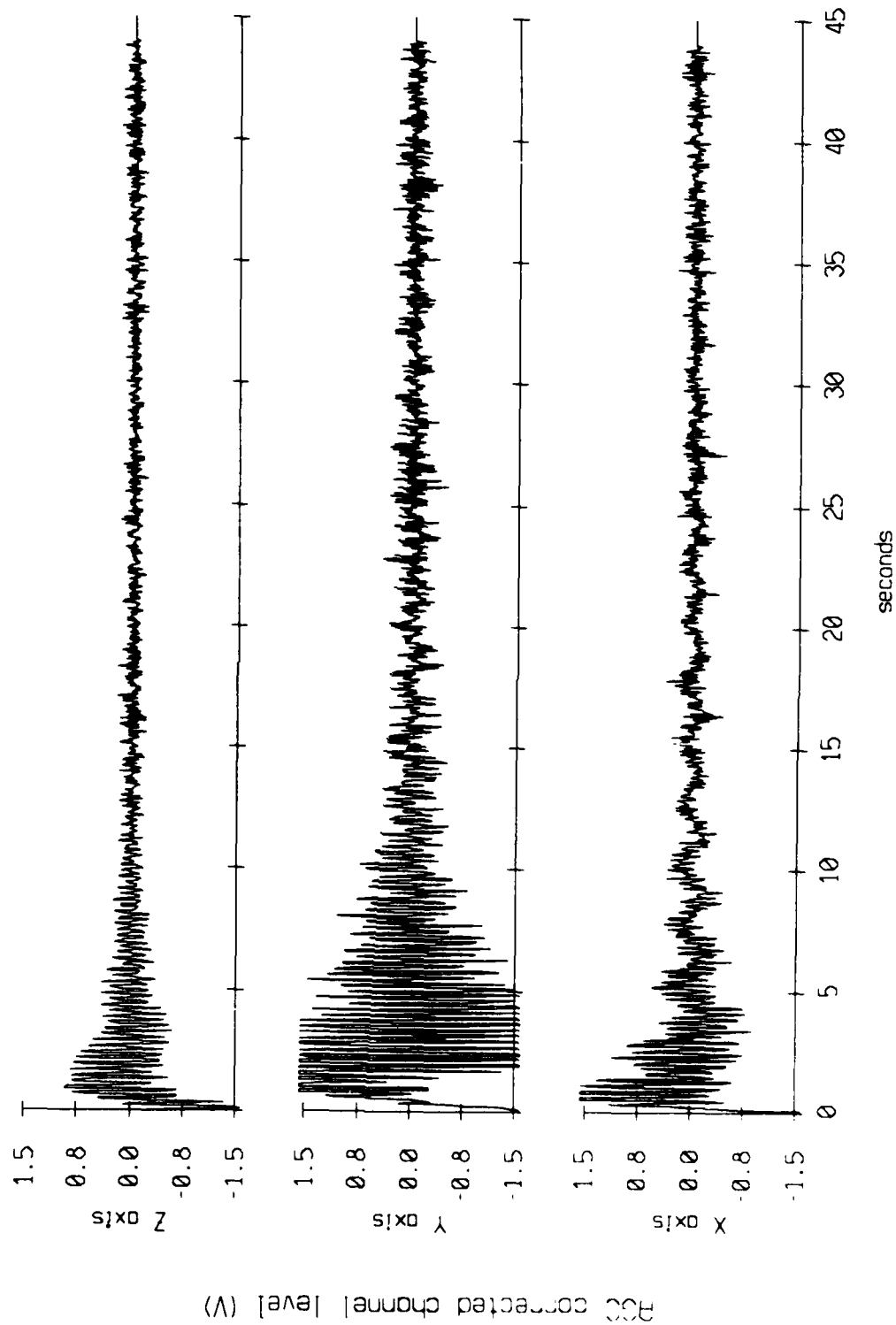


Figure 4.12a

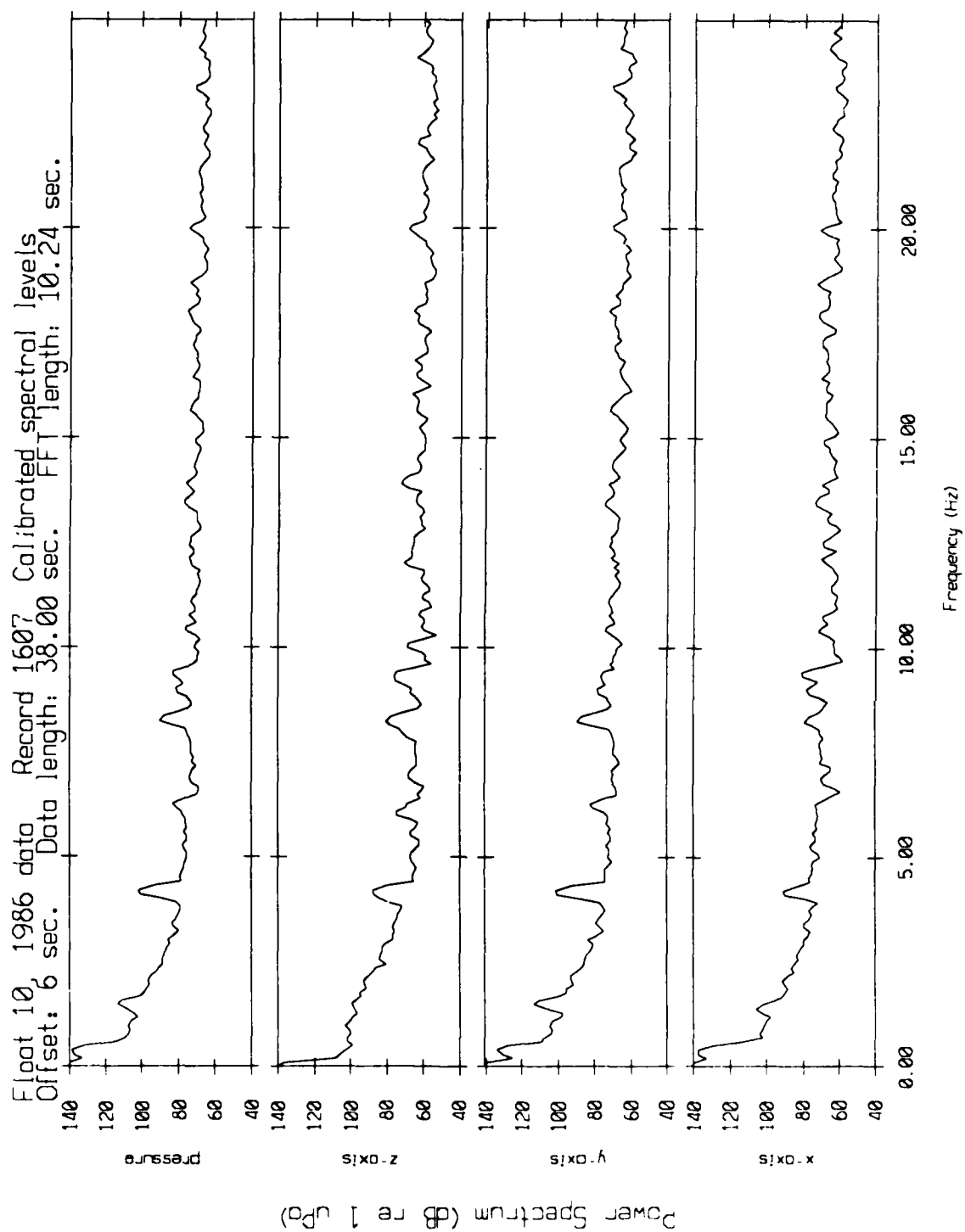
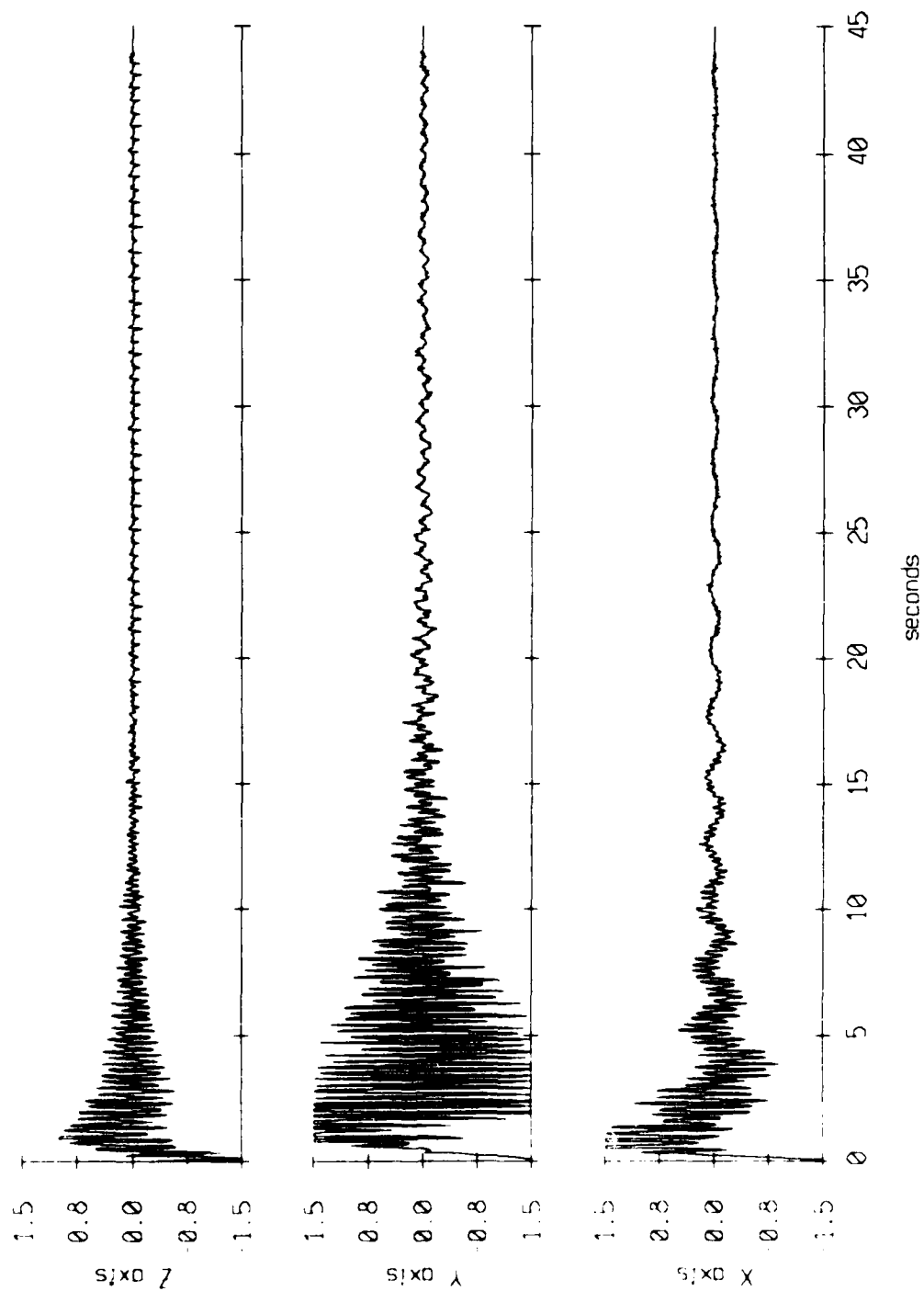


Figure 4.12b

Float 10, September 1986 Trip
 40 record average, starting with record 1601



FOO corrected channel level (V)

Figure 4.12c

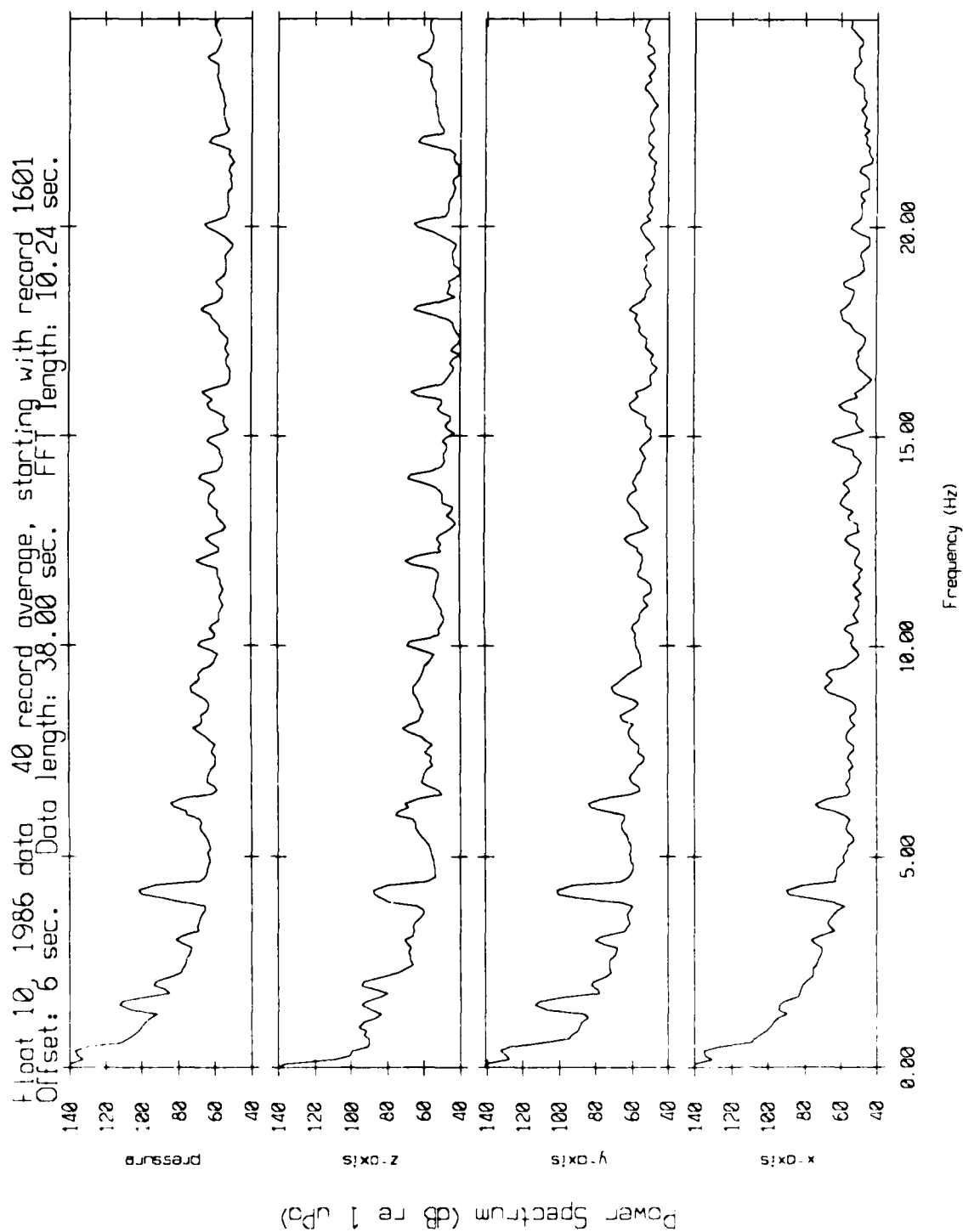


Figure 4.12d

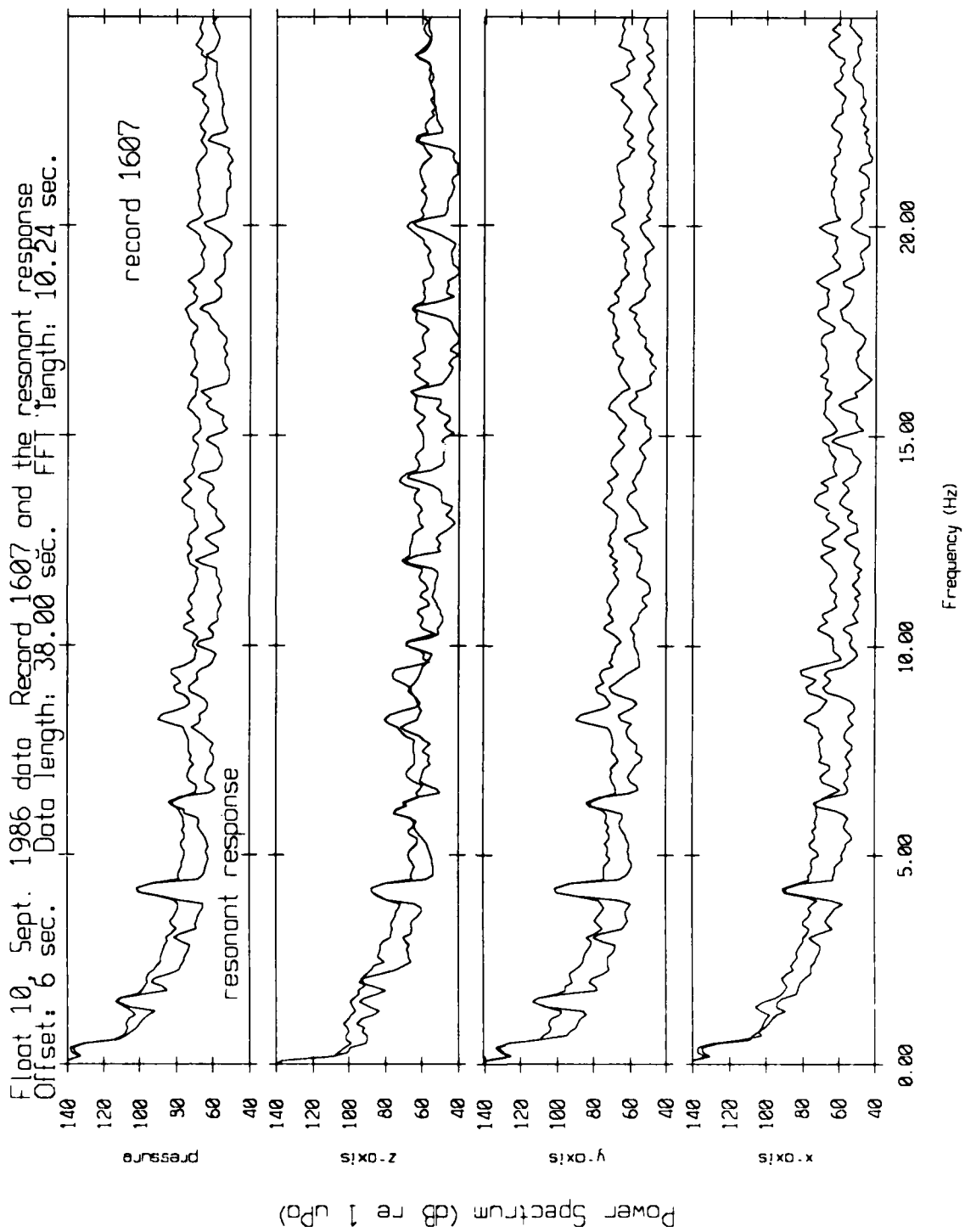


Figure 4.12e

Floot 10, September 1986 Trip
 record 1607 with (0.96406 1.0374 0.99367) * r(n) subtracted

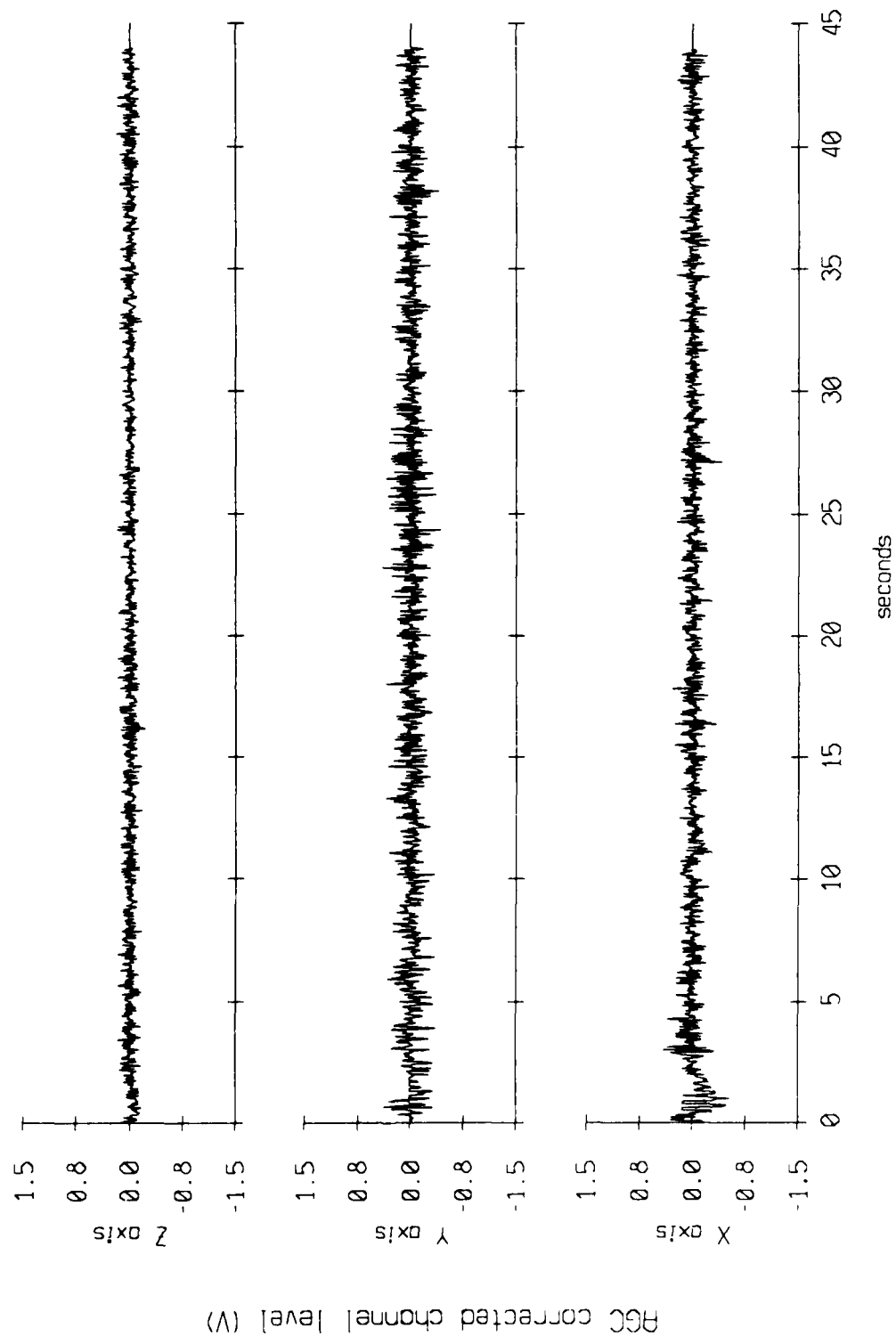


Figure 4.12f

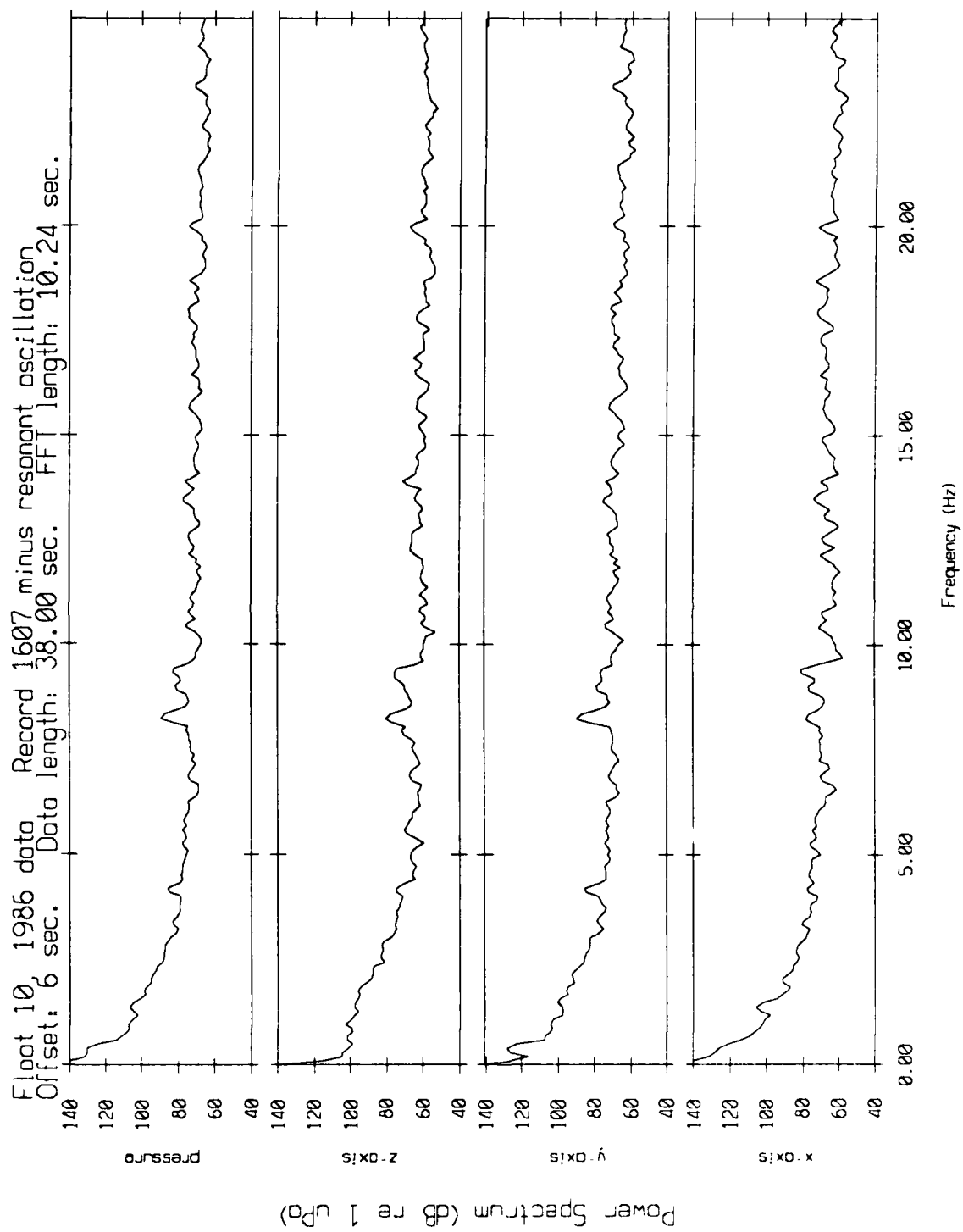


Figure 4.12g

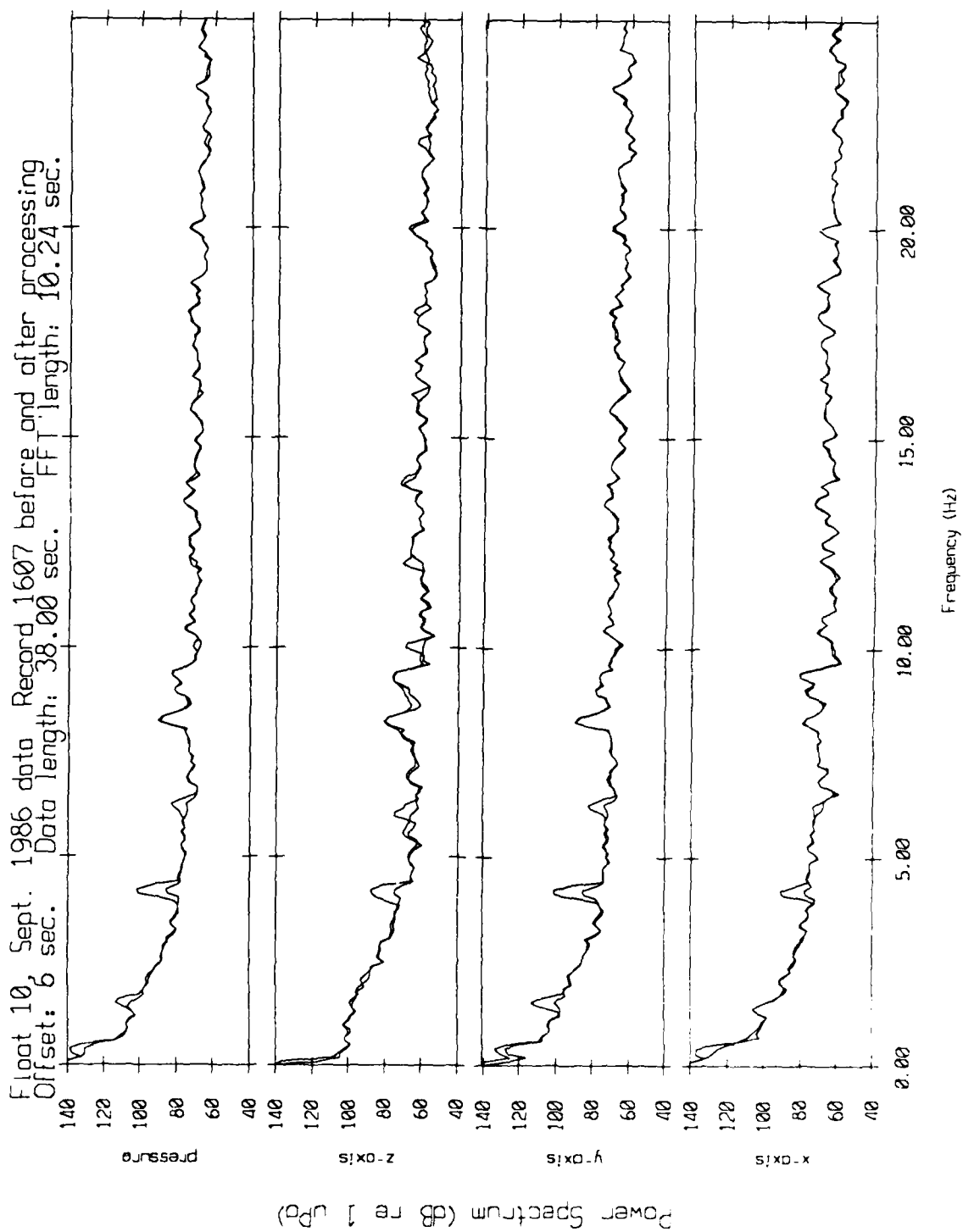


Figure 4.12h

END

FILMED

MARCH, 19 88

DTIC